Dynamic Behavior of Steel Pipe Sheet Pile Foundation in a Slope Revetment during Liquefaction

July 2014

NGUYEN Thanh Trung

Dynamic Behavior of Steel Pipe Sheet Pile Foundation in a Slope Revetment during Liquefaction

July 2014

Waseda University
Graduate School of Creative Science and Engineering
Department of Civil and Environmental Engineering,
Research on Structural Engineering

NGUYEN Thanh Trung

ACKNOWLEDGMENT

Firstly, I would like to express my honest appreciation to Professor Osamu Kiyomiya. During three years of doctoral course of studying in his laboratory I have learned a lot of wonderful academic lessons not only relating my research topic but also being how to become a good researcher and how to apply these studies to my country. It is really useful to me and the development of my country in the future. I am going to maintain these experiences and lessons and to transfer them to students in my university in Viet Nam. I think that the graduation of good research students is my deputy and is the best thank to my professor.

I would like to thank the referee committee of my dissertation, Professor Teruhiko Yoda, Professor Akiyama and Professor Atsushi Kuzumi for useful recommendations and suggestions in improving my research topic.

I also would like to thank the Associate professor Tongxiang An for his support and sharing many good experiences of research work during three years. When I have any troubles and problems about the living life in Japan and researches he is one of the most believable persons.

The living in the first steps in Japan was little difficult for me but with the major helps from Mrs. Endo, Dr. Hung, Mr. Vu and all members in Kiyomiya Laboratory, it became more comfortable. I really appreciate their helps a lot.

I would like to thank the Nippon Steel & Sumitomo Metal Corporation supported me a three years Scholarship. Especially to Dr. Kinoshita and Mr. Muchizuki, they also provided interesting trips to their construction site and office to me. This helps me to understand more about working behavior and characteristics of Japanese engineers.

I would like to thank my members in the Division of Transport and Communication, especially to Prof. Nguyen Viet Trung and Dr. Nguyen Thi Tuyet Trinh. Their supports and advices help me much to pass the difficult steps in the researches.

Finally, this is an honest thank to my parent who always encourages me and give the useful advices to solve every difficulties in living. Especially, the love and encourages from my wife and little daughter who shared both happiness and difficulties during two years staying with me in Japan are huge motivations to me. These were happy memories in Japan I have never forgotten.

Dynamic Behavior of a Steel Pipe Sheet Pile Foundation in a Slope Revetment during Liquefaction

By

NGUYEN THANH TRUNG

The dissertation presents the research on the dynamic behavior of Steel Pipe Sheet Pile Foundation (SPSP foundation) of long stayed cable bridge in a slope revetment during liquefaction by large scale earthquakes. The vibration test using 1G Shaking table test was conducted to study the seismic responses of SPSP foundation. Both the numerical method in the JRA 2002 approach and dynamic stress analysis also were mentioned to verify the validity of vibration test and applicability of simulation method in the investigation of SPSP foundation in the engineering practice.

The various damages to the pile and caisson foundation structures have been observed in areas of liquefaction in past earthquakes. Some of these damages were pipe failures near the bottom of the liquefied layer, whereas others were pile failures near the pile head. These failures were likely caused by the liquefaction that occurs due to a decrease in the soil strength and lateral movement of the liquefied layer. Moreover, significant damages were observed at both the pile body and pile head in the sites located near or on the revetment with a sloped surface ground along riverbanks or sea coasts. This damage was likely caused by the unstable ground movement during liquefaction.

In recent years, many important lessons and insights regarding the basic mechanisms of soil-pile interaction in liquefied soil and their effect on superstructure performance during liquefaction have been understood from field observations, shaking model tests, and numerical analysis. However, most of these studies were conducted on flat ground or ground with a mild slope line for a pile foundation structure. Ramin Motamed (2013) conducted a large shaking table test on the pile foundation near a gravity-type quay with flat ground. S. Mohsen Haeri (2008) investigated the response of a group of piles to liquefaction-induced lateral spreading by large-scale shake testing using a sloped ground with an angle of 5°. In addition, Tokida (1994) conducted tests on various sloped ground models of 5° with varying slope length. Miyajima (1991) performed a shaking table test and determined that the pile response depends on the sloping surface of the ground, with a range from 2° to 6° considered. Tokimatsu and Suzuki (2004)) performed seismic behavior of soil-pile-superstructure system during soil liquefaction and liquefaction-induced ground displacement by shaking table test. Therefore, the above researches almost performed the dynamic behavior of pile foundation on the flat ground or with the mild slope from 2^o to 6^o. However, the SPSP foundation, a kind of the caisson foundation, works as not only a support structure but also a retaining wall in the revetment, may be not discussed before.

Consequently, in this study the behavior of SPSP foundation with a slope of 15^0 will be investigated.

Moreover, in the current bridge seismic design specification JRA (2002) the liquefaction verification for the foundation structure is stipulated for flat ground. The verification of liquefaction-induced lateral spreading is conducted for a foundation that is less than 100 m from the waterfront. Therefore, the foundation in the revetment with a slope, whether affected by liquefaction-induced lateral spreading or not, is not clearly mentioned, and further investigations and studies are required.

In this study, a 1-G shaking table test with a 1:60-scale model was designed for two test models of a steel pipe sheet pile (SPSP) foundation to study the behavior of the bridge foundation during vibration. The first model was on a flat ground surface (denoted the flat model), and the second model was on a 15°-sloped ground (denoted the slope model). Additionally, a 2-D numerical finite element method using the effective stress analysis (ESA) and total stress analysis techniques considering the superstructure of the bridge was conducted to simulate the behavior of the liquefied ground and bridge foundation during vibration. The total stress analysis technique is used to investigate the dynamic characteristics of models. Furthermore, the ESA technique was used to consider the liquefaction of the loose sand for both a drain condition and an undrain condition.

This dissertation consists of six chapters

Chapter 1 presents the background, objectives and approach methodology of the research. It summarizes some damages of bridge foundation, previous researches and the design method of specification to clarify objectives and necessaries of this research. The result illustrates that the damages due to liquefaction and lateral spreading are really serious on the bridge foundation. Meanwhile, the previous researches using both vibration test and numerical analysis almost focused on the investigation of behavior of pile foundation on the flat or mild slope ground during liquefaction. The SPSP foundation, a quite special structure and works as not only the supporting structure but also a retaining wall, which located in the revetment with a slope of 15^o may be not investigated before. Moreover, the verification of liquefaction and liquefaction induced lateral spreading in the specification JRA 2002 only stipulates for the foundation in the flat ground or/and near revetment. Therefore, the behavior of SPSP foundation in the slope revetment during liquefaction is necessary to investigated in this research.

Chapter 2 reviews some major items that are necessary for a setup of models in both the vibration test and numerical methods. Firstly, the characteristics of SPSP foundation of the long stayed cable bridge and its design models by mass- spring model in the specification JRA 2002 are displayed. Secondly, the adopted theories in liquefaction analysis of foundation structure are summarized to show the effect of liquefaction parameters on the soil-foundation system. This is very significant to determine the analysis conditions. Finally, the total stress analysis and effective stress analysis are descried to explain their applicability in the later chapters.

Chapter 3 describes the vibration test using shaking table testing facility and explains the methodology used to perform the tests, the testing program and the test model. The two

models of foundation in the flat model and slope model are determined and conducted on this experiment to shows the difference of dynamic response of the foundation system and the ground such as excess pore water pressure, acceleration, displacement and strain, etc. Since then, there are some given evaluations to clarify the influence of slope on the behavior of SPSP foundation.

Chapter 4 presents the numerical method by the mass spring model using a total stress analysis calculated according to the specification JRA 2002. Total stress analysis is a simple calculation in the practical engineering approach using the reduction factor of shear modulus or strength of soil. The factors are determined in the specification JRA 2002 and depend on strength of earthquake and soil properties of ground. The result of research shows the validity of applicability of specification JRA in design work for SPSP foundation in both the flat and slope ground.

Chapter 5 presents the more advantaged numerical method using an effective stress analysis for the two dimension model. A particular advantage of this analysis is that it considers the dynamic response of the entire soil-foundation- superstructure system. Moreover, soil elements of ground are considered as plane strain elements using advanced models are that: a multi-spring model in un-drained condition; a glass cocktail model for drained condition. These models can explain the behavior of real soil more precisely. They consider the generation of excess pore water pressure in case of multi –spring model and both generation and dissipation of pore water pressure in case of cocktail glass model. The comparison between two models in this analysis represents the significant difference of their dynamic response to clarify the effect of slope ground on the foundation as mentioned in the experimental result of Chapter 3. Chapter 5 presents the comparison between experimental and analysis results also gives some evaluations and commentaries about the effective stress analysis in practical engineering.

Chapter 6 summarizes the key conclusions from this work. The implications of this research work are also highlighted. The scope for future work is also suggested.

In conclusion, the dissertation produces main findings as follows:

1) The effect of slope ground on seismic response of SPSP foundation is significant. It means that the lateral movement of liquefaction layer due to slope may partially affect to the foundation when liquefaction occurred. The effective stress analysis (ESA) has almost same trend as the dynamic responses in the experiment. The difference in dynamic response of the foundation, superstructure, and ground between the flat and the slope models is minimal in the low-amplitude input ground motion, indicating that the effect of the ground slope is not significant. In cases of higher amplitude when liquefaction is observed, the effect of the ground slope becomes more significant, with the following trends: The slope causes an increase in the maximum and residual displacements of the pile cap and superstructure and a decrease in the horizontal acceleration. Furthermore, the slope causes an increase in the inclination of the foundation and the maximum value of the bending and axial strain in the foundation pile.
2) Numerical method in the specification JRA 2002 approach can produce the good

agreement with the vibration test in the flat model but not in case of slope model.

3) The ESA using both the Multi-spring model and Cocktail glass model can explain the behavior of the foundation with regard to maximum displacements, EPWP ratios and bending strains during liquefaction. However, the calculated values of the residual displacement, etc. did not display a good agreement with the values observed in the vibration test.
4) The bending and axial strains along the foundation axial were nearly uniform before the liquefaction of sand occurred. When liquefaction occurred, the strains in the non-liquefaction layer became larger instead of the strains in the liquefied layer. The reaction stress of the slope model was small in the liquefied layer. The reaction force at the front wall was small in the liquefied layer for the slope model. However, the reaction at the back wall was large to move the foundation to front direction. The foundation resisted the movement due to the non-liquefaction layer.

TABLE OF CONTENTS

This page intentionally left blank

LIST OF FIGURES

This page intentionally left blank

LIST OF TABLES

This page intentionally left blank

Chapter 1

Introduction

1.1 Research Background

1.1.1 Damages of the bridge foundation during liquefaction

1.1.1.2 Introduction

Although the past strong earthquakes such as 1964 Niigata Earthquake and 1995 Kobe Earthquake have long passed but their damages on the foundation, superstructure and other structures due to liquefaction phenomenon were really serious and complicated. Triggered this, there are a lot of experimental and numerical researches were conducted to investigate and to evaluate the effects of liquefaction.

The observations of earthquakes show that these damages to bridge foundations during earthquake were mainly caused by liquefaction and/or lateral movement of ground (Pile Damage Investigation Committee et al. 1996, Editorial Committee et al. 1998). Some of them are failures of piles near the bottom of liquefied layer. They were caused by kinematic force from its lateral movement and some cases are pile failures near the pile head which are likely influenced by inertial force from superstructure. Other cases are failures caused by both kinematic and inertial force (Kawamura et al. 1985, Yoshida and Hamada et al. 1990, Matsui and Oda et al. 1996, Tokimatsu et al. 1996, 1998, Fuji et al. 1998, Nishizawa et al. 1998). These observations of damages became the concept theories of failure in areas of liquefaction, as shown in **Fig.1.1**. This figure shows that the crack of pile in the pile foundation appears near a pile head and bottom of liquefied layer during liquefaction or liquefaction induced lateral movement. Most of significant damages were clearly observed in the site located near or in the revetment along the river banks and sea coasts where the lateral movement of ground is large. Some typical damages due to the liquefaction and lateral movement observed in the history strong earthquake cases are summarized in the **Table 1**.

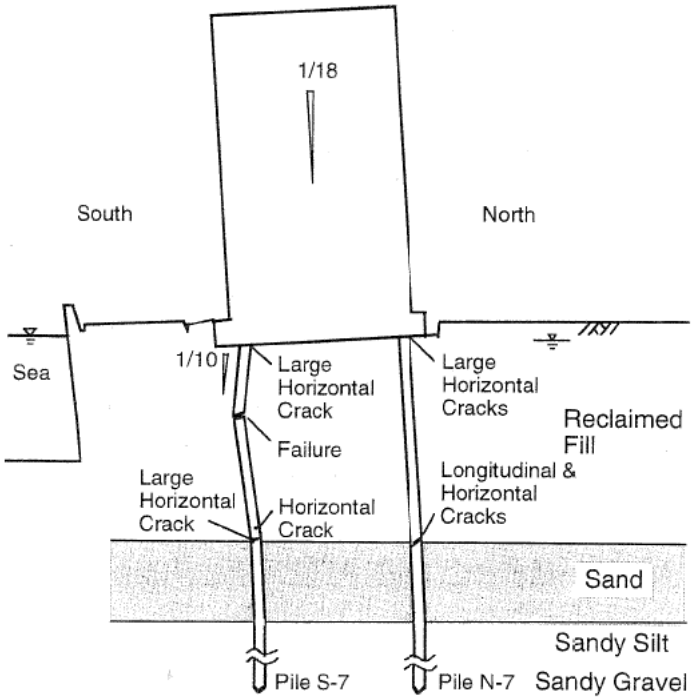

Fig.1.1 Concept failure patterns of piles due to liquefaction (Tokimatsu et al. 1997)

Table 1.1 Typical case histories of seismic liquefaction observation

No	Case Histories of seismic liquefaction	Pile length	Liquefiable layer	Pile section	Lateral spreading observation
1	Landing bridge, 1987 Edgecumbe earthquake, Berrill et al. (2001)	9	4	0.4m square PSC	Ground cracked and sand ejected.
2	14 stores building in American park, 1995 Kobe earthquake, Tokimatsu et al. (1996)	33	11	2.5m Dia. RCC	Quay walls on the west, south and east moved.
3	Hanshin expressway pier, 1995 Kobe earthquake, Ishihara et al. (1997)	41	15.9	1.5m Dia. RCC	Ground moved by 0.62m.
4	NFCH building, 1964 Niigata earthquake, Hamada et al. (1992)	9	7	0.35m Dia. RCC hollow	Nearby ground moved by 1 to 2m.
5	Showa bridge, 1964 Niigata earthquake, Hamada et al. (1992)	25	19	0.6m Dia. Steel tube	Width of river decreased.
6	Yachiyo Bridge, 1964 Niigata earthquake, Hamada (1992)	11	8	0.3m Dia. RCC	Width of river decreased.

Fig.1.2 Permanent Ground Displacements in the Upstream Area of the Shinano River

1.1.1.2 Niigata Earthquake 1964

The Niigata Earthquake caused soil liquefaction phenomenon in Niigata City and the surrounding areas. The earthquake motion was not large but it caused the liquefaction and lateral movement of ground (Hamada et al. 1986). The liquefaction mostly occurred along bank lines of the Shinano Rivers in Niigata City. **Fig.1.2** shows the horizontal movements of the permanent ground displacements. The maximum horizontal ground displacements were until 8m occurred in the area along the Shinano river toward the waterfront. The Yachiyo bridge across Shinano river consists of 14 spans which is made of pre-stressed concrete slab and composite girders with 304 m long and 10 m width. Some damages were observed at the substructure of the pier during the earthquake. **Figs.1.3** and **1.4** show that the damages of the abutment and the piers of the Yachiyo Bridge were on the left bank. The pier 2 was broken in the middle and the deformation between the bridge footing center and the lower part of the pier was 1.1 m. The damages were also observed at the abutment and the piers on the right bank. The permanent ground displacements on both banks were from 2 to 4 m towards the river and it caused the damage to the abutments and the piers.

Fig.1.3 Damages at the abutments and piers of Yachiyo Bridge (Hamada et. al, 1986)

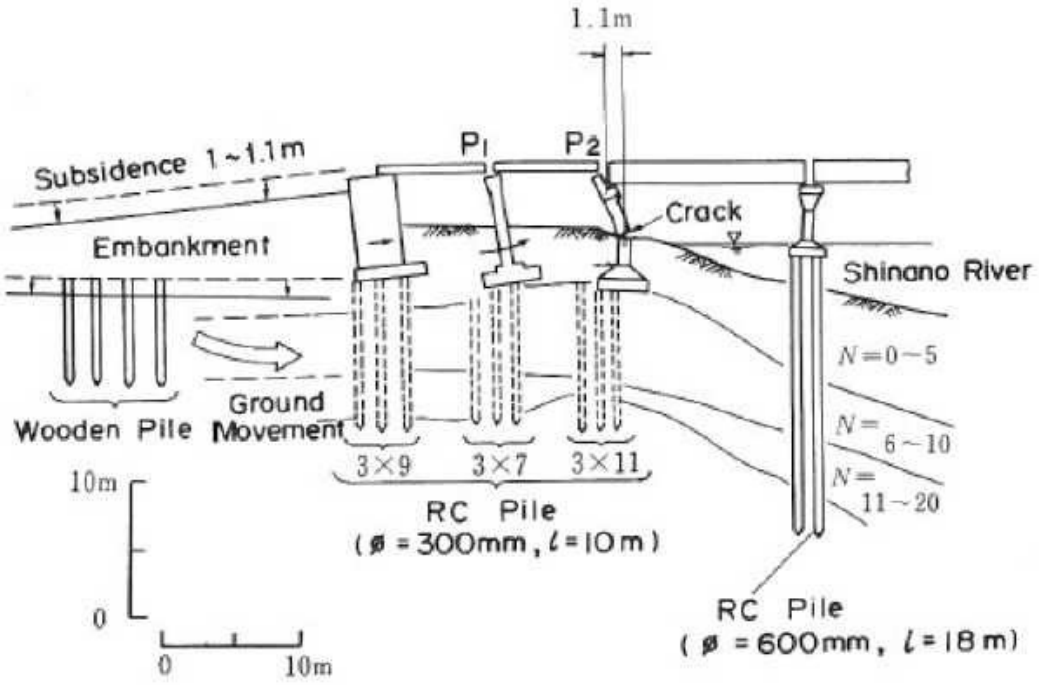

Fig.1.4 Damage to Yachiyo Bridge due to lateral spreading

1.1.1.3. Kobe Earthquake 1995

The Hyogoken-Nambu Earthquake (Kobe earthquake) in 1995 with 7.3 Richter magnitude scales. In this earthquake, there were lateral movements of ground observed in the southern area of Uozakihama bridge. **Fig.1.5** shows that the area near the revetment line the lateral displacement is directed southwards to the waterfront with its maximum value of 186cm. The lateral displacement of the pier P211 of Uozakihama bridge near the revetment was

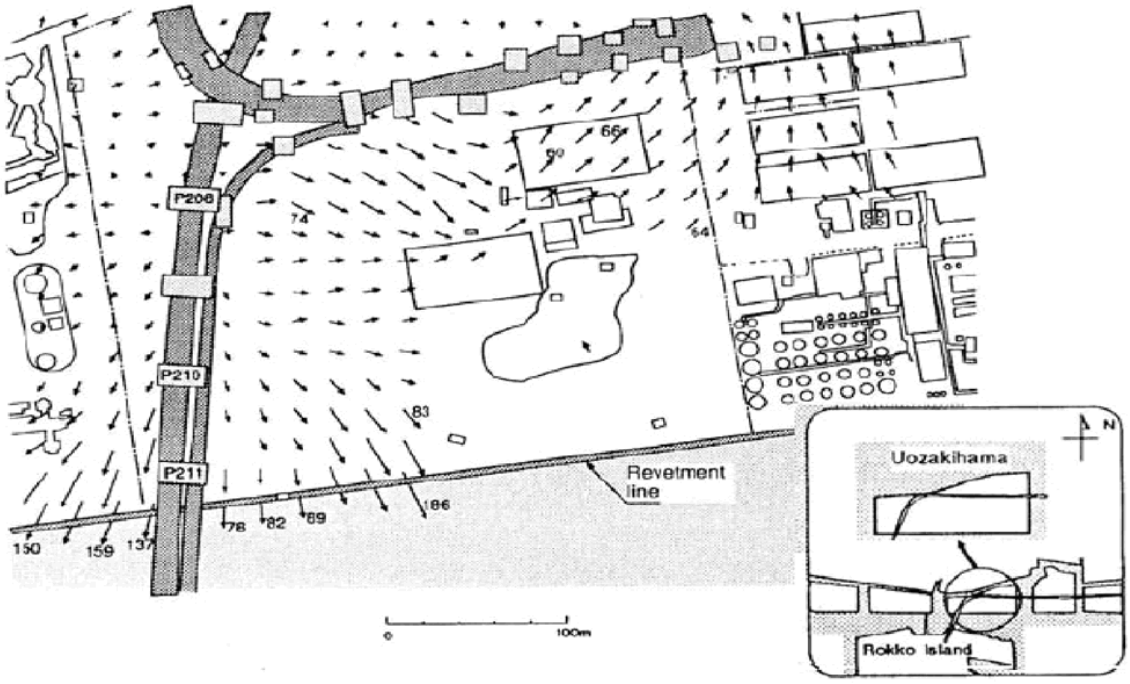

Fig.1.5 General area of Uozakihama bridge near revetment line

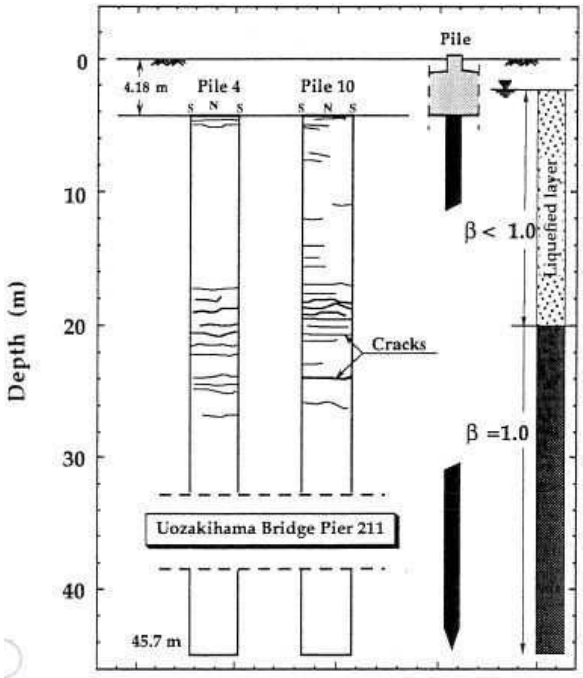

Fig.1.6 Crack distribution of the large diameter bored piles of pier 211 (Ishihara and Cubrinovski **1998)**

62cm. The pile damages took place around three positions along the depth of pile. The cracks are observed at the pile head and at depth of the interface between the liquefied layer and the base non-liquefied layer, as shown in **Fig.1.6**

1.1.1.4 Conclusions

Most of major failures of pile were observed on the pile foundation structure near a river bank or coastal line during liquefaction or liquefaction-induced lateral spreading. There may be no investigations work for damages of caisson or SPSP foundation but the influence of liquefaction is really serious. Moreover, in recent years some new projects using SPSP foundation structure have been conducted near river banks or coastal lines where poor construction site such as a depth water and/or soft surface ground conditions. For example, in Kawasaki Port Ring Road Project under planning is one of typical examples. The tower MP4 of Higashi Ogijima cable stayed bridge used a SPSP foundation in design work. In Vietnam, Nhat Tan bridge project under construction and Thanh tri project using the SPSP foundation for towers located near river banks. Therefore, it is necessary to previously estimate the seismic behavior of SPSP foundation structure during liquefaction and lateral ground movement.

1.1.2 Previous researches

1.1.2.1 Introduction

In recent years, the researches of liquefaction and liquefaction induced lateral spreading have been considerably conducted on pile foundation structure. Liquefaction and/or lateral movement of ground is really complicated phenomenon. The change of soil strength depends on the generation and dissipation of pore water pressure along with contractive and dilative characteristic of soil element. Therefore, the numerical model, experimental and theory models still have been improved to more closely approach the behavior of real soil elements.

1.1.2.2 Experimental researches

Experiments provide a tool for investigating specific features of pile response. The researchers can accurately observe and measure pile behavior during shakings. While experiments can be well modeled the features of real life structures, soil condition and liquefaction earthquakes, they remain a vital instrument in investigating of the behavior of pile foundations during liquefaction.

Ramin Motamed et al. (2013) conducted a large shaking table test on the pile foundation near a gravity-type quay on flat ground, as shown in **Fig.1.7**. This research showed that the liquefaction induced lateral spreading occurred in this experiment and the

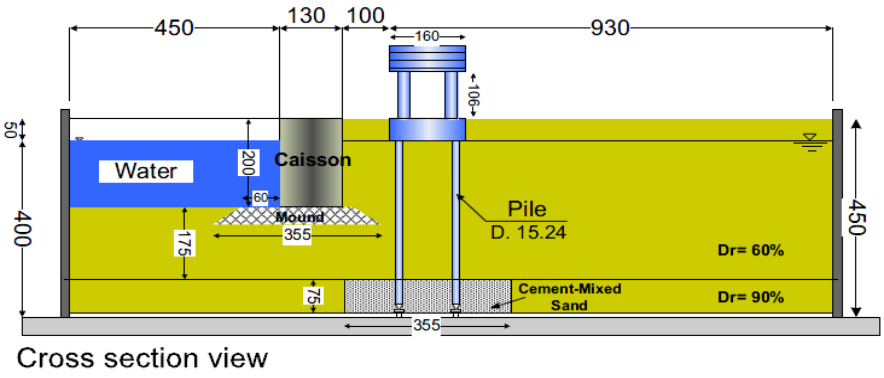

Fig.1.7 Shaking table test on pile foundation near a gravity quay

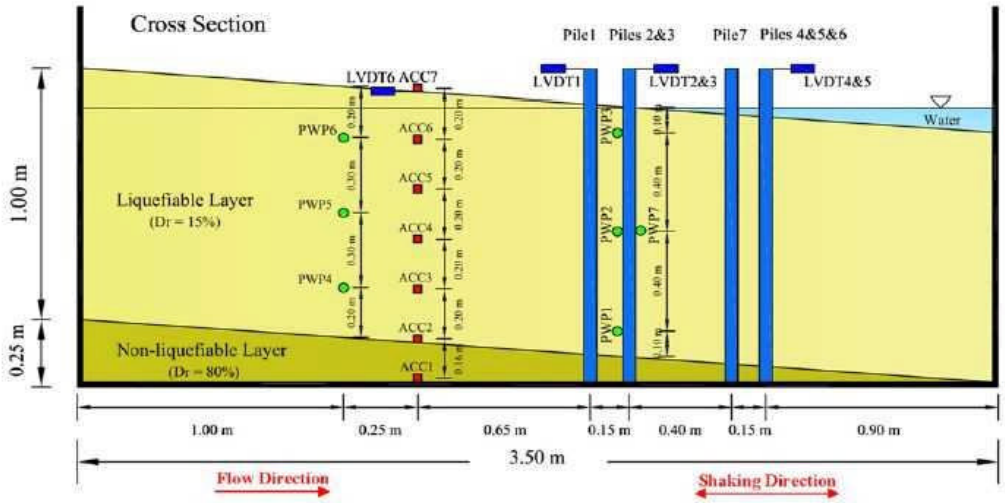

Fig.1.8 Shaking table test on pile group on the slope ground of 8^{o}

lateral displacement of soil depends on the distance from the foundation to the quay wall. S. Mohsen Haeri et al. (2012) and Ramin Motamed et al. (2008) investigated the response of a group of piles to liquefaction-induced lateral spreading by large-scale shake testing using a sloped ground with an angle of 5°, as shown in **Fig.1.8.** In addition, Tokida et al. (1992) conducted tests on various sloped ground models of 5° with varying slope length. Miyajima et al. (1991) performed a shaking table test and determined that the ground displacement depends on a layer thickness and a ground slope with a range from 2° to 6° considered, however the test model in the experiment was a slope revetment. Consequently, the effect of liquefaction in the revetment with a ground slope and large inclination may have been investigated in these previous studies.

Kyohei Ueda et al. (2012) performed the behavior of embankment on liquefaction sand deposit using Multi-spring model. This research considered the effect of large deformation analysis on the seismic response by extending the model based on the finite

strain theory of large strain and rotation phenomenon. It assumed the significant effect of seepage of pore water pressure on the seismic response of this structure and recommended the drained condition was necessary in the liquefaction analysis.

Hatsukazu Mizuno et al. (2004) clarified the effect of the stiffness and damping of soil-pile system in the liquefaction process. Its result presented that pore water pressure was high, the damping and stiffness of the system was small. Inversely, when dissipation of pore water pressure occurred the damping and stiffness increased. This is in accordance with previous researches. Shintaro Yao and Koichi Kobayashi et al. (2003) performed the interactive behavior of soil-pile-superstructure system in the transient state to liquefaction during earthquake by a shaking table test. The transient state to liquefaction was necessary to consider in liquefaction analysis because effect of both inertial and kinematic force in this state simultaneously occurred and was greatly significant. Shunichi Sawada et al. (2000) presented the liquefaction analysis induced residual deformation for two quays using FLIP program and Jun Wang et al. (2000) also performed behavior of seawall structure in both un-drained and drained condition during liquefaction.

As a result, these researches and studies of liquefaction and lateral spreading movement were conducted carefully and detail. However, most of them almost focus on flat ground or ground with a mild slope line for a pile foundation structure or pile group. The SPSP foundation, a type of caisson foundation, works not only as a supported structure but also as a retaining wall and is located in the slope revetment. It is necessary to have further studies to investigate its dynamic behavior. Therefore, it is necessary to have the further researches..

1.1.2.3 Analysis researches

A number of constitutive models have been developed to simulate soil response during liquefaction (e.g., Ishihara et al. 1985; Iai, 1991; Li and Dafalias 2000; Kimura et al., 1993; Tobita and Yoshida, 1995; Lade and Yamamuro et al. 1999; Arduino et al. 2001). However, there are two satisfied soil models mainly used in modeling the behavior of soil elements under liquefaction condition.

The first one is a strain space multiple mechanism model. It was firstly suggested by Iai et al. (1991) named as a Multi Spring Model in the un-drained condition. Then, the model was also improved by Iai et al. (2011) names as a Glass Cocktail Model in the drained condition. The model is one of the most advanced models in geotechnical

engineering. The second one is a Stress Density Model suggested by Misko Cubrinovski et al. (1993, 2010). The model considers the dependence of the plastic strain increment direction on the stress increment direction, or hypo-plasticity (the effects of rotation of principal stresses), modifies the hyperbolic relationship between stress and strain and establishes the relationship between the stress and dilatancy factor of soil element.

These advanced models were applied to the strong FEM programs to perform the behavior of ground with many kinds of foundation structure during liquefaction. M. Yoshida, M. Mitou and O. Kyomiya et al. (2012) investigated the effect of seismic reinforcement on sheet pile quay way by using a strain space multiple mechanism model for a soil element, as shown in **Fig.1.9**. Kyohei Ueda et al. (2008) also used the model in modeling a self-supported sheet pile wall. M.W.Wang et al. (2008) investigated the seismic behaviors of inclined micro-piles during liquefaction by using Multi-spring models. The Sawada and Iai et al. (2000) presents the behavior of quay and pile foundation under liquefaction-induced lateral spreading, as shown in **Fig.1.10**. Bowen and Cubrinovski et al. (2007) using the numerical model to perform behavior of pile foundation during liquefaction, as shown in **Fig.1.11**.

In summary, the same with researches from the vibration test such as shaking table or a centrifuge test. The advanced numerical models in the previous researches also performed the behavior of structures such as a pile foundation, quay wall and sheet pile retaining during liquefaction. Moreover, these researches were almost conducted in the flat ground and/or far away the revetment. As a result, the numerical behavior of SPSP foundation in the slope revetment may be studied before.

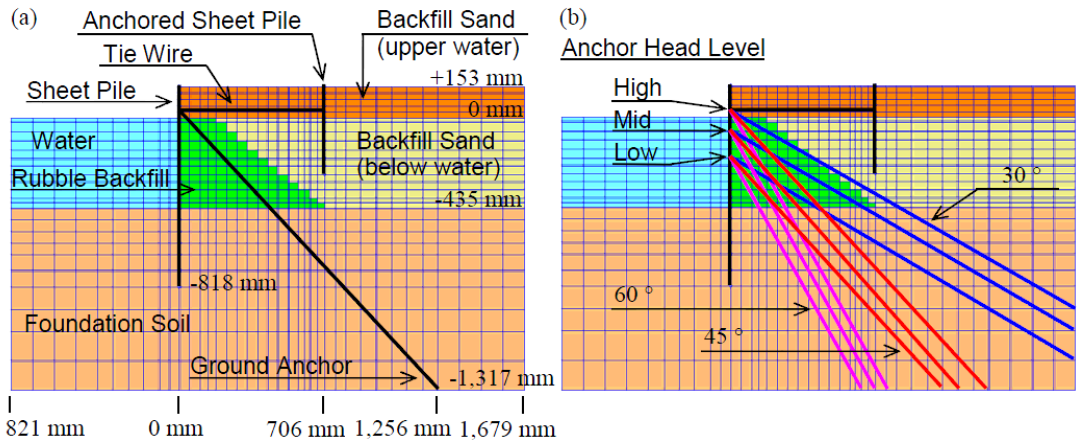

Fig.1.9 Numerical model of steel sheet pile in FLIP (Yoshida and Kiyomiya et al. 2012)

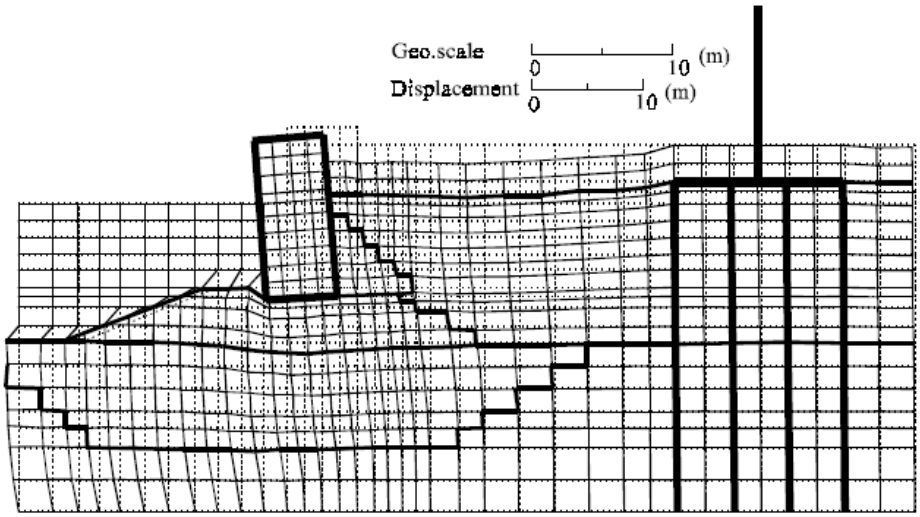

Fig.1.10 Residual displacement of quay and pile foundation in the Flip program (Sawada and Iai et al. 2000)

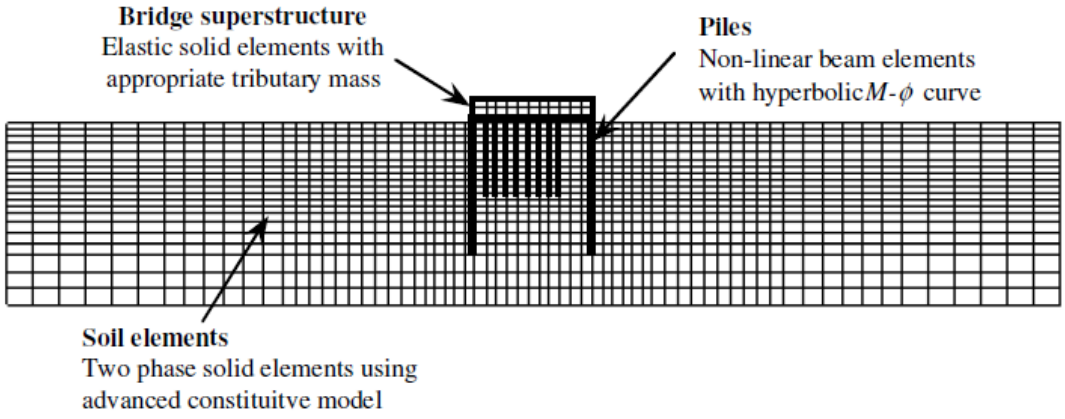

Fig.1.11 Numerical model of pile foundation (Bowen and Cubrinovski et al. 2007)

1.1.3 Design verification of liquefaction in the specification JRA 2002

The Japan Road Association (JRA 2002) specifications for highway bridges stipulates a verification of liquefaction induced lateral spreading in seismic design work (as shown in **Fig.1.12**) by multiplying the reduction factor (D_E) with initial shear modulus or soil strength. This F_L is taken as dependent on the level of earthquake (as represented by the factor of safety against liquefaction, F_L), the relative density of the soil (as represented by the dynamic shear strength ratios R), as shown in equation: F_L=R/L. However, this equation is only stipulated for the foundation on the flat ground. The foundation in the slope ground is not mentioned. This may be because of the complex in the determination of overburden pressure with a change of ground slopes.

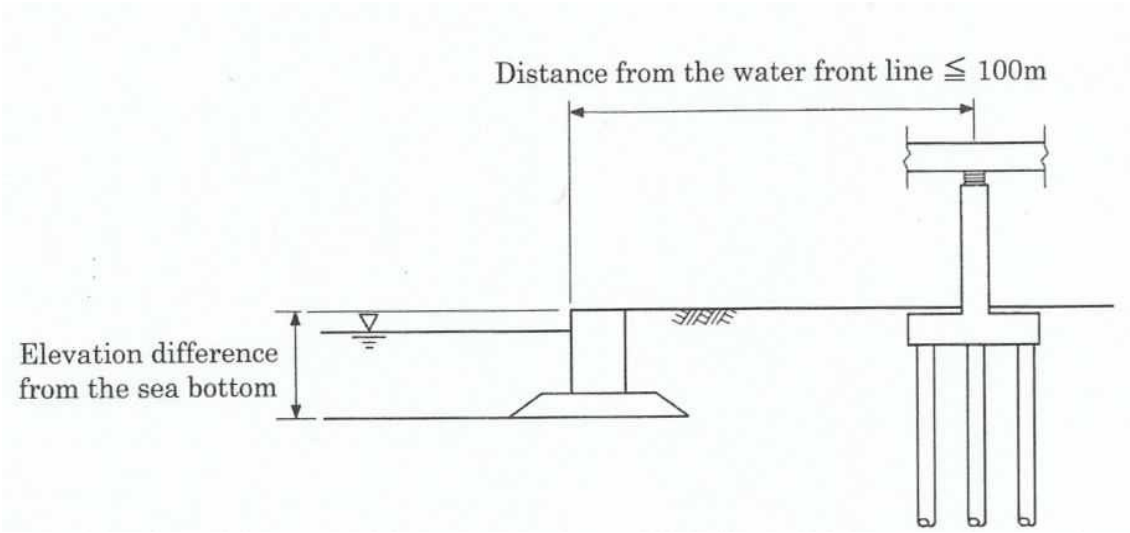

Fig.1.12 Verification of liquefaction induced lateral spreading in JRA et al. (2002)

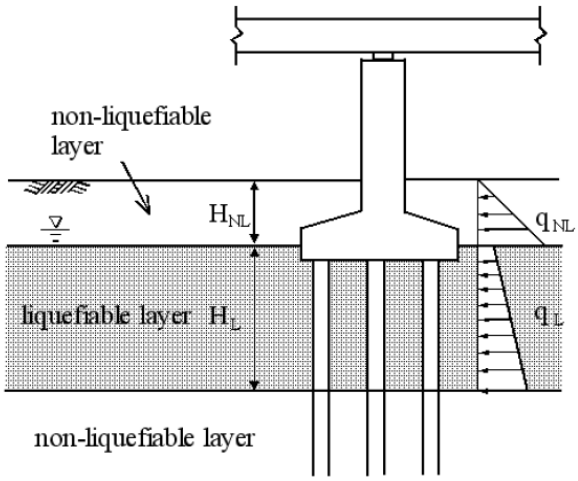

Fig.1.13 Lateral spreading pressure in JRA 2002

Moreover, regarding as the liquefaction induced lateral spreading the JRA (2002) guidelines impose lateral pressures from the liquefied layer and from any overlying non-liquefied layers (as shown in **Fig.1.13**)**.** The non-liquefied layers are considered as imposing passive earth pressures. The liquefied layers are considered as imposing a lateral pressure equal to 30% of the total overburden stress. The verification is conducted for a foundation that is less than 100 m from the waterfront. It is one of two conditions shall be treated as a ground with possible lateral movement is that ground within a distance less than 100 m from a water front in the shore area that formed by revetment with an elevation difference of 5 m and more between the water bottom and the ground surface. The distance of this methodology is partly based on analyses of case histories of pile performance in the 1995 Kobe earthquake. Therefore, the foundation in the revetment with a slope, whether

affected by liquefaction-induced lateral spreading or not, is not clearly mentioned, and further investigations and studies are required.

1.1.4 Conclusions

As a result, there are many damages of foundation due to liquefaction and liquefaction induced lateral spreading during past earthquakes; especially serious for the foundation located in the site near the slope revetment, river banks or coastal lines. Many numerical and experiment researches have been conducted to investigate but only focused on the pile foundation on a flat or mild ground. Therefore, the behavior of SPSP foundation in the revetment with a slope of 15^{o} may not be investigated before. Moreover, the specification JRA 2002 also does not clearly mentioned about a calculation work for the foundation in the large slope ground. Consequently, it is necessary to have a further investigation to perform the behavior of SPSP foundation in the large slope ground.

1.2 Research Objectives

The fundamental aims of this research are to investigate the dynamic behavior of SPSP foundation in the flat ground and the slope revetment during liquefaction earthquake by using the vibration experiment and numerical analysis. Their result is compared and evaluated to present the salient features of seismic response of the foundation in the slope revetment. Moreover, the aim is also to produce some commentaries in seismic design work and future studies. Therefore, the objectives of the present research are:

1) To review the previous researches about the effects of liquefaction on the seismic behavior of foundation and to investigate the applicability of numerical models stipulated in the specification JRA to explain the seismic behavior of SPSP foundation.
2) To capture the basic foundation of test set up, program verification, loading procedure, test model in the vibration experiment using shaking table test.
3) To investigate the dynamic behavior of pier foundation system of experimental model on the both flat and slope ground during seismic liquefaction through the seismic response of the superstructure, foundation and ground. Then, the results are examined to express the effects of the slope ground and lateral spreading on the foundation.
4) To investigate the response of test models by using a simple numerical method (Total stress analysis) based on the specification JRA 2002 and to evaluate and give some

commentaries to the seismic design of the foundation in the slope ground following the specification.

5) To perform numerical study on the dynamic behavior of above test models by using the current advanced analysis (Effective stress analysis) that considers the liquefaction behavior of soil elements in the un-drained and drained conditions. Then, to evaluate some contractive and dilative parameters of soil models in liquefaction analysis and to contribute commentaries and new ideas for future research

1.3 Structure of the Thesis

Chapter 1 presents the background, objectives and approach methodology of the research. It summarizes some damages of bridge foundation, previous researches and the design method of specification to clarify objectives and necessaries of this research. The result illustrates that the damages due to liquefaction and lateral spreading are really serious on the bridge foundation. Meanwhile, the previous researches using both vibration test and numerical analysis almost focused on the investigation of behavior of pile foundation on the flat or mild slope ground during liquefaction. The SPSP foundation, a quite special structure and works as not only the supporting structure but also a retaining wall, which located in the revetment with a slope of 15^{o} may be not investigated before. Moreover, the verification of liquefaction and liquefaction induced lateral spreading in the specification JRA 2002 only stipulates for the foundation in the flat ground or/and near revetment. Therefore, the behavior of SPSP foundation in the slope revetment during liquefaction is necessary to investigated in this research.

Chapter 2 reviews some major items that are necessary for a setup of models in both the vibration test and numerical methods. Firstly, the characteristics of SPSP foundation and its design models in the specification JRA 2002 are displayed. Secondly, the adopted theories in liquefaction analysis of foundation structure are summarized to show the effect of liquefaction parameters on the soil-foundation system. This is very significant to determine the analysis conditions. Finally, the total stress analysis and effective stress analysis are descried to explain their applicability in the later chapters.

Chapter 3 describes the vibration test using shaking table testing facility and explains the methodology used to perform the tests, the testing program and the test model. The two models of foundation in the flat model and slope model are determined and

conducted on this experiment to shows the difference of dynamic response of the foundation system and the ground such as excess pore water pressure, acceleration, displacement and strain, etc. Since then, there are some given evaluations to clarify the influence of slope on the behavior of SPSP foundation.

Chapter 4 presents the numerical method using a total stress analysis calculated according to the specification JRA 2002. Total stress analysis is a simple calculation in the practical engineering approach using the reduction factor of shear modulus or strength of soil. The factors are determined in the specification JRA 2002 and depend on strength of earthquake and soil properties of ground. The result of research shows the validity of applicability of specification JRA in design work for SPSP foundation in both the flat and slope ground.

Chapter 5 presents the more advantaged numerical method using an effective stress analysis for the two dimension model. A particular advantage of this analysis is that it considers the dynamic response of the entire soil-foundation- superstructure system. Moreover, soil elements of ground are considered as plane strain elements using advanced models are that: a multi-spring model in un-drained condition; a glass cocktail model for drained condition. These models approach the behavior of real soil more closely. They consider the generation of excess pore water pressure in case of multi –spring model and both generation and dissipation of pore water pressure in case of cocktail glass model. The comparison between two models in this analysis represents the significant difference of their dynamic response to clarify the effect of slope ground on the foundation as mentioned in the experimental result of Chapter 3. Chapter 5 presents the comparison between experimental and analysis results also gives some evaluations and commentaries about the effective stress analysis in practical engineering.

Chapter 6 summarizes the key conclusions from this work. The implications of this research work are also highlighted. The scope for future work is also suggested.

References

1) Miles, J. W. : On the generation of surface waves by shear flows, *J. Fluid Mech*., Vol. 3, Pt. 2, pp. 185-204, 1957.
2) Pile Damage Investigation Committee (1996). Report of damage to building foundation during Hyogoken-Nambu earthquake, Kinki Branch of AIJ, 399p.
3) Editorial Committee (1998). Report on the Hanshin-Awaji Earthquake Disaster, Report on the Hanshin-Awaji earthquake disaster, building, Vol. 4, 548p.
4) Tokimatsu, K., Oh-Oka, H., Shamoto, Y., Nakazawa, A., and Asaka, Y. (1997). Failure and deformation modes of piles caused by liquefaction-induced lateral spreading in 1995 Hyogoken-Nanbu earthquake. *Geotechnical Engineering in Recovery from Urban Earthquake Disaster, 3rd Kansai International Geotechnical Forum on Comparative* R-8.
5) Matsui, T., Kitazawa, M., Nanjo, A. and Yasuda, F. (1997). Investigation of damaged foundations in the Great Hanshin earthquake disaster. *Seismic Behavior of Ground and Geotechnical Structures*, Secoe Pinto (ed.), Balkema, Rotterdam, pp.235-242. *Geotechnical Engineering (KIG – Forum 97)*, Kansai Branch, Japanese Geotechnical Society, Osaka, Japan.
6) Yoshida, N., and Hamada, M. (1991). Damage to foundation piles and deformation pattern of ground due to liquefaction induced permanent ground deformations. *Tech. Rep.NCEER 91-0001*, NCEER, Buffalo, N.Y.
7) Tamura, S., Suzuki, Y., Tsuchiya, T., Fujii, S., and Kagawa, T. (2000). Dynamic response and failure mechanisms of a pile foundation during soil liquefaction by shaking table test with a large-scale laminar shear box. *12th World Conference on Earthquake Engineering*, CD ROM Paper No. 0903.
8) Ramin , M., Towhata, I., Honda, T., Tabata, K. and Abe, A. (2013). Pile group response to liquefaction-induced lateral spreading: E-Defence large shake table test. *Journal Soil Dynamics and Earthquake Engineering*, Vol. 51, pp.35-46.
9) Haeri, S.M., Kavand, A., Rahmani, I., Torabi, H. (2012). Response of a group of piles to liquefaction-induced lateral spreading by large scale shaking testing. *Journal of Soil Dynamic and Earthquake Engineering*. Vol. 38, pp.25-45.
10) Ramin , M., Sesove, V., and Towhata, I. (2008). Shaking model test on behavior of group piles undergoing lateral follow of liquefied subsoil. *Proc. 14th World Conference on Earthquake Engineering.* Beijing, China, pp.12-17.
11) Tokida, K., Matsumota, H., & Iwasaki, H. (1992). Experimental study on drag acting on piles in ground flowing by soil liquefaction. *Proc. 4th US-Japan Workshop on Earthquake Resistant Design of Lifeline Facilities and Countermeasures for Soil Liquefaction*, NCEER report 92-0019, SUNY, Buffalo, pp.511-523.

12) Miyajima M, Kitaura M, Ando K. (1991). Experiments on liquefaction-induced large ground deformation. *Proceedings of the third Japan–U.S. workshop on earthquake resistant design of lifeline facilities and countermeasures for soil liquefaction*, Technical report NCEER, New York: SUNY, Vol. 1, pp. 269-278.

13) Tokida, K., Iwasaki, H., Matsumoto, H. and Hamada, T. (1993). Liquefaction potential and drag force acting on piles in flowing soils. *Soil Dynamics and Earthquake Engineering*, 1, pp. 244-259.

14) Tokimatsu, K., Suzuki, H. and Sato, M. (2004). Influence of inertial and Kinematic components on pile response during earthquakes. *Proc., 11th International Conference on Soil Dynamics and Earthquake Engineering*, pp.768-775.

15) Tokimatsu, K., Suzuki, H and Suzuki, Y (2001). Back-calculated p-y relation of liquefied soils from large shaking table tests", *Proceedings of the 4th International Conference on Recent Advances in Geotechnical Earthquake Engineering and Soil Dynamics and Symposium,* in Honor of Professor W.D.Liam Finn, San Diego, California.

16) Tokimatsu, K (1999). Performance of pile foundations in laterally spreading soils", *Proceedings of the 2nd International Conference on Earthquake Geotechnical Engineering*, Lisbon, Portugal, June 21-25, Vol 3, pp. 957-964.

17) Suzuki, H., Tokimatsu, K. (2002). Loading combinations for inertial and kinematic components in dynamic soil-pile-structure interaction during soil liquefaction. *Proc., US-Japan Seminar on Seismic Disaster Mitigation in Urban Area by Geotechnical Engineering*.

18) JRA (2002): Specifications for highway bridges. Japan Road Association, Preliminary English Version, prepared by Public Works Research Institute (PWRI) and Civil Engineering Research Laboratory (CRL), Japan.

19) Kagawa, T., Taji, Y., Sato, M., and Minowa, C. (1997b). Soil-piles-structure interaction in liquefying sand from large-scale shaking table tests and centrifuge tests. *ASCE Annual Convention,* ASCE, Reston, Va.

20) Kagawa, T., Abe, A., Ogawa, N., and Minowa, C. (1997a). Shaking table tests on a real-size pile foundation in liquefying sand. *Proc., SMIRT 14 Conf., International Association of Structural Mechanics in Reactor Technology*.

21) Cubrinovski M, Ishihara K. (2004). Simplified method for analysis of piles undergoing lateral spreading in liquefied soils. *Soils Foundation* 44(5).

22) Cubrinovski, M., and Ishihara, K. (1998a). Modeling of sand behavior based on state concept. *Soils and Foundations*, 38(3), pp. 115-127.

23) Ishihara, K., Yoshida, K., and Kato, M. (1997). Characteristics of lateral spreading in liquefied deposits during the 1995 Hanshin-Awaji Earthquake. Journal of Earthquake Engineering, 1(1), pp. 23-55.

24) Ishihara, K. and Cubrinovski, M. (1998). Performance of large-diameter piles subjected to

lateral spreading of liquefied soils, *Keynote Lecture, Proc. 13th Southeast Asian Geotechnical Conf.*, Taipei: pp. 1-14.

25) Uzuoka, R., Cubrinovski, M., Zhang, F., Yashima, A., and Oka, F. (2006). Accuracy of prediction with effective stress analysis for liquefaction-induced earth pressure on a pile group. *New Zealand Workshop on Geotechnical Earthquake Engineering*, pp.120-132.

26) Boulanger, R. W., Wilson, D. W., Kutter, B. L., Brandenberg, S. J., and Chang, D. (2004). Nonlinear FE analyses of soil-pile interaction in liquefying sand. *ASCE Geotechnical Special Publication 126*, pp. 403-410.

27) Yasuda, S., Kobayashi, T., Nomura, H., and Terauchi, T. (1996). Shaking table tests on the lateral flow of the liquefied ground behind quay walls. *Sixth Japan -U. S. Workshop on Earthquake Resistant Design of Lifeline Facilities and Countermeasures Against Soil Liquefaction*, Report NCEER-96-0012, SUNY, Buffalo, NY, pp. 275 - 288.

28) Taji, Y., Sato, M., and Yanagisawa (1998). Modeling of a prototype soil-pile-structure system during seismic ground liquefaction. *Proc. Intl. Conf. Centrifuge '98*, (T. Kimura, O. Kusakabe, and J. Takemura, eds.), Tokyo, Japan, Sept. 23-25, Vol. 1, pp. 283 – 288.

29) Takahashi, A., Takemura, J., Kawaguchi, Y., Kusakabe, O., and Kawabata, N. (1998). Stability of piles pier subjected to lateral flow of soils during earthquake. *J. Geotechnical and Geo-environmental Engineering,* ASCE, Vol. 124, No. 12, pp. 1195 - 1206.

30) Towhata, I., and Mizutani, T. (1999). Effect of subsurface liquefaction on stability of embankment resting on surface. *Proc., 2nd Int. Conf. on Earthquake Geotech. Engrg.*, P. S. Seco e Pinto, ed., Balkema, Rotterdam, The Netherlands, 3, pp. 1045–1058.

31) Imamura, S., T. Hagiwara, Y. Tsukamoto, and K. Ishihara (2004). Response of pile groups against seismically induced lateral flow in centrifuge model tests. *Soils and Foundations*, 44(3), pp. 39-55.

32) Hamada, M. (2000). Performances of foundations against liquefaction-induced permanent ground displacements, *Proceedings of the 12th World Conference on earthquake engineering*, Auckland, New Zealand, p. 1754.

33) Hamada, M. (1992a). Large ground deformations and their effects on lifelines: 1964 Niigata earthquake. Case Studies of liquefaction and lifelines performance during past earthquake, *Technical Report NCEER-92-0001, Vol.1, Japanese case studies*, National Centre for Earthquake Engineering Research, Buffalo, NY.

34) Hamada, M. (1992b). Large ground deformations and their effects on lifelines: 1983 Nihonkai-Chubu earthquake. Case Studies of liquefaction and lifelines performance during past earthquake", *Technical Report NCEER-92-0001, Volume-1*, Japanese case studies, National Centre for Earthquake Engineering Research, Buffalo, NY.

This page intentionally left blank

Chapter 2

Literature Review

2.1 Introduction

In the previous chapter, the background and objectives were summarized to express the validity of the research in civil engineering practices. This chapter will present an overview of SPSP foundation characteristics, its design accepts. Especially, it explains two dynamic methods (a total stress analysis and an effective stress analysis) using in this research and summarizes some adopted researches about the effects of liquefaction conditions such as a drainage, relative density of sand and an interaction soil-structure, etc. on the behavior of foundation. The review work provides initial foundations for installing a numerical and test model in both vibration test and simulation method in the next chapters. Furthermore, the SSI (Soil-Structure-Interaction) and SFSI (Soil-Structure-Foundation-Interaction) models of SPSP foundation stipulated in the specification JRA 2002 during strong earthquakes were also investigated and discussed to show an applicability of JRA 2002 in performing the seismic behavior of SPSP foundation.

2.2 Steel Pipe Sheet Pile Foundation

2.2.1 Introduction

Steel Pipe Sheet Pile (SPSP) foundation was firstly applied to build a sheet pile wall in 1964 in Japan. It was then used as a foundation for a blast furnace in 1967 with the first bridge foundation that was constructed across Ishikari River in Hokkaido in 1969. Up to now, more than 1600 foundations have been constructed using SPSP foundation structures. Application of SPSP has expanded widely to harbor constructions (supporting piers and breakwaters), infrastructure of civil engineering project (building bridges, rail roads, and sheet piles). The studies of SPSP foundation have been conducted and developed by both

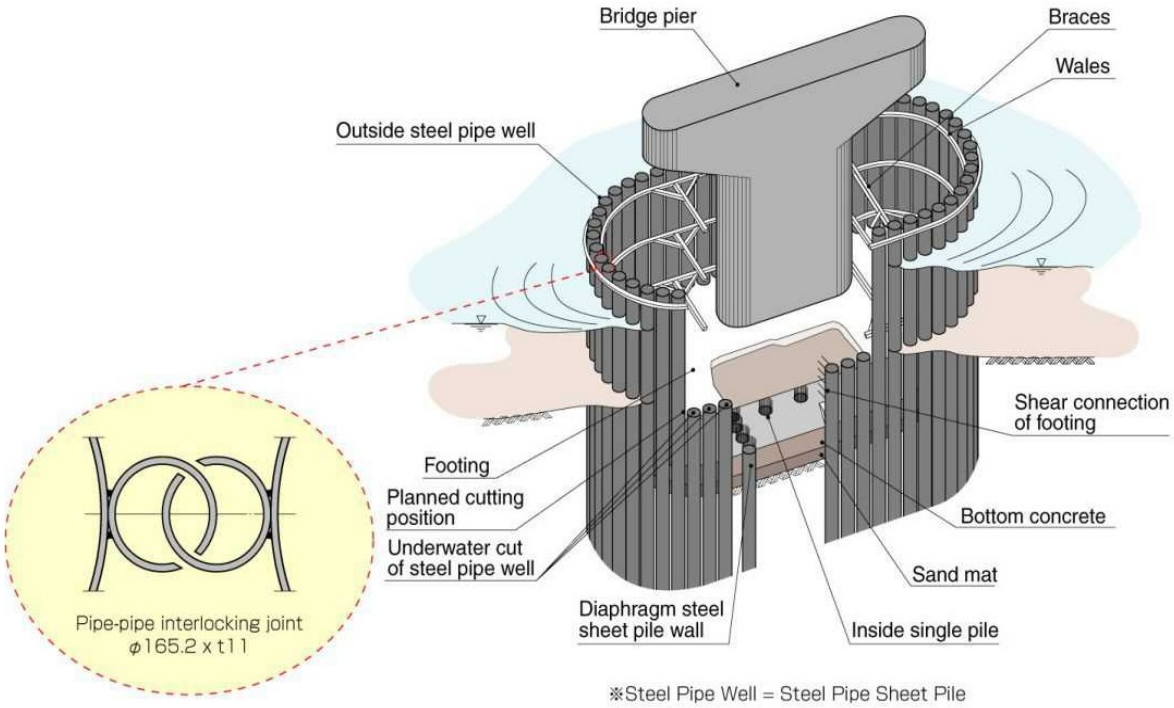

Fig.2.1 Overview of Steel Pipe Sheet Pile foundation

the numerical method and experiment. Its design criteria have also specified Japan Road Association, JRA et al. (2002).

2.2.2 Characteristic of SPSP foundation

Steel pipe sheet pile (SPSP) is a combination of steel pipe piles that are connected by two interlockings. They are welded either side to form a closed structure of arbitrary shape such as a circle, rectangular, oval. The interlockings will be filled concrete into, the heads of piles are connected together rigidly by constructing work of footing. The overview of SPSP foundation is shown in **Fig.2.1**. The most commonly used interlocking in SPSP are the P-P, P-T and L-T types. Therefore, SPSP foundation has some typical characteristics as follows:

1) It is suitable to foundation system in areas with adverse conditions such as in deep waters and/or soft soil, especially in region of strong strength earthquake and liquefaction phenomenon.

2) The position of the SPSP component above the ground level is used as a temporary cofferdam for drying up the excavation area. The method using steel pipe piles as a temporary cofferdam, putting up the pile to water elevation, filling material to prevent water into interlocking. After installing the footing and pier, the cofferdam will be

Fig.2.2 Installment stage of SPSP foundation of Nhat Tan Bridge in Viet Nam (from http://www.antarakoh.com.sg/contact-us.php)

temporarily cut and pull up. Foundation of this type can take advantages of cofferdam foundation, so it has some advantages over the short construction time.

3) The bearing capacity is very high to construct near existing structures or work as a retaining wall.

4) It has a high resistance against earthquakes and liquefaction.

The **Fig.2.2** shows the installment stage of SPSP foundation of Nhat Tan Brigde project in Viet Nam

2.2.3 Design method

After 1995 Kobe Earthquake in Japan, the design codes for highway and railway bridges were revised to meet the needs of much higher strength and reliability levels for structures. The specification JRA 2002 (Japan Road Association, 2002), consists of a Seismic Design (Part IV) and a Substructure (part V) Design, is used for design of SPSP foundation. Seismic design of SPSP foundation is divided into two steps: Firstly, the design of SPSP foundation is calculated under ordinary, storm and Level 1 earthquake conditions to verify the vertical ground capacity, displacement, stress of each member. Secondly, the verification of foundation strength that is considered the liquefaction of ground under level 2 earthquake will be carried out. **Fig.2.3** shows the design and calculation procedure of SPSP foundation. Therefore, verification of liquefaction is one of the most important steps in the seismic design work of SPSP foundation.

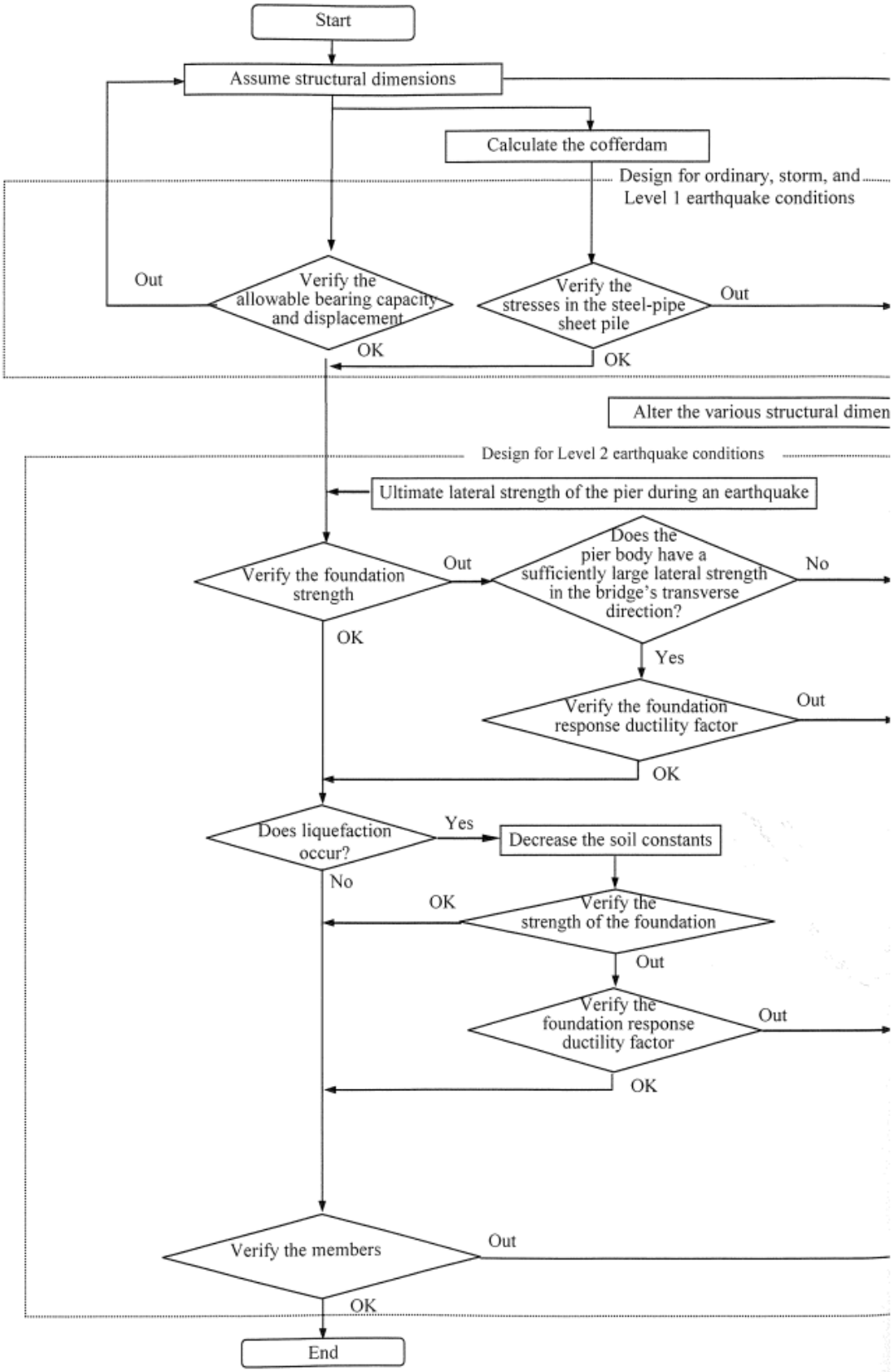

Fig.2.3 Design and calculation flow of Steel Pipe Sheet Pile Foundation

There are three adopted design approaches stipulated in the part IV Substructure Design of specification JRA 2002 as follows:

1) The finite length beam on elastic foundation.

This is a simple model considering the composite efficiency (μ:=0.75). The SPSP foundation is modeled as a beam on the elastic ground. The stiffness of the beam is calculated by the entire rigidity of SPSP foundation with an effect of composite joint between two piles. The elastic springs are determined by soil properties surrounding the foundation. The model is shown in **Fig.2.4**.

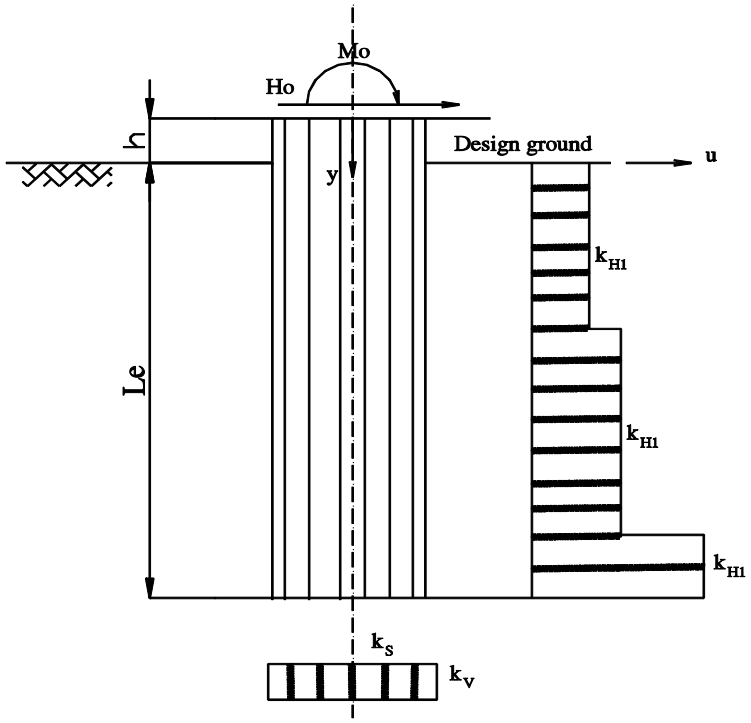

Fig.2.4 The finite length beam on elastic foundation

2) The imaginary well considering the shear slippage.

The well body was treated as a beam free of shear deformation. On the other hand, this analysis method is based on a beam theory that considers shear deformation. That is, an imaginary well is assumed by tying up steel pipe sheet piles at their central axes, as shown in **Fig.2.5.** Assuming that the central axis of each steel pipe sheet pile is fixed to the central plane of the imaginary well wall, establish the following assumptions in order to render the well into one dimension as a beam theory: the imaginary well based on a beam theory that considers shear displacement; each individual steel pipe sheet pile based on a beam theory that neglects shear displacement.

3) Three dimension model of SPSP foundation

3D numerical model of foundation is shown in **Fig.2.6**. The foundation of steel pipe pile is considered as a three dimension frame model. The steel pipe pile is modeled as a frame, the footing as a solid element; interlocking as elastic spring, the joints between steel pipe pile and soil as a spring. The input forces of the model are a moment, a vertical reaction and a displacement or stress of each steel pipe pile. The important basis of modeling the foundation is a model of connection between steel pipe pile and ground and a model of connection of steel pipe piles together. Therefore, it must consider ground reactions in three directions and reactions of interlocking in three directions carefully due to a difference between the piles.

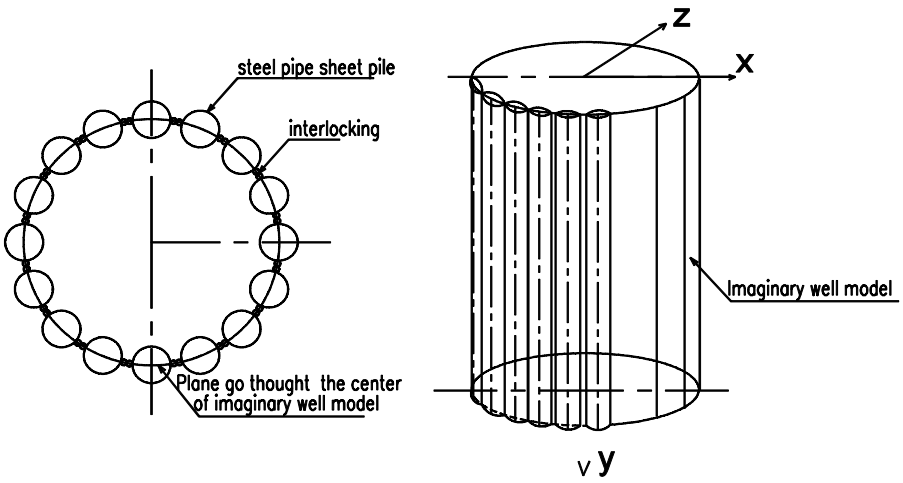

Fig.2.5 Imaginary well model of SPSP foundation

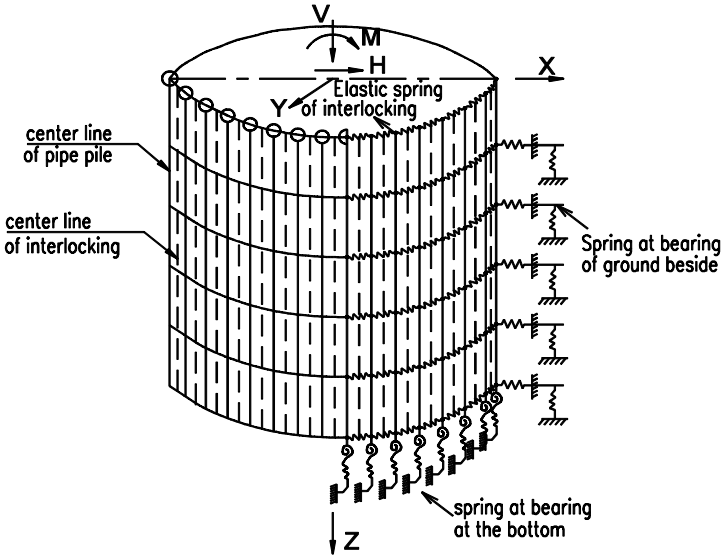

Fig.2.6 Three dimension model of cofferdam foundation

2.2.4 Verification of seismic behavior of SPSP foundation based on the design models in JRA 2002

Trung, N.T and Kiyomiya, O. et al. (2012, 2013) investigated the 2D nonlinear behavior of SPSP foundation under 1995 Kobe earthquake, 2011 Tohoku Pacific Coast. The proposed pier foundation system using SPSP had a RC column with height of 13 m and a sectional dimension of 2.5 m x 7.5 m. The SPSP foundation has a circular shape in plan with an outside diameter of 12.145m and a steel pipe has a diameter of 1.0 m and a thickness of 0.012 m, as shown in **Fig.2.7**. Both the finite length beam on elastic foundation and imaginary well stipulated in the specification JRA 2002 were applied in these researches. The interaction between soil, foundation and structure was considered by the SSI model (Soil-Structure-Interaction) and SFSI model (Soil-Foundation-Structure-Interaction). The soil - structure interactions were considered as springs whose stiffness was also determined from the stiffness of soil and foundation according to JRA-2002

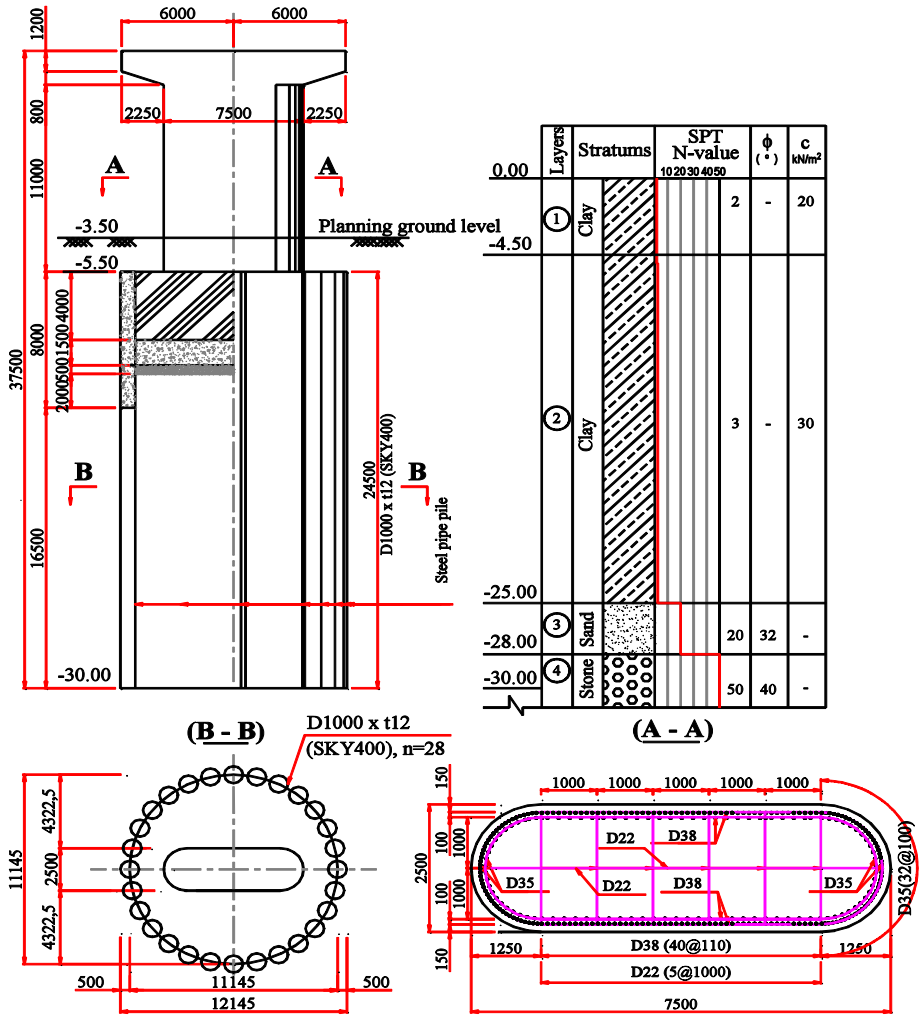

Fig.2.7 Prototype bridge pier with Steel Pipe Sheet Pile, foundation and soil properties

2.2.4.1 Calculation models

The analysis was carried out on three models in this work. The pier column was modeled as beam elements. As to Model 1, the SPSP foundation was modeled as concentrated springs, while the SPSP was modeled as beam elements and the soil was modeled as soil springs for Model 2 and Model 3. The stiffness of the soil springs was determined from the stiffness of the soil and SPSP according to Highway Bridge Design Specifications 2002 (JRA-2002).

(a) *Concentrated spring model (SSI, model 1)*: as shown in **Fig.2.8**, the SPSP foundation was modeled as three concentrated springs K_v, K_h and K_r in the horizontal, vertical and rotational direction, respectively. The pier column and top slab was supported by these three springs whose stiffness was calculated as follows:

$$K = F\delta^{-1} \tag{2.1}$$

Where, K: the stiffness matrix of springs; δ: the displacement matrix at the bottom of footing. The stiffness of soil surrounding the footing was modeled in the horizontal, K_{fh}, and in the vertical, K_{fv}.

(b) *One column with soil spring model (SFSI, model 2)*: as shown in **Fig.2.9**, the SPSP foundation was modeled as one column supported by soil springs that represented the function of the soil, and the pier column and top slab were supported by this column. The foundation column was divided into 15 segments in its axial direction. The flexural rigidity of this beam was derived by:

$$E_S I_Z = E_S\left(\sum_{i=1}^{n1+n2} I_{0i} + \mu\sum_{i=1}^{n1+n2} A_{0i}x_i^2\right) \tag{2.2}$$

Where, I_Z: second moment of area of steel pipe sheet pile foundation (m^4); E_S : Young's modulus of steel pipe pile foundation (kN/m^2); A_{0i}: net cross-sectional area of i^{th} steel pipe body (m^2); I_{0i}: second moment of area of i^{th} steel pipe sheet pile and inner single pile (m^4);μ: composite efficiency (=0.75); x_i: the distance from centroid of i^{th} steel pipe sheet pile and inner single pile to neutral axis in horizontal section of foundation (m); n_1: number of steel pipe sheet piles at periphery of well part (pile); n_2: number of steel pipe sheet piles in bulkhead. The surrounding soil was represented by 15 couple of concentrated springs: K_{ih} in horizontal direction and K_{iv} in vertical direction (i: i^{th} soil layer) were derived by:

$$K_{ih} = Dl_r k_{hi} \tag{2.3}$$

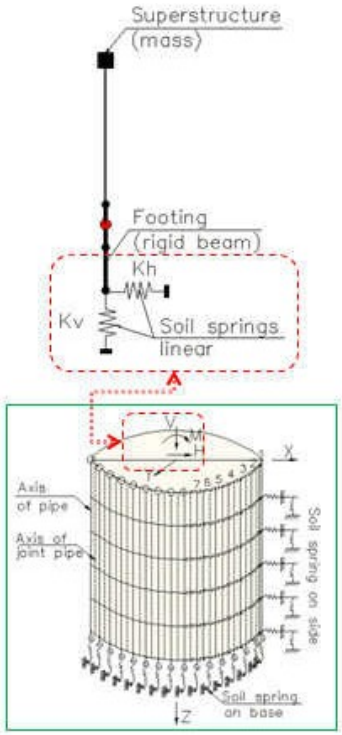

Fig.2.8 A column model with concentrated spring (SSI model)

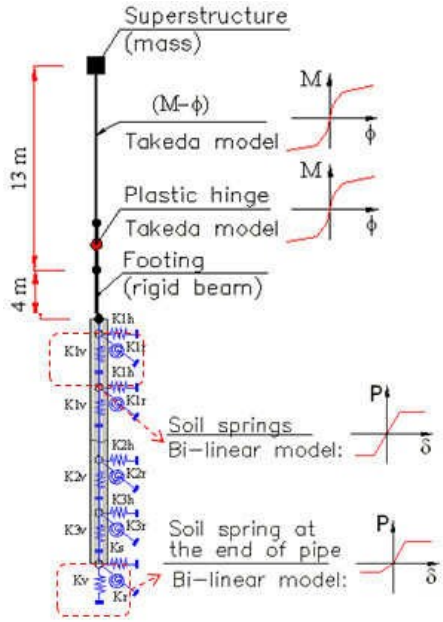

Fig.2.9 2D frame model with soil springs (SFSI model)

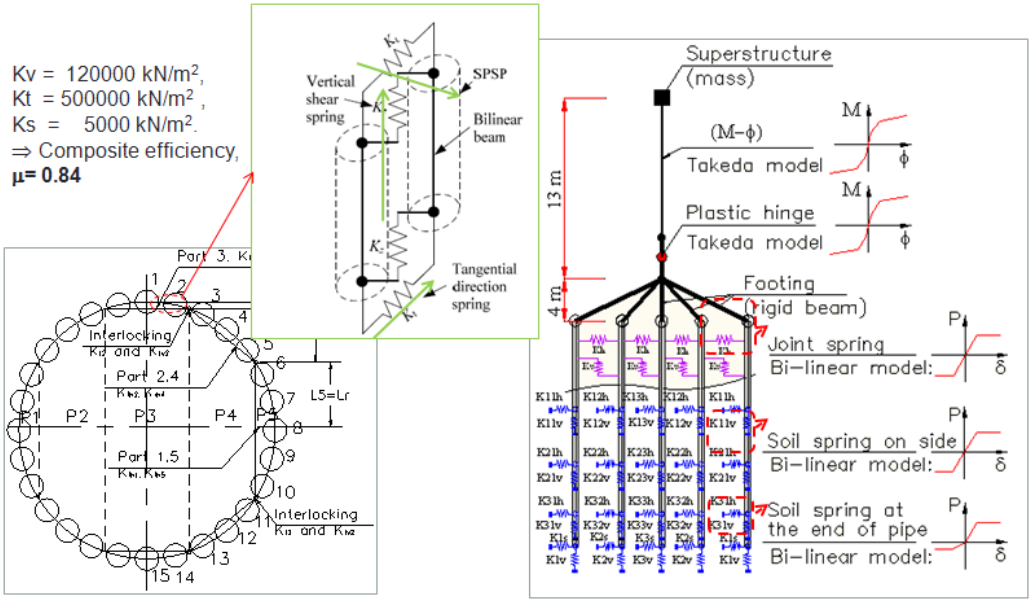

Fig.2.10 A column model with soil springs (SFSI model)

$$K_{iv} = Dl_r k_{vi} \tag{2.4}$$

Where, D: the outside diameter of foundation (m), l_r: the length of r^{th} segment (m), k_{hi}: the coefficient of reaction of i^{th} soil layer in the horizontal and vertical direction (kN/m^3). Theywere determined following JRA-2002.

(c) *2D frame with soil spring model (SFSI, model 3)*: as shown in **Fig.2.10**, the SPSP was divided into five parts with equal width in horizontal direction in plan, and each part was represented by a beam at its center. Each beam was supported by 15 couple of concentrated soil springs (K_{ihj}, K_{ivj}) (i: the i^{th} soil layer, j: the j^{th} beam, $j \in \{1,5\}$) whose stiffness were derived by:

$$K_{ihi} = L_i l_r k_{hi} \tag{2.5}$$

$$K_{ivi} = L_i l_r k_{vi} \tag{2.6}$$

Where, L_j: the length of the j^{th} part (m); l_r: the length of the r^{th} segment (m); k_{hi}, k_{vi}: the cofficients of reaction of the i^{th} soil layer in the horizontal and vertical direction determined in JRA-2002 (kN/m^3). Adjacent beams were jointed with each other by 15 couple of concentrated springs, (K_{lhi}, K_{lvi})(i:1,2) which have the stiffness were determined from the relationship between the shear capacity and the displacement of site experiment. The stiffness of spring K_{lvi} is a compressive modulus in longitude direction of pile. Regard to the stiffness of spring K_{lhi} in the horizontal direction was derived by:

$$K_{lhi} = L_i(K_c cos\theta_j + K_s sin\theta_j) \tag{2.7}$$

Where, L_j: the length of the j^{th} part (m); K_c: compressive modulus of j^{th} interlocking part (kN/m^2); K_s: shear modulus of stiffness of j^{th} interlocking part (kN/m^2); θ_j: the angle between the horizontal axis and tangent axis at the point of j^{th} interlocking part (rad).

2.2.4.2 Methodology

The hysteretic behavior of plastic hinge of the pier column was considered by Takeda model. The soil springs and interlocking springs were considered by bilinear model for nonlinear models. The upper limits of interlocking springs were calculated according to compression, tension and shear tests of interlocking. To verify the effects of the nonlinear properties of the structure on the vibration behavior and seismic performance of the substructure, the analysis was carried out on six cases (as shown in Table 1). Case 1a, case 2a and case 3a were conducted by Jma Kobe wave (IK) and other cases including case 1b, 2b and 3c were inputted by Tsukidate wave. The ground resistance was bilinear for all cases and the nonlinearity of interlocking behavior between two pipes was also considered by bilinear model for case 3a and 3b. As to case 2a, case 2b, the efficiency coefficient μ of interlocking was 0.75. The coefficient for case 3a, case 3b determined by the nonlinear static analysis on Model 3 was 0.84. These cases are shown in **Table 2.1**

Table 2.1 Analytical cases

No	Analytical cases	Model	Ground property	Interlocking property	Input type
1	Case 1a	Model 1	Bilinear	-	IK
2	Case 1b		Bilinear	-	IT
3	Case 2a	Model 2	Bilinear	-	IK
4	Case 2b		Bilinear	-	IT
5	Case 3a	Model 3	Bilinear	Bilinear	IK
6	Case 3b		Bilinear	Bilinear	IT

Note:

1. IK: Jma Kobe 1995 input ground motion
2. IT: Tsukidate 2011 input ground motion

Table 2.2 Results of Eigen - value Analysis

Mode No	Model	Frequency (Hz)	Period (s)	Mode damping (%)	Mass ratio (%)
First mode	Model 1	2.10	0.476	8.30	42
	Model 2	2.06	0.485	6.42	64
	Model 3	2.17	0.461	5.40	53
Second mode	Model 1	6.69	0.149	12.61	45
	Model 2	7.97	0.125	10.44	34
	Model 3	5.01	0.200	10.23	41

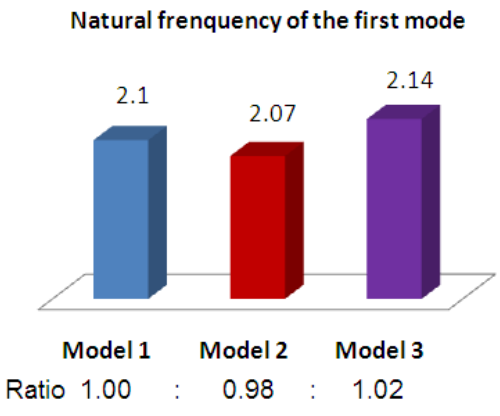

Fig.2.11 Comparison of the first natural frequency between three models

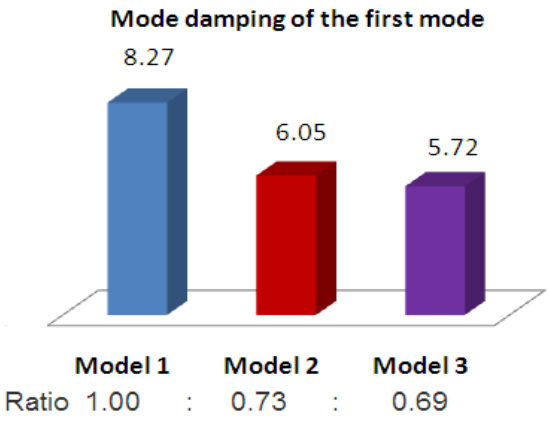

Fig.2.12 Comparison of the first mode damping between three models

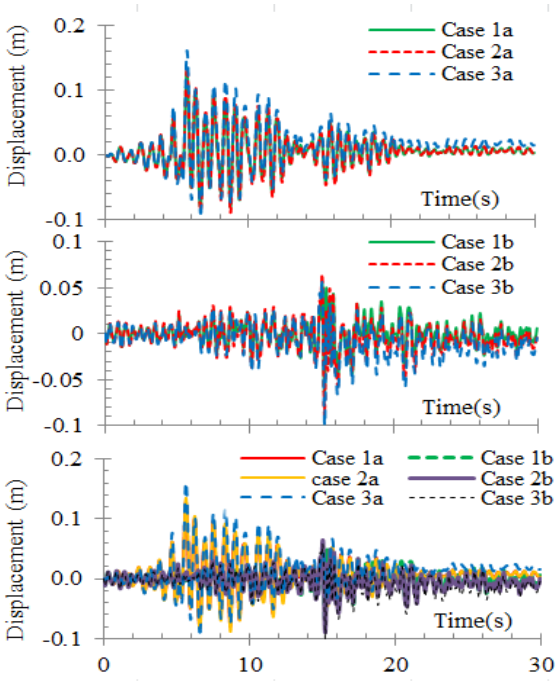

Fig.2.13 Displacement response at top of pier

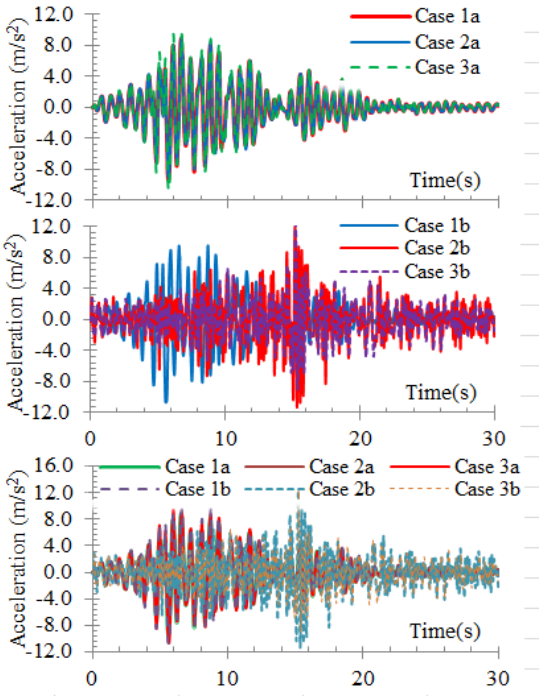

Fig.2.14 Acceleration response at top of pier

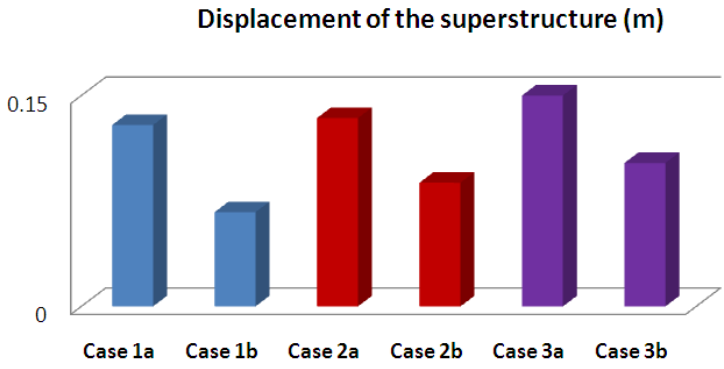

Fig.2.15 Comparison the maximum displacements between three models

2.2.4.3 Eigen analysis

The fundamental frequencies and mode damping of three models are shown in the **Table 2.2**. The comparison of the first frequency and mode damping between them are presented in Figs. 2.1 and 2.2, respectively.

The natural frequency ratio of Model 1, Model 2 and Model 3 was 1.00:0.98:1.03 respectively. The natural frequency of Model 2 was smallest. Because flexural rigidity of SPSP foundation was calculated by using composite efficiency of 0.75, while the equivalent composite efficiency calculated by Model 3 was 0.84. It means that the shear

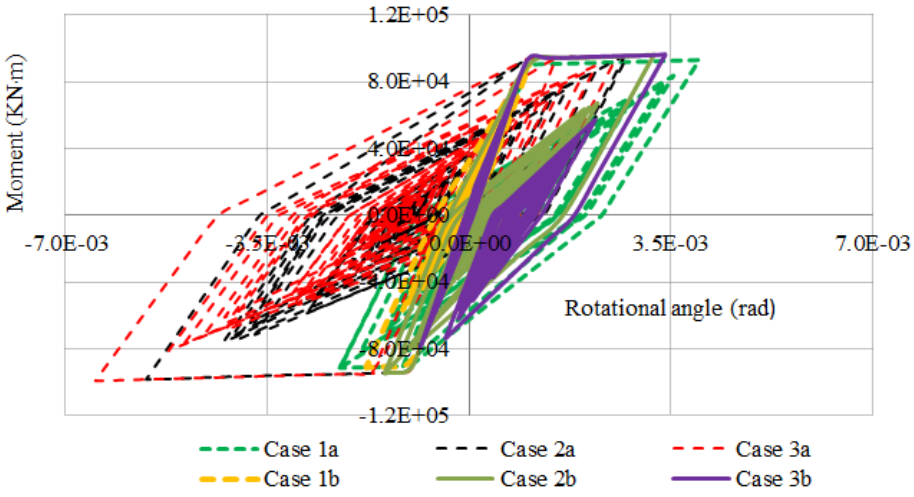

Fig.2.16 Displacement response at the top of pier in three models

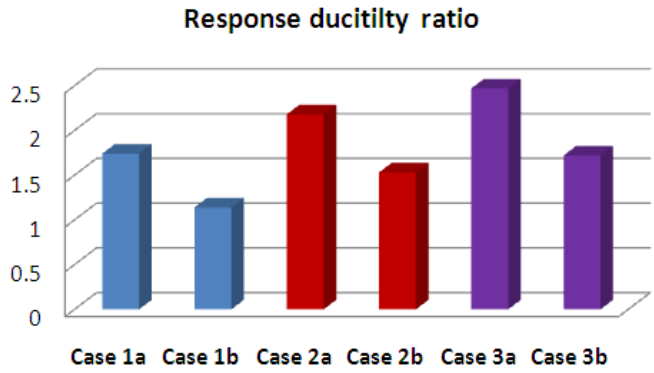

Fig.2.17 Comparison of ductility ratio between three models

stiffness of interlocking between two pipes effected to fundamental frequencies of bridge substructure system and the larger the stiffness is, the lower the natural frequency is.

Regard as mode damping, Model 3 was the smallest and the ratio with Model 1, Model 2 was 1.00:1.54:1.18 for mode 1 and 1.00:1.23:1.02 for mode 2. It was thought that the damping ratio 0.03 of SPSP foundation in Model 2 and Model 3 makes a decrease of damping ratios of entire structure.

2.2.4.4 Seismic responses

The time histories of horizontal displacement and acceleration of three models are shown in **Figs.2.12** and **2.13**, respectively. As to case 1a, case 2a and case 3a, the ratio of the maximum displacement and that of the maximum acceleration were 1.00:1.04:1.25 and 1.00:1.12:1.14, respectively. For case 1b, case 2b and case 3c, the ratios were 1.00:1.31:1.52 of displacement and 1.00:1.12:1.19 of acceleration. As the results, the

maximum displacement and maximum acceleration at the top of pier of model 3 were largest among three models. Especially, the displacement of all cases caused by IT wave was less than that of cases by IK wave approximately 0.52-0.66 times, the difference is quite great. Comparing with the cases by IK wave, the difference of acceleration between them was 1.13-1.18 times, the difference is not so much significant. The comparison of displacement between them is shown in **Fig.2.15**. Therefore, vibration behavior of SPSP foundation through SSI model and SFSI model with the Tsukidate wave gave the smaller displacement and the larger acceleration of superstructure.

The seismic performance of the structure was verified based on dynamic response of the pier column. The hysteresis loops of the bending moment against the rotational angle of the plastic hinge are shown in **Fig.2.16**

The maximum rotational angles of the case 1a, case 2a and case 3a were 4.34 mrad, 5.64 mrad and 6.51 mrad respectively, the ratio among them was 1.00:1.30:1.50 respectively. The rotational angles of case 1b, case 2b and case 3b were respectively 1.87 mrad, 2.63 mrad and 3.43 mrad and their ratio was 1.00:1.09:1.63 respectively. As to group of (case 1a; case 1b), (case 2a; 2b) and (case 3a; 3b), the ratios of ductility were (1.00:0.52), (1.00:0.47) and (1.00:0.53), respectively. Based on the above ratios, the maximum rotational angle of Model 1 was minimal and that of Model 3 was maximum. And the rotational angle under IK input ground motion was larger than that under IT input ground motion approximately 2 times. As to the ratio of ductility, among case 1a, case 2a and case 3a was 1.00:1.25:1.42. For case 1b, case 2b and case 3b, the ratio was 1.00:1.34:1.51. As to group of (case 1a; case 1b), (case 2a; 2b) and (case 3a; 3b), the ratios of ductility were (1.00:0.66), (1.00:0.70) and (1.00:0.70), respectively.

The above ratios showed that the ductility ratio of model 1 (SSI) was minimum and that of Model 3(SFSI) was maximum. The ductility ratio of all cases of Mode1, Model 2 and Model 3 under IT input ground motion was less than that under IK input ground motion. The comparison of ductility ratio between three models is shown in **Fig.2.17**.

2.2.4.5 Conclusions

The vibration behavior and seismic performance of Steel Pipe Sheet Pile foundation were verified on three models using both SSI model and SFSI model by nonlinear dynamic analysis method in this study.

Regarding the characteristic of substructure using SPSP foundation in this study, SFSI model gave the larger displacement and ductility ratio than that of SSI model under large scale earthquakes. Moreover, the mode damping in the SFSI models was larger than that in the SSI model. The 2D imaginary well model (SFSI, model 3) in the specification approach can perform the dynamic behavior of SPSP foundation during strong earthquake. On the other hand, the verification of liquefaction is recommended in the specification for the design work of SPSP foundation, as shown in **Fig.2.3** Therefore, this study is one of basic foundations to produce the proposal model in verifying the dynamic behavior of SPSP foundation during liquefaction and/or lateral ground movement.

2.3 Adopted researches

The captured results of past researches using numerical methods or experiments are summarized as follows:

2.3.1 Effect of liquefied thickness

Some researchers have conducted on the effects of the thickness of the liquefied layer on the behavior of surface ground and structure. The effects have been observed in vibration test (Yasuda et al. 1992a; Tokida et al. 1993 and O'Rourke and Pease et al. 1997). As the thickness of the liquefied layer increases, a greater buildup of pore water may occur, as shown in **Fig.2.18**. The drainage path for excess pore pressures of the thickness of the liquefied layer is large. It causes portions of a thicker liquefied layer will keep liquefied for a longer time period and then causes greater surface displacements.

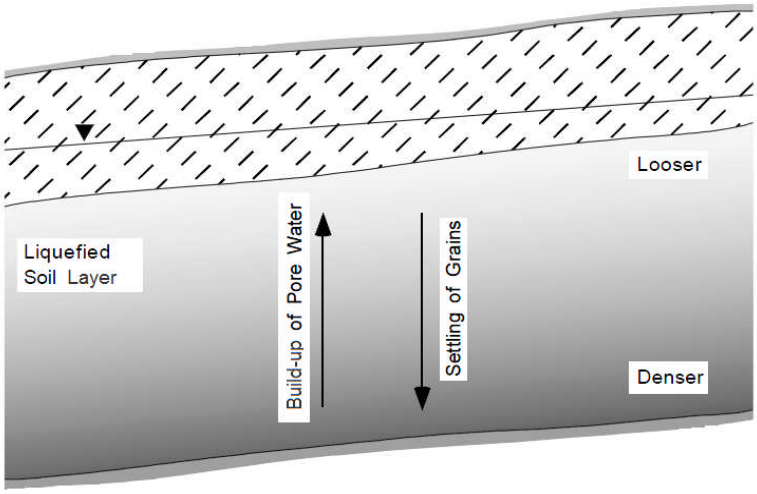

Fig.2.18 Effect of liquefied thickness on the surface displacement due to the build-up of pore water pressure.

2.3.2 Effect of drainage

Liquefaction is generally considered to result from the generation of excess pore pressures in the un-drained conditions. However, the pore water drainage always occurs in nature, the generation and dissipation of pore water in partially drained conditions may have a significant effect on the magnitude of ground movement. Stark and Mesri et al. (1992) note that the excess pore pressures in the drained condition can give an increase in shear resistance. It means that this can contribute to smaller slope movements.

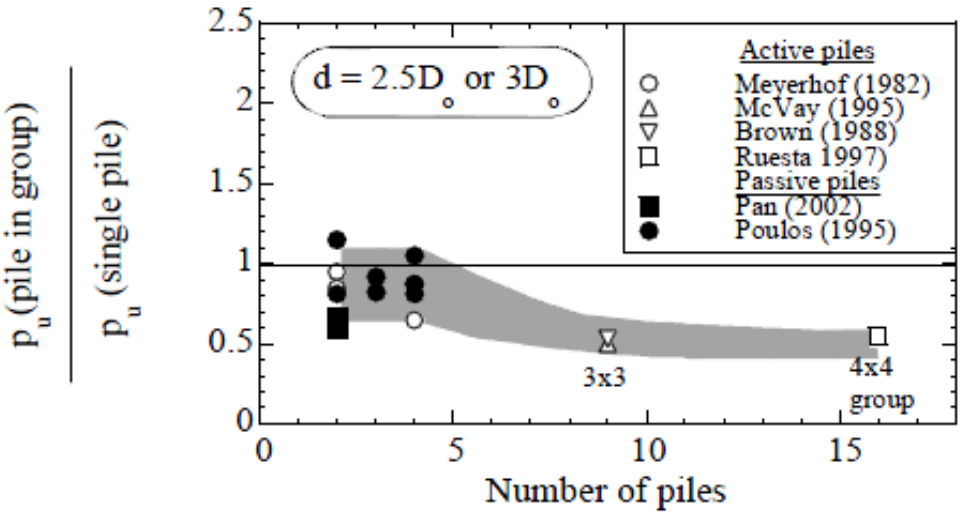

Fig.2.19 Reduction of lateral pressure depends on the number of piles

2.3.3 Effect of inertial and kinematic force

Tokimatsu and Suzuki et al. (2004) presented the effects of inertial and kinematic forces on pile stresses during earthquakes based on large shaking table tests. The research results show that if the natural frequency of the superstructure is larger than that of the ground, the inertial force is in phase with the kinematic force. Inversely, if the natural frequency of the structure is less than that of the ground, the inertial force is out of phase with the kinematic force.

2.3.4 Effect of pile group

The effects of pile groups on the behavior of piles in liquefaction soils were investigated in recent years. These researches focused on the effect of the interaction between the piles within the ground and the influences of magnitude and distribution of lateral ground displacements, stiffness characteristics of soil. **Fig.2.19** presents the effect of number of pile group on the reduction of lateral pressure. The more piles are in the group, the smaller

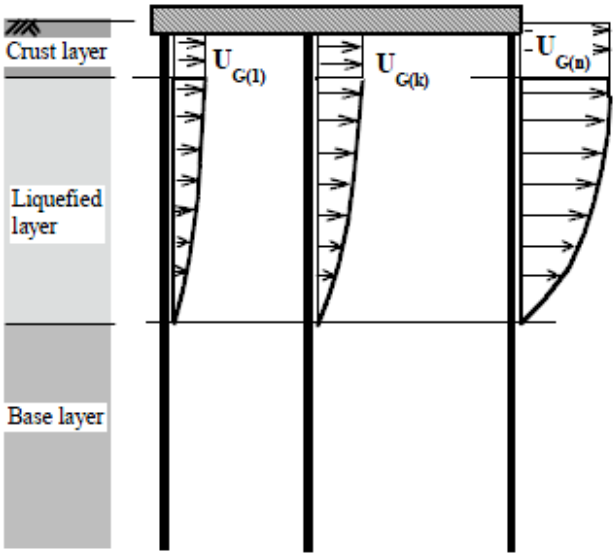

Fig.2.20 Different lateral pressure on the piles in the group

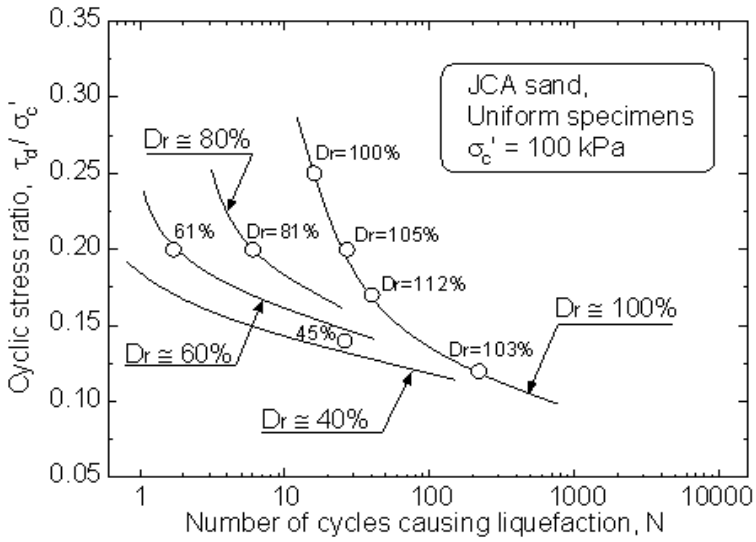

Fig.2.21 The effect of JCA sand on the liquefaction strength (M. Yoshimine at al. 2005)

lateral soil pressure is on the each pile. Cubrinovski and Ishihara et al. (2005) investigated the pile-group effects can be captured by a simple method of analysis using a single pile model.

Under the lateral movement of ground, all piles have almost the same horizontal displacements at the pile cap because they are rigid at the pile cap. However, each of the piles will be attacked by a different lateral pressure from liquefaction layer. This may depend on its position in the group and the distribution of the lateral pressure, as shown in **Fig.2.20** presents a distribution of lateral pressure on group piles.

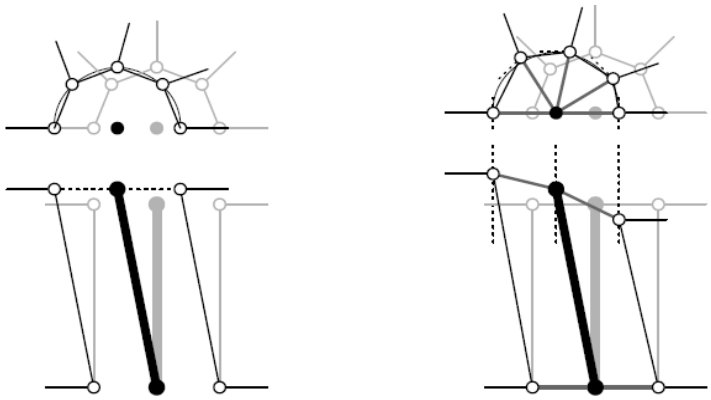

Pile without slippage

(a) For rough pile.

Pile with slippage

(b) For smooth pile.

Fig.2.22 Displacements of nodes of solid elements for soil adjacent to beam element for piles

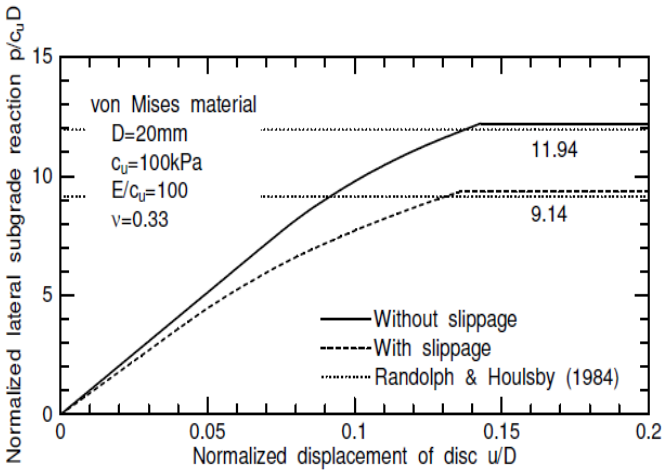

Figure 6.5: Normalized load–displacement relations of disc in von Mises material.

Fig.2.23 Lateral reaction and displacement relationship of pile with and without slippage

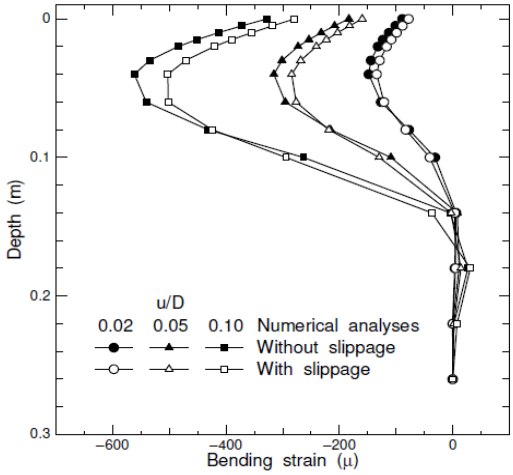

(b) Comparison between the pile with and without slippage.

Fig.2.24 Bending strain of pile with and without slippage

2.3.5 Effect of relative density

The liquefaction resistance, the cyclic shear modulus and build-up of pore water pressure of cohesion soil are influenced by the relative density. Toyota and Towhata et al. (1994) conducted on model tests to investigate the effect relative density of soil on displacement. Bartlett and Youd et al. (1992, 1995) showed the correlation between soil density and the lateral spreading displacements during liquefaction. M. Yoshimine and R. Koike et al. (2005) presented the effect of relative density on the liquefaction characteristics by un-drained tri-axial compression tests and cyclic tri-axial loading tests. The result is shown in the **Fig.2.21**.

2.3.6 Effect of soil-pile interaction

Takahashi Akihiro et al. (2002) researched the effect of soil-pile interaction on behavior of pile by both numerical method and experiment during liquefaction-induced lateral spreading. The pile models with and without the slippage were conducted to model for a smooth and rough pile surfaces, respectively, as shown in **Fig.2.22**. The research result showed that the lateral subgrade reaction and bending strain response of pile with slippage were larger than that of pile without slippage, as shown in **Figs.2.23** and **2.24**, respectively.

2.3.7 Summaries

In summary, the liquefaction researches almost all performed the behavior of soil-foundation system during earthquake. They are very useful for directing and improving the next researches. The result of above researches will be used for verifications in this study.

2.4 Dynamic Analysis

2.4.1 Introduction

There are two kinds of analysis generally used for modeling the soil elements in the FEM program. The first is a total stress analysis and this is a simple calculation in the practical engineering approach. The second is an effective stress analysis that details more parameters of soil and is more completed to perform the behavior of soil-structure system during liquefaction.

2.4.2 Total stress analysis

The total stress analysis is also used for the evaluation of foundation structure and embankments. The total stress analysis usually is used in the un-drained condition. The actual analysis is performed for rapid loading or unloading conditions often encountered during the construction phase or at the end of construction period. The analysis considers a change of shear stress that occurs quickly enough that soil does not have time to re-setup. Therefore, the total stress analysis is often applied to a short-term time. The total stress analysis uses the total unit weight of the soil, and the location of the groundwater is not considered in the analysis. The dash line in **Fig.2.25** shows the nonlinear relationship between the total shear stress and strain using Ramberg-Osgood model in the analysis

2.4.3 Effective stress analysis

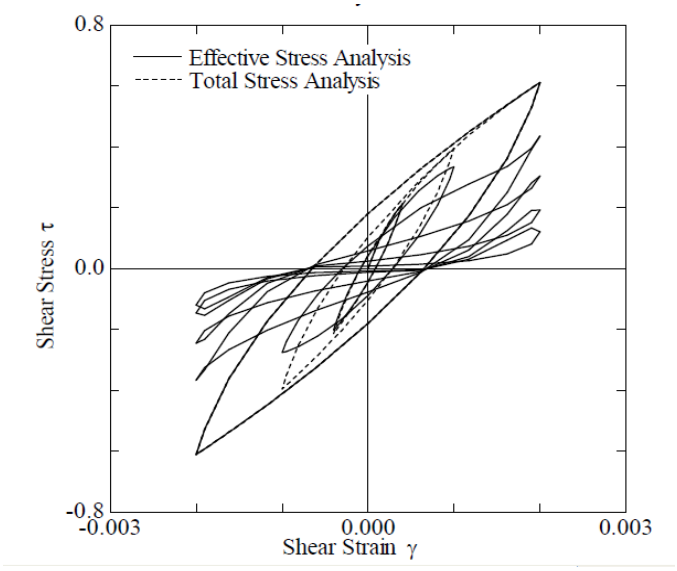

Fig.2.26 Shear stress and strain relationship of total and effective stress analysis

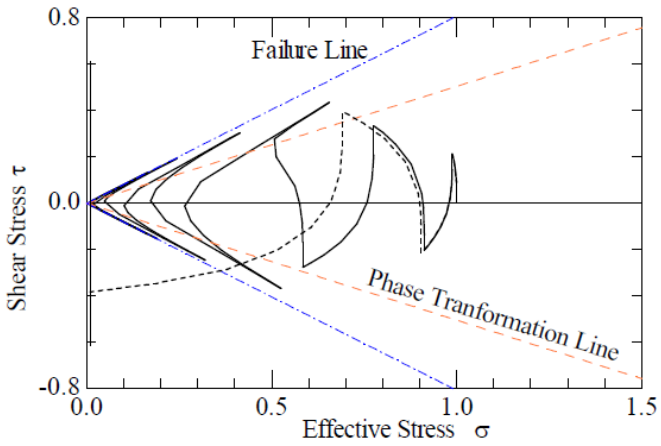

Fig.2.26 Shear stress and mean effective stress relationship in the effective stress analysis

Effective stress analysis is used in the long-term analysis and considers effects of pore water pressure immigration in the ground. The difference between the total and effective stress analysis is a dilatancy behavior of soil elements. The continuous line in **Fig.2.25** shows the nonlinear relationship between stress and strain during liquefaction with a reduction of shear modulus or soil strength. The shear stress reduces when soil is liquefied, while strain of soil is almost constant. The **Fig.2.26** presents the relationship between shear stress and effective stress during liquefaction. The cyclic behavior in this figure expresses that the effective stress of soil decreases due to the increase of pore water pressure, the shear stress increases. While, when effective stress increases due to the decrease of pore water pressure the shear stress still increases. The cyclic line will approach to transformation line and the failure line of Mohr-Coulomb step by step.

As a result, the effective stress analysis is more advantageous than the total stress analysis in a consideration of the development of pore water pressure of soil with a reduction of soil strength or shear modulus.

2.4 Conclusions

This Chapter reviewed the characteristics of SPSP foundation, its calculation models in JRA 2002 and the effect of liquefaction parameters of adopted researches. There are some findings as follows:

(1) The SPSP foundation is a special and complicated structure located in poor sites such as soft surface soil and/or water depth. Its calculation models and liquefaction verification are detail stipulated in the specification. The review work is very necessary in building and determining the characteristics of the analysis models and conditions for both the vibration test and numerical methods in the next researches.

(2) The 2D imagery well model (SFSI) stipulated in the specification JRA 2002 well performed the seismic behavior of SPSP foundation during strong earthquakes but the liquefaction condition was not considered in this calculation. However, with the accepted good advantages this SFSI model will be chosen to perform the dynamic behavior of the SPSP foundation in the slope ground during liquefaction in the next step.

References

1) JRA (2002): Specifications for highway bridges. Japan Road Association, Preliminary English Version, *Public Works Research Institute (PWRI) and Civil Engineering Research Laboratory (CRL)*, Japan.
2) Uchida, A., and Tokimatsu, K. (2006): Comparison of current Japanese design specifications for pile foundations in liquefiable and laterally spreading ground. *ASCE Geotechnical Special Publication* 145, pp. 61-70.
3) Kimura, M., Too, A.J.K., Inazumi, S., Isobe, K. and Nishiyama, Y. (2004): Innovative development of steel pipe sheet pile joint, *Proceedings of the Third Civil Engineering Conference in the Asian Region*, pp.373-377.
4) Inazumi, S., Kimura, M., Too, A.J.K., Nishiyama, Y. and Kamon, M. (2004): Permeability of H-H joint in H-jointed steel pipe sheet piles at coastal landfill site, *Proceedings of Fifteenth Southeast Asian Geotechnical Conference*, pp.635-640.
5) Isobe, K., Kimura, M., Yoshizawa, Y., Kohono, K., Harata, N. and Makino, T. (2005). Evaluation of effect of strengthening existing caisson foundation against earthquake by steel pipe sheet piles using 3D elasto-plastic FEM analysis, *Proc.11th Int. Conf. of IACMAG* , No.2, pp.459-466.
6) Isobe, K. and Kimura, M. (2004). Centrifugal model tests on effect of steel pipe sheet pile reinforcement on existing caisson foundation, *The Seventeenth KKCNN Symposium on Civil Engineering*, pp.463-468.
7) Cubrinovski, M., and Ishihara, K. (2006): Assessment of pile group response to lateral spreading by single pile analysis. *ASCE Geotechnical Special Publication 145*, pp. 242-254.
8) Boulanger, R. W., Wilson, D. W., Kutter, B. L., Brandenberg, S. J., and Chang, D. (2004): Nonlinear FE analyses of soil-pile interaction in liquefying sand. *ASCE Geotechnical Special Publication 126*, pp. 403-410.
9) Trung, N.T. Kiyomiya, O. An, T.X. (3/2012): Response analysis of steel sheet pipe pile foundation by three simple types of models. *Proceedings of the 39th Annual Conference of JSCE*, Yokohama, Japan, Kanto Branch, I-3-P-401.
10) Trung, N.T. Kiyomiya, O. An, T.X. (7/2012): Comparison of three seismic analysis models of Steel sheet pile bridge foundation. *Proceedings of the 15th Symposium on Performance-based Seismic Design Method for Bridges of JSCE*, Tokyo, Japan, P.137-142.
11) Trung, N.T. Kiyomiya, O. An, T.X. (9/2012): Dynamic response analysis of steel sheet pipe pile foundation conducted on three simple models. *Proceedings of the 14th International summer Symposium of JSCE*, Nagoya, Japan, CS4-0019.

12) An, T.X. Kiyomiya, O. Trung, N.T. (9/2013): Impact on the Seismic Performance of Steel Pipe Sheet Pile Foundation by the Joint Mechanical Properties. *Proceedings of the 36th of IABSE Symposium in Long Span Bridge and Roofs-Development, Design and Implementation,* Kolkata, India.

This page intentionally left blank

Chapter 3

Vibration Experiment on SPSP Foundation

3.1 Introduction

The vibration experiment using a shaking table is one of the most advanced approaches of investigating the behavior of soil-foundation system during liquefaction. Up to now, the researchers have conducted a series of large shaking table tests to investigate the behavior of foundation during liquefaction. The effects of surface, bottom slope, thickness of liquefiable layers, relative density, etc. summarized in the chapter 2 were studied carefully and detail. The shaking table test was conducted in this study to perform the dynamic behavior of SPSP foundation during liquefaction. It was designed for a test model of soil-pier foundation of a cable stayed bridge on both the flat and slope ground. They were denoted a flat model and a slope model, respectively. This experiment would produce their dynamic responses during shaking and especially investigated them during liquefaction phenomenon. Furthermore, the difference of the responses between two models also evaluated to express the effect of ground slope on the behavior of SPSP foundation, as described in the following sections. This experiment was conducted using the 1-G shaking table facility of the Penta-Ocean Construction Corporation in Japan. The steel rigid container of shaking table test with 1.5 m in height, 4.0 m in width, and a depth of 2.5 m was installed on the underwater shaking table, as shown in **Fig.3.1**.

3.2 Prototype

The prototype of test model in shaking table test is a tower foundation system of cable stayed bridge. The tower with a high of 95.5 m supported by the SPSP foundation on the ground was modeled in the shaking table test by using the similarity law. The SPSP foundation has 165 steel pipe piles and dimensions of 36.456 m in length and 29.469 m in width. Each steel pipe pile has a diameter of 150 cm and a thickness of 2.5 cm. The outline of the tower and SPSP foundation is shown in **Fig.3.2**.

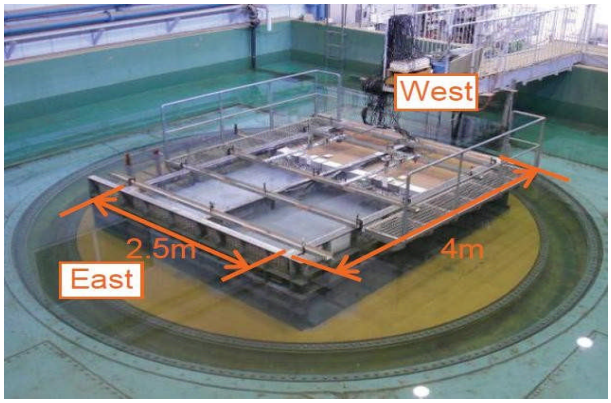

Fig.3.1 Overview of shaking table test 1-G

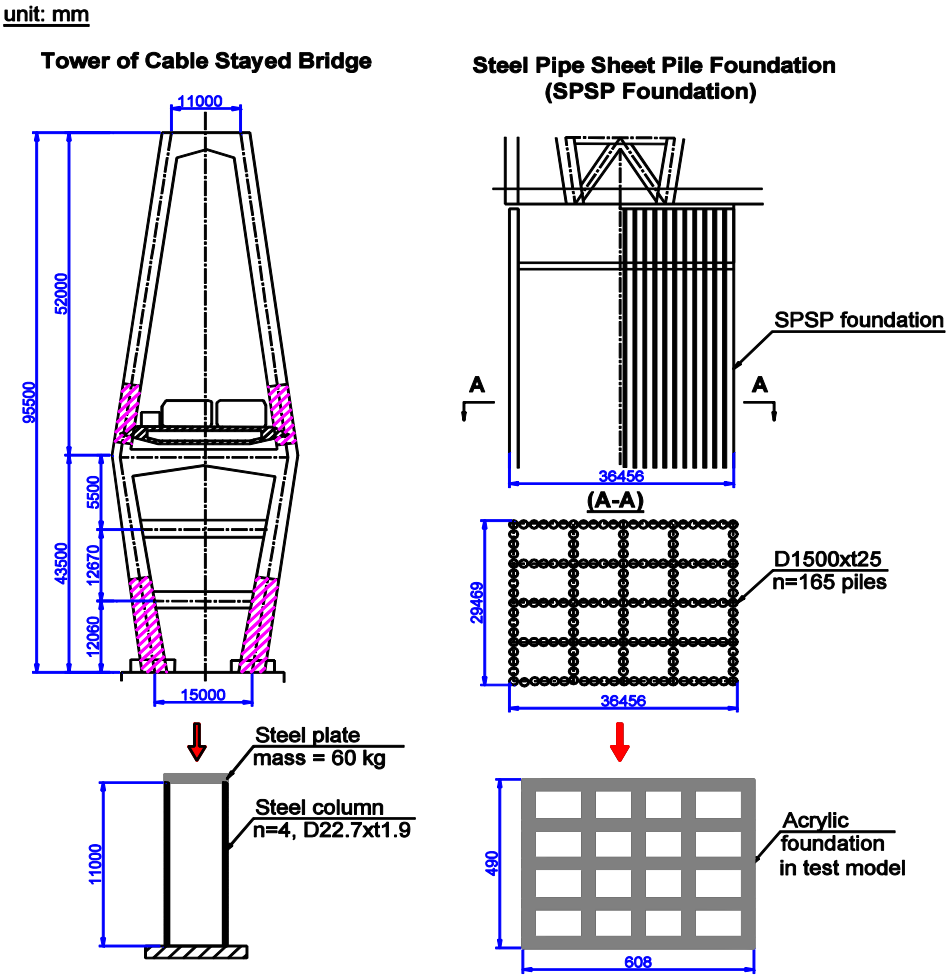

Fig.3.2 Cable stayed bridge prototype

To simplify the structure for constructing the physical model, the superstructure-tower system of the prototype was modeled as a single-degree-of-freedom (SDOF) system. The mass of the system, including the mass of the superstructure and tower at the top of the column, and the natural frequency of the system were calculated as suggested by Yoneda et al. (1990) as follows:

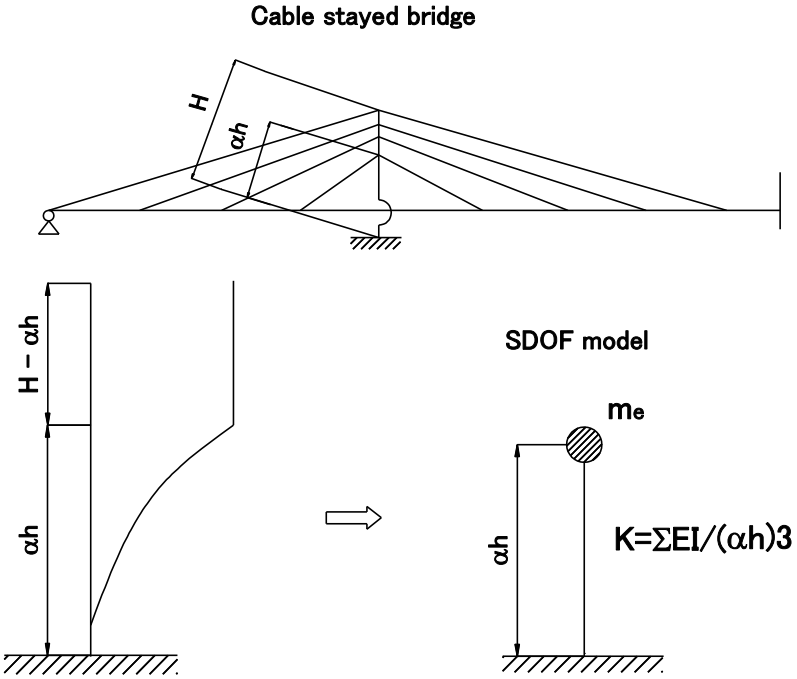

Fig.3.3 SDOF model of superstructure tower system of a cable stayed bridge (Yoneda et al. 2009)

$$f_L = \frac{1}{2\pi}\sqrt{\frac{\sum_0^i 3EI/(\alpha h)^3}{m_e}} \tag{3.1}$$

Where m_e: is the mass of the superstructure; h is the height from the bottom of the pier to the position of the lowest cable; α: is a factor that depends on the ratio of stiffness between the tower and girder and depends on the parameter P_{TG} is determined by **Eq. 3.2**; and I: is the area moment of inertia of the tower.

$$P_{TG} = \frac{\sum_1^i (\frac{EI}{H})_{TOWER}}{\sum_1^i (\frac{EI}{L_c})_{GIRDER}} \tag{3.2}$$

Where $(EI/H)_{TOWER}$: is a rigidity of tower and $(EI/L_c)_{GIRDER}$: is a rigidity of girder; H : is a total height of tower.

3.3 Test set up

3.3.1 Similarity law

The similarity law is derived for shaking table test on soil-structure –fluid system in 1 G gravitational field. These scaling factors were established based on the typical characteristics of soil-structure structure such as soil, fluid elements, immigration of pore

Table 3.1 Scaling factors of shaking table test

Parameter	λ = prototype /model	Scale
Length	λ	60
Density	1	1
Time	$\lambda^{0.75}$	21.56
Stress	λ	60
Pore water pressure	λ	60
Displacement	$\lambda^{1.5}$	464.76
Acceleration	1	1
Strain	$\lambda^{0.5}$	7.75
Water permeability coefficient	$\lambda^{0.75}$	21.56
Bending stiffness	$\lambda^{4.5}$	100,387,728

Table 3.2 Material and buildup method of component of test model

Item	Material	Standard	Quality	Method
Foundation	Steel	B490×L608mm	1	Shop fabrication
Sand filling	No. 6 silica sand	Dr=80%	$0.7m^3$	Air dropping method
Superstructure	Weight steel		1	Shop fabrication
Liquefaction layer	No. 6 silica sand	Dr=50%	$21m^3$	Air dropping method
Non-liquefaction layer	No. 6 silica sand	Dr=80%		
Surface	No. 7 crushed stone		$0.7m^3$	Air dropping method

water pressure and type of structure. Moreover, the influence of constitutive law of soil was also considered as a stress-strain relationship, a confining pressure. All material properties of the physical model and ground were scaled using a similitude law suggested by Iai et al. (1988). In this experiment, the fundamental scaling factor, λ =1/60. **Table 3.1** shows the scaling factors of parameters such as length, time, acceleration, density, pore water pressure, bending stiffness, etc.

3.3.2 Test model

The material and buildup method of component of test models in the vibration test is shown in **Table 3.2.** Firstly, the foundation structure was firstly manufactured in the laboratory and then it was installed with the superstructure in the site. The liquefaction, non-liquefaction layers and ground surface were made by air dropping method using silica sand No.6.

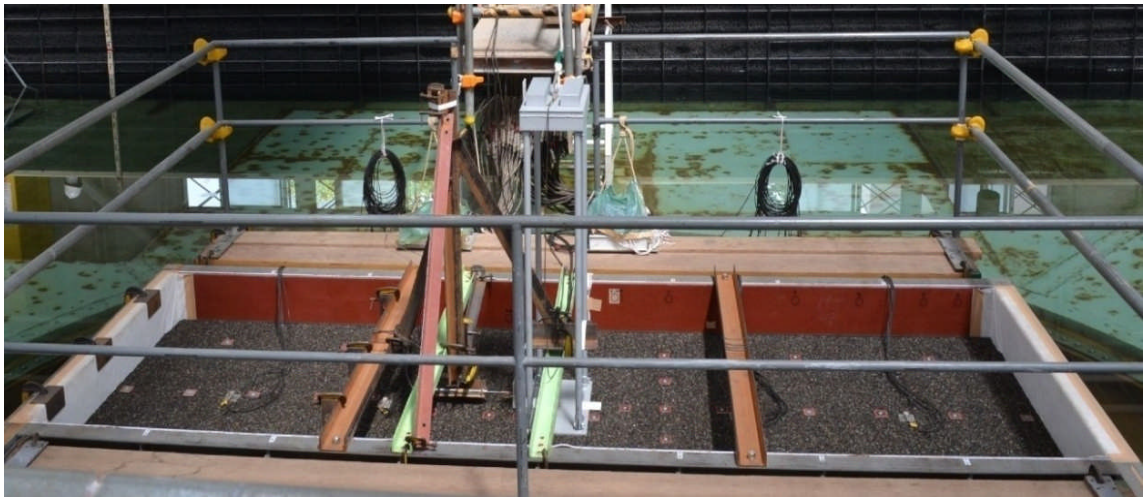

Fig.3.4 1-G shaking table test on the flat model

Fig.3.4 shows a set-up of the flat model on the shaking table. The test model includes the pier, superstructure, and foundation in the sand ground. The natural frequency of the pier-superstructure system of the model was determined by dynamic characteristics of the single-degree-of-freedom system of the prototype using a scale of 1:60. The pier in the model consists of four steel columns that are rigidly fixed together by a steel plate at the top with a mass of 60 kg. Each column has dimensions of 1.1 m in height and a cross section in a tubular shape of 2.27 cm in diameter and 0.19 cm in thickness. The foundation is a caisson made of acrylic materials with a dimension of 49 cm in width, 60.8 cm in length, and 83.4 cm in height. The cap at the top of the foundation is an acrylic plate that is 60.8 cm long, 49 cm wide and 9.8 cm thick. The footing of the pier is constructed of steel with dimensions of 26.6 cm in length, 46.6 cm in width, and 18.5 cm in thickness. The test model in the shaking table test is shown in **Fig.3.4**.

3.3.3 Material properties of ground

Soil properties of liquefaction and non –liquefaction layers are shown in the **Table 3.3**. The ground in the models consists of a 48.8 cm liquefiable sand layer with a relative density of 50% using Yamagata-sand No. 6 (D50 = 0.3 mm) overlying a 74.3 cm non-liquefiable layer with a relative density of 90%. The soil layers of the model ground were constructed using a sand drop method. The sand was gradually dropped into the vessel up to the water level step. However, the relative density of the non-liquefiable layer was controlled by the amount of tamping and the measured weight of the sand layer. The thickness of the sand layer for each tamping period was 10 cm. The rubble layer consists of Grade 6 crushed stone with a particle size of 13-20 mm.

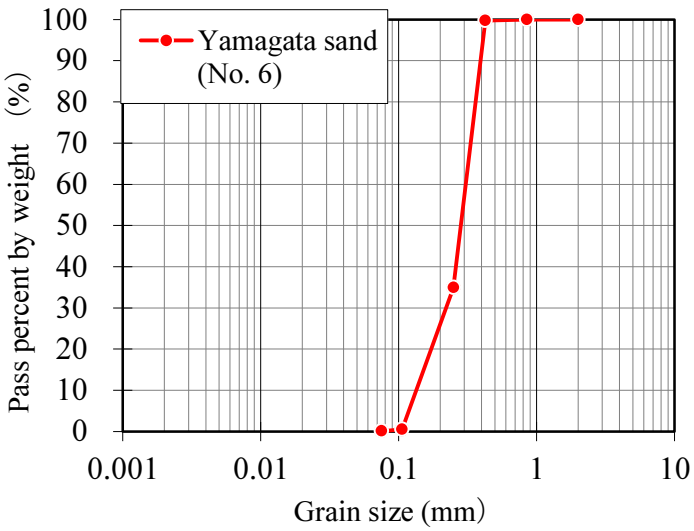

Fig.3.5 Grain size distribution of Yamagata sand

The grain size distribution of the Yamagata sand used for the ground is provided in **Fig.3.5**. It is seen that the grain size of Yamagata sand was dominant at the size less than 0.25 mmm. The slope of the ground in the case of the slope model was 15° in the longitudinal direction. The maximum shear modulus (G_o) of the sand layer was calculated using the following equation:

$$G_o = \rho v_s^2 \tag{3.3}$$

Where G_o is the initial shear modulus, ρ is the mass density of sand and v_s is the shear wave velocity of the soil layer.

A pulse method was used to determine the shear velocity of the sand. An impulsive sin wave (amplitude: 100 Gal, period: 0.0176 s) was inputted at the bottom of the shaking table by the electrohydraulic vibration machine The acceleration responses at two locations, one at the top of the soil layer and another at the bottom of the layer, were recorded in time-history waves to capture the difference of the peak time between the two locations. The method is shown in the **Fig.36**. Then, the shear wave velocity (v_S) was calculated by the following equation:

$$v_s = \frac{H}{\Delta T} \tag{3.4}$$

Where v_S is a shear wave velocity; H is the height of the soil layer or distance between the two locations and ΔT: is the difference of the peak time between the two locations

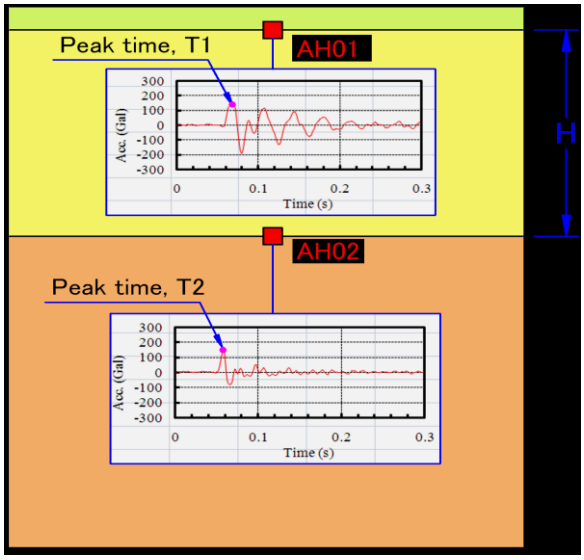

Fig.3.6 A pulse method

Table 3.3 List of soil parameters.

Parameter		Symbol	Liquefaction layer	Non-Liquefaction layer	Rubble layer
Parameters for deformation characteristics	Wet unit weight	ρ (t/m^3)	1.96	2.05	1.37
	Initial shear modulus	G_{ma} (kPa)	3,866	21,788	2,993
	Initial bulk modulus	K_{ma}(kPa)	10,083	56,819	7,805
	Confining pressure	σ_{ma}'(kPa)	2.27	6.85	0.28
	Poisson's ratio	ν	0.33	0.33	0.33
	Internal friction angle	ϕ_f(degree)	36.55	42.80	41.60
	Hysteretic damping ratio	h_{max}	0.24	0.24	0.24

3.3.4 Instrument and deployment

The **Fig.3.7** shows the arrangement of accelerometers and acrylic foundation of test model in the soil layers before vibration test. The instruments and their placement are shown in **Figs.3.8** and **3.9,** respectively. The accelerometers and pore water pressure transducers were arranged in the near- and far-field areas of the ground at various depths of the liquefaction and non-liquefaction layers. The accelerometers were attached at the top and bottom of the pier. Two horizontal laser displacement transducers were installed at the top and bottom of the pier, and two vertical displacement transducers were installed at the bottom of the pier. The strain gauges were installed on opposite sides of the foundation at different depths. The small, circular targets were embedded in the ground surface to record their movements before and after shaking.

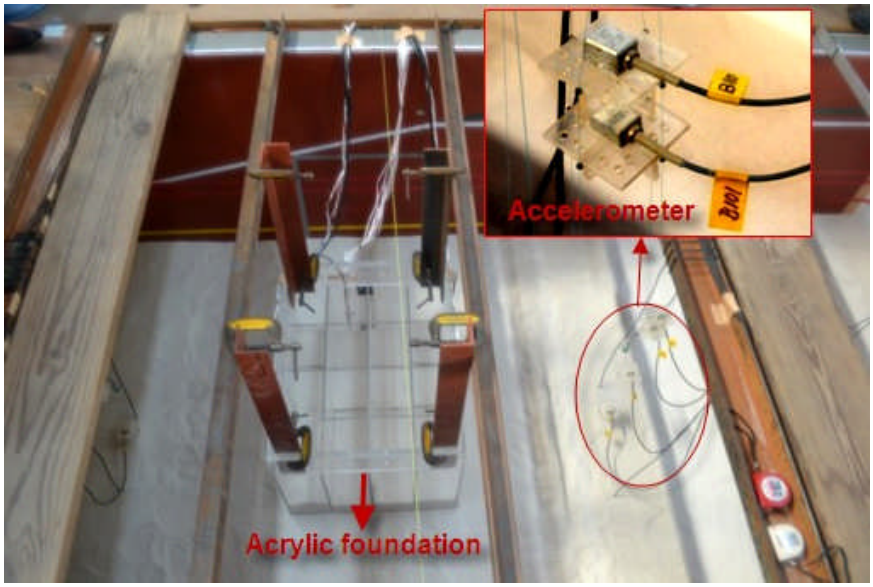

Fig.3.7 Acrylic foundation and accelerometers arrangement in the ground

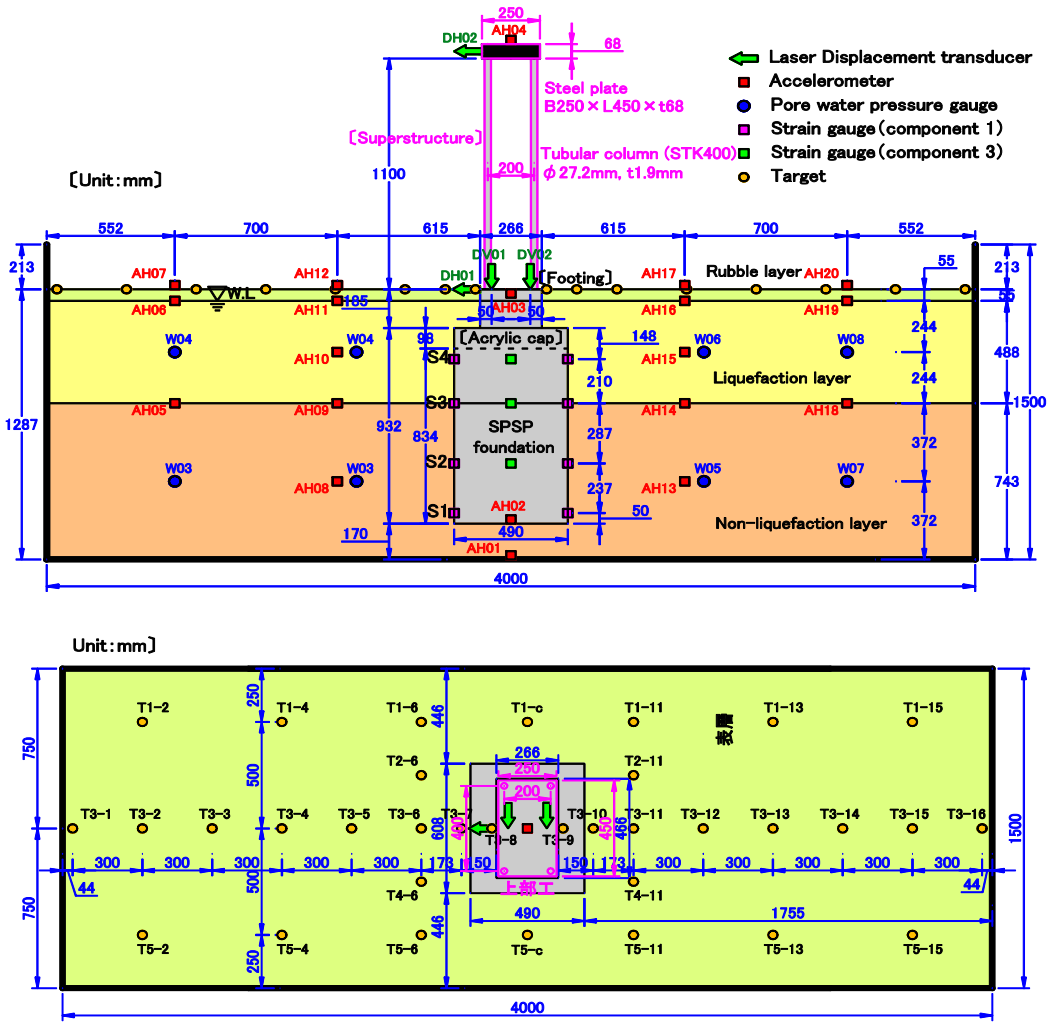

Fig.3.8 General view of the flat model and transducers arrangement.

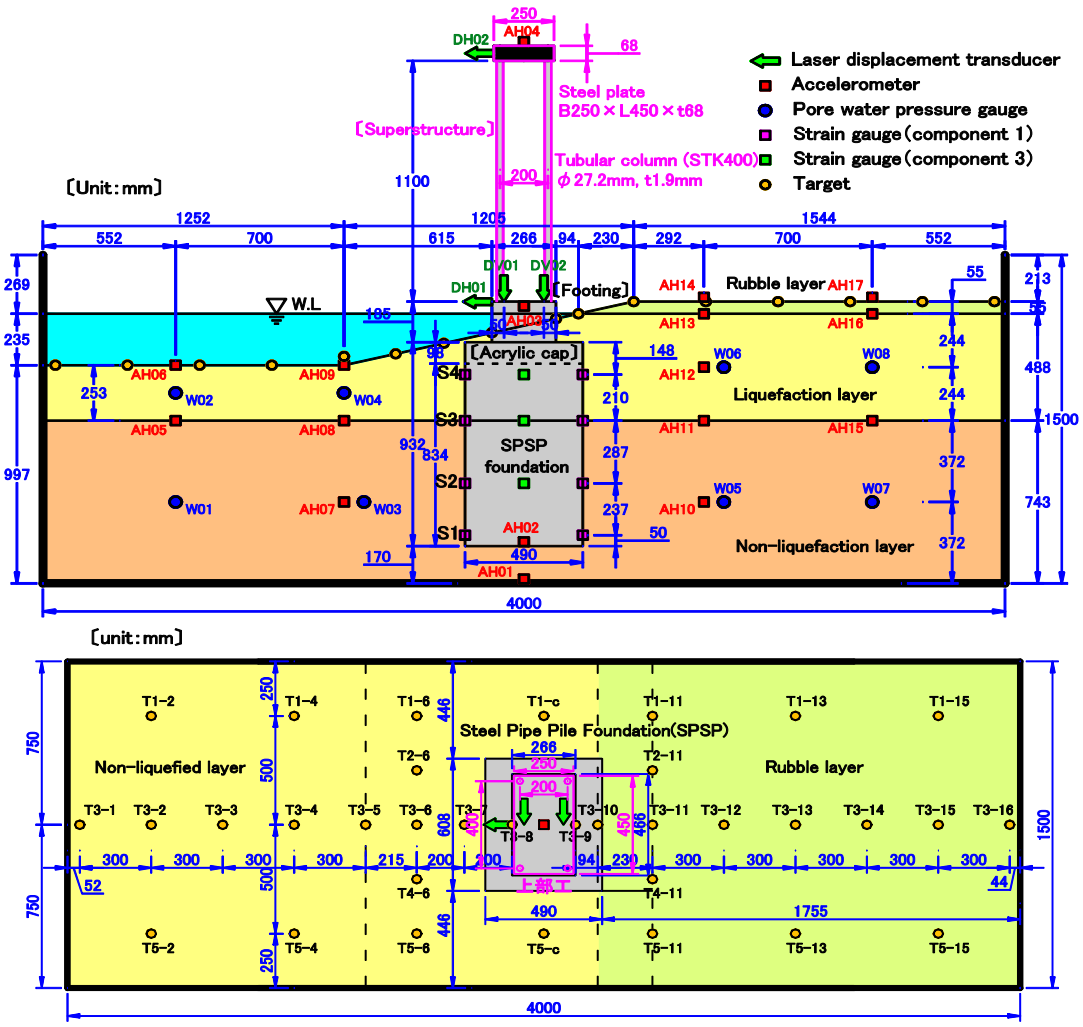

Fig.3.9 General view of the slope model and transducers arrangement.

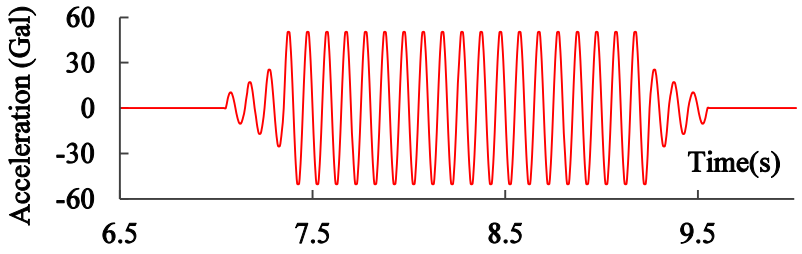

Fig.3.10 Acceleration wave input of 50 Gal at the base.

3.3.5 Base excitation

The models were shaken with a base harmonic acceleration at a constant frequency of 10 Hz. The duration time was 2 s. The amplitude increased incrementally from 50 to 300 Gal, and one of the input stages is shown in **Fig.3.10.** The frequency and wave numbers of input ground motion was selected in the consideration of the sub-duction zone earthquakes (level 2 earthquake motion) and the similarity law.

3.4 Behavior of Ground

3.4.1. Excess pore water pressure of ground

The time histories of the EPWP at various depths in both liquefaction layer and non-liquefaction layer for cases 100, 200 and 300 Gal input ground motion are shown in **Figs.3.11** and **3.12** for both the flat and slope models, respectively.

The time history records of pore water pressure are divided into the following main stages:

1) Stage 1 (from 7 s to 7.5 s).

The stage took place very quickly around 0.5 s. In the stage, there was a generation of pore water pressure and the maximum horizontal acceleration at time of 7.5 s. However, the rise of EPWP ratio only increased to values from 20% to 30 % after the maximum acceleration approached a peak.

2) Stage 2 (from 7.5 s to 10 s).

The pore water pressure keeps generation to the peak at 10 s, the recorded acceleration had decreased amplitude. EPWP ratio was observed in the stage.

3) Stage 3 (from 10 s to 13.5 s).

In this stage, there was a dissipation of pore water pressure. The starting time was at around 10 s and gradually decreased.

Fig.3.11 shows that the pore water pressure at W2, W4, W6 and W8 of ground in the liquefied layer of the flat model almost increased according to the increase of the input acceleration amplitude from 100 to 300 Gal. However, at W4 point the EWP of 100 Gal was largest among other input cases. It may be because the sand at the point was much looser than other cases of higher input ground motions. Regarding to the base layer, EPWP ratio at W3 from 100 to 300 Gal was very small. It means that liquefaction phenomenon did not occur in this layer. The different of EPWP between W2 and W8 was not significant and the generation of W8 was little faster than that of W2, so PWP distribution was quite symmetric in the flat model. EPWP at W2, W4, W6 and W8 of ground in the slope model are shown in **Fig.3.12**. Similar to the flat model, an increase of pore water pressure was accordance with input ground motion. In the ground of the waterfront, the EPWP ratio at W4 of the near field was larger than that in W2 of the far field and the generation of pore

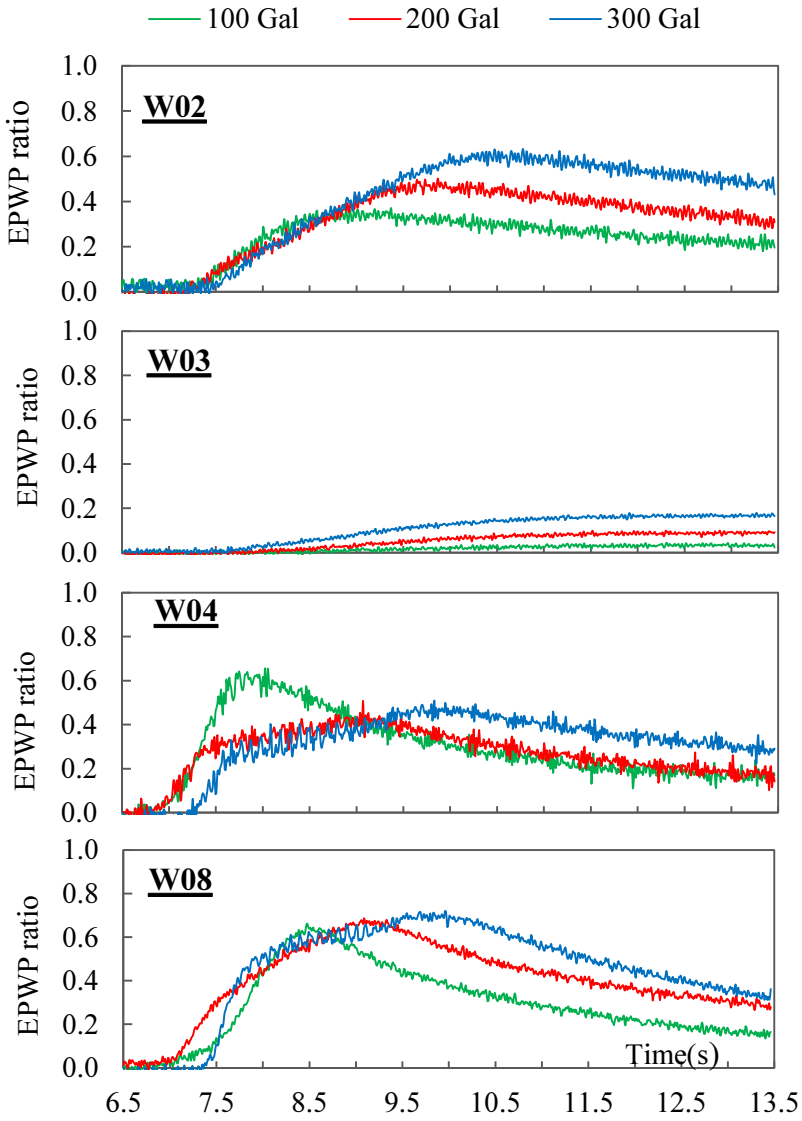

Fig.3.11 Time histories of pore water pressure in the flat model from 100 to 300 Gal

water at W4 also faster than that of W2. The increase of pore water also did not appear in the base layer in the slope model.

The comparisons of maximum EPWP ratio from 50 to 300 Gal between two models are shown in **Fig.3.13**. It is seen that in the liquefaction layer the EPWP ratio at W4 of near field in the slope model was almost larger than that in the flat model, while the ratio at W8 of far field was less than that in flat model during shaking from 50 to 300 Gal.

The liquefaction time in the 300 Gal case occurred quite quickly during shaking of 2 s. It means that the sand was not kept liquefied in a long time. This is because the time for drainage was reduced by a factor of 60^2.

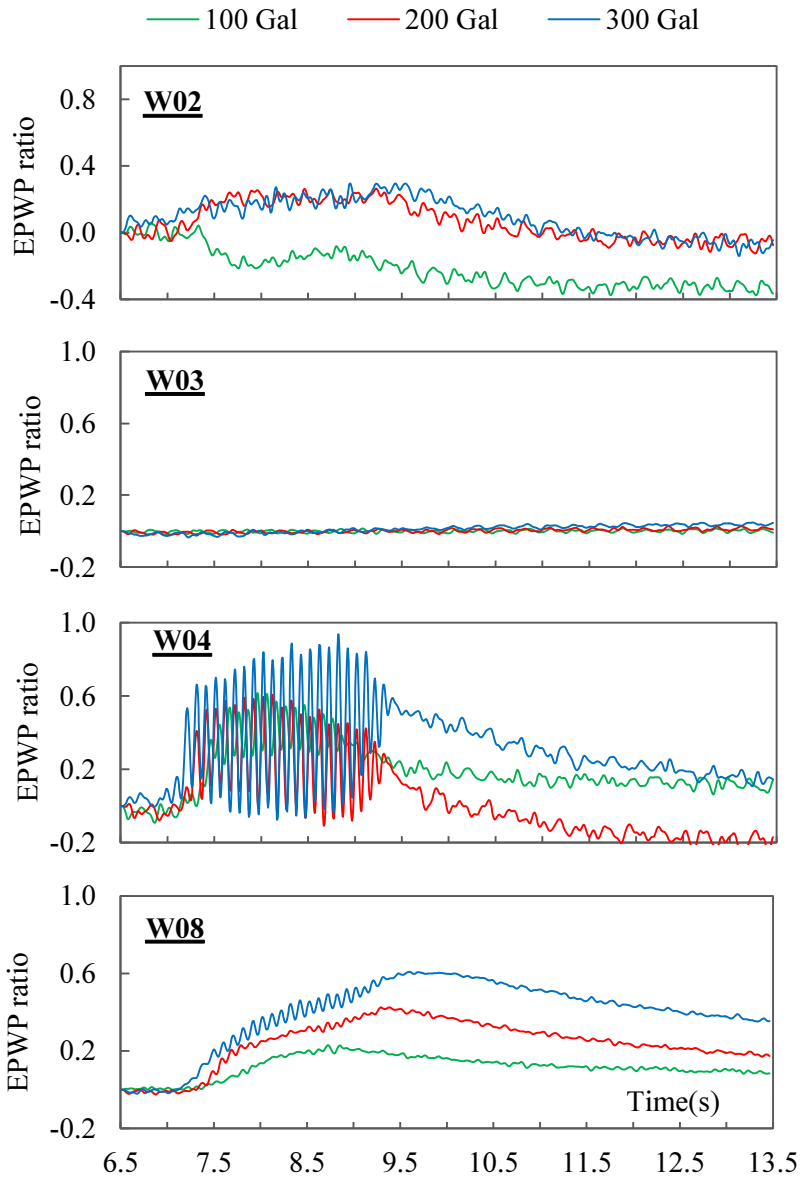

Fig.3.12 Time histories of pore water pressure in the slope model from 100 to 300 Gal

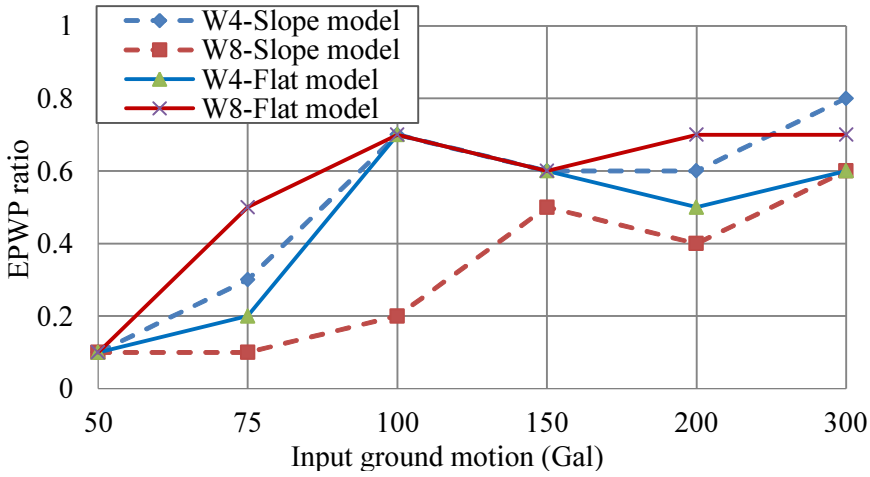

Fig.3.13 Comparison of EPWP ratio between models from 50 to 300 Gal

There are some conclusions as follows:

1) The increase of pore water pressure in two models is accordance with the increase of input ground motion

2) When liquefaction occurred in the slope model the value of pore water pressure ratio in the near field was higher than that in the flat model, while the smaller values was observed in the far field.

3) The development of pore water pressure including the water generation and dissipation in the lower ground of slope model was more complex than in the flat model, as displayed in records of W2 and W4 in both models. There was an appearance of cyclic component in the recorded time histories. This might be because the instability of slope ground due to soil liquefaction.

3.4.2 Acceleration of ground

Fig.3.14 presents the time histories of the horizontal accelerations in the ground in the flat model from 100 to 300 Gal. The records of the acceleration observed from accelerometers in the vibration test show that the increase of acceleration was in accordance with an increase of input ground motion from 100 to 300 Gal.

The acceleration amplitude gradually decreased from the bottom of shaking tank to the ground surface as displayed in records at AH8, AH10 and AH19. The acceleration records at AH10, AH15 of the near field and AH10, AH19 of the far field indicate that distribution of acceleration in the flat model was quite symmetric and the difference of acceleration amplitude between the points at near field and far field was not much significant.

The all records in the liquefaction layer shows that during liquefaction the acceleration amplitude gradually decreased but disappeared in the non-liquefaction layer, and during shaking of 100 and 200 Gal the acceleration amplitude almost did not decrease. The declination time of acceleration in the records in the liquefaction layers was approximately 2s that ranges from 8 s to 10s. It means that the liquefaction phenomenon gave a declination of horizontal acceleration. This is because when ground was liquefied the shear modulus or soil strength increased. These are suitable to adopted theories of liquefaction.

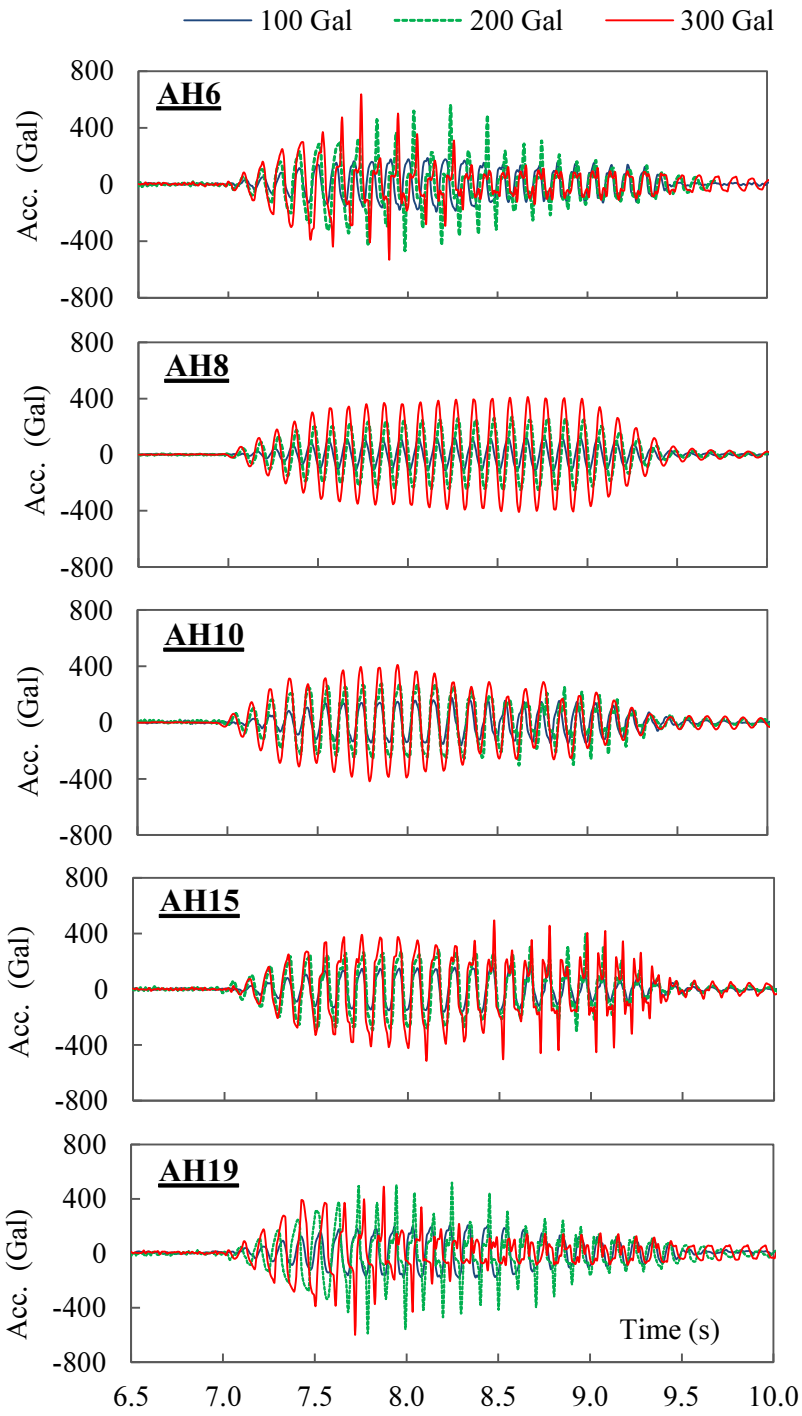

Fig.3.14 Time histories of acceleration in the flat model from 100 to 300 Gal

The time histories of the horizontal accelerations at points in the ground in the slope model are shown in **Fig.3.15**. Similar to the flat model, all acceleration records in the slope were in the same trend except the symmetric distribution of acceleration. The observed records at AH9 and AH16 show a distinct difference compared with the flat model about acceleration distributions. It means that when the liquefaction occurred the acceleration amplitude toward the waterfront (as represented by a negative value of acceleration) was

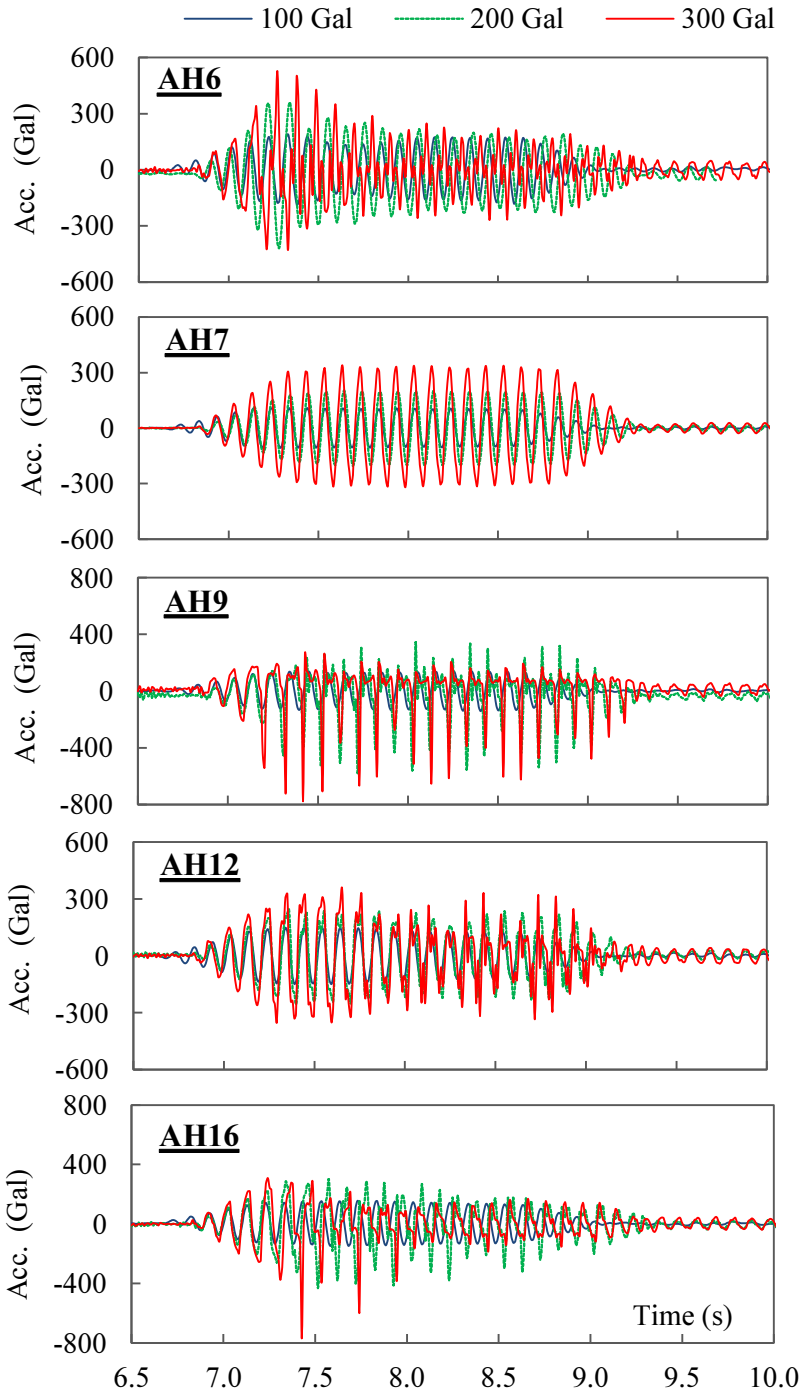

Fig.3.15 Time histories of acceleration in the flat model from 100 to 300 Gal

much larger than that in the opposite direction (as presented by positive one). It is expected that the instability of slope ground generated the high acceleration. This phenomenon also occurred in the flat model in the liquefaction case of 300 Gal input ground motion, but it was not clear. Moreover, the declination of acceleration was considerably observed in the slope model in cases of 200 Gal.

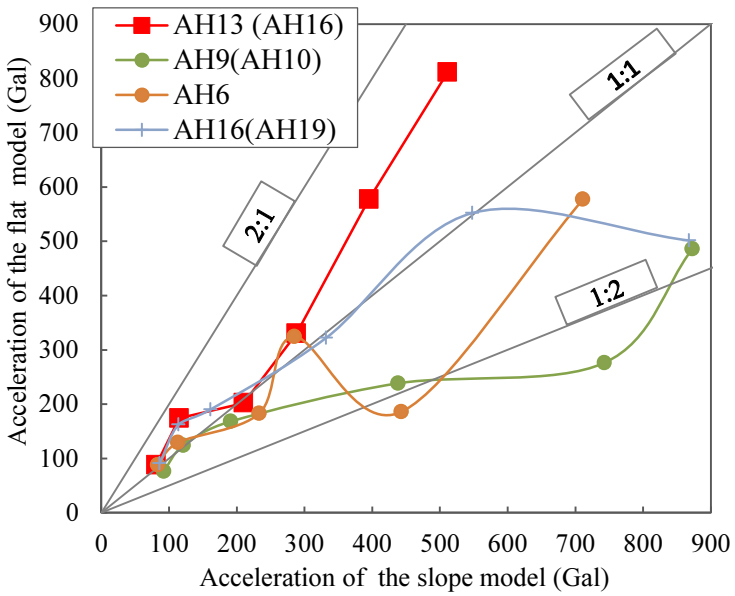

Fig.3.16 Comparison of acceleration between two models from 100 to 300 Gal

The comparison of ground acceleration between two models from 50 to 300 Gal is shown in **Fig.3.16**. It is seen that from 50 to 100 Gal the difference of acceleration in the ground was quite small but in cases of higher input ground motion the difference became greatly large. During shaking the accelerations at in the far field in the slope model were larger than that in flat model, as shown at AH6 and AH16 of the slope model (AH19 of the flat model). The acceleration at AH9 of the lower ground of near field in the slope was also larger than AH10 at the same coordination in the flat model, while AH13 at the high ground of slope model had a smaller acceleration than AH19 of the flat model. It thinks that soil moved down on the slope ground so the sand in the higher ground became looser, while the sand at the bottom of ground was denser.

The comparisons and time histories of ground acceleration give some findings:

1) The increase of ground acceleration amplitude is in accordance with an increase of input ground motion.

2) There is a declination of acceleration phenomenon during liquefaction. This phenomenon also occurred in the slope model but the rate of declination happen more quickly than in the flat model.

3) When liquefaction occurred the acceleration at the bottom in the slope model is influenced by the soil movement of slope ground, the acceleration part is much taken advantage toward the waterfront direction.

4) In the low input ground motion the acceleration between two models is not much significant but in the higher input ground motions the ground accelerations are almost larger and greatly increase in the slope model.

3.4.3 Displacement of the surface ground

Fig.3.17 displays the distribution of the measured residual horizontal displacement at the maximum input ground motion of 300 Gal in the slope model. The figure illustrates that the movement of the slope ground was in the direction from T3-11 toward the land to T3-6 toward the water when liquefaction occurred. The displacement distribution from T1-6 to T5-6 in front of the foundation was nearly uniform. However, the displacement at T3-6 in front of the foundation was slightly smaller than that of the other points. The displacement of the points near the foundation was less than that in the free field from T1-11 to T5-11 behind the foundation. The residual displacements at the front and back of the foundation were smaller than those of other points. A lateral relative soil movement around the foundation was occurred due to sand liquefaction in the slope model. The foundation that was inserted into non-liquefaction layer blocked the horizontal displacement of the points in the free field.

The measured horizontal displacement value of points near the foundation is shown in **Fig.3.19.** The figure illustrates that in the 50-100 Gal cases, there was a slight difference in the displacement between points, including points T3-6, T3-11, T1-c, and T5-c near the front, back, and two sides of the foundation, respectively. However, the difference became significantly larger in the 150-300 Gal cases. The displacement of the footing was the smallest in these cases. The foundation clearly retained the movement of soil on the back side and pushed the soil forward on the front side.

Fig.3.18 presents the distribution of the measured residual horizontal displacement under the 300 Gal case in the flat model. The figure illustrates that the displacement distribution on the back side of the foundation from T1-6 to T5-6 was nearly uniform. However, the displacements of points from T2-11 to T4-11 on the front of the foundation were larger than that of T1-11 and T5-11 in the free field. Moreover, the displacement on the right side was larger than that on the left side. The foundation vibration created a disturbed adjacent sand layer.

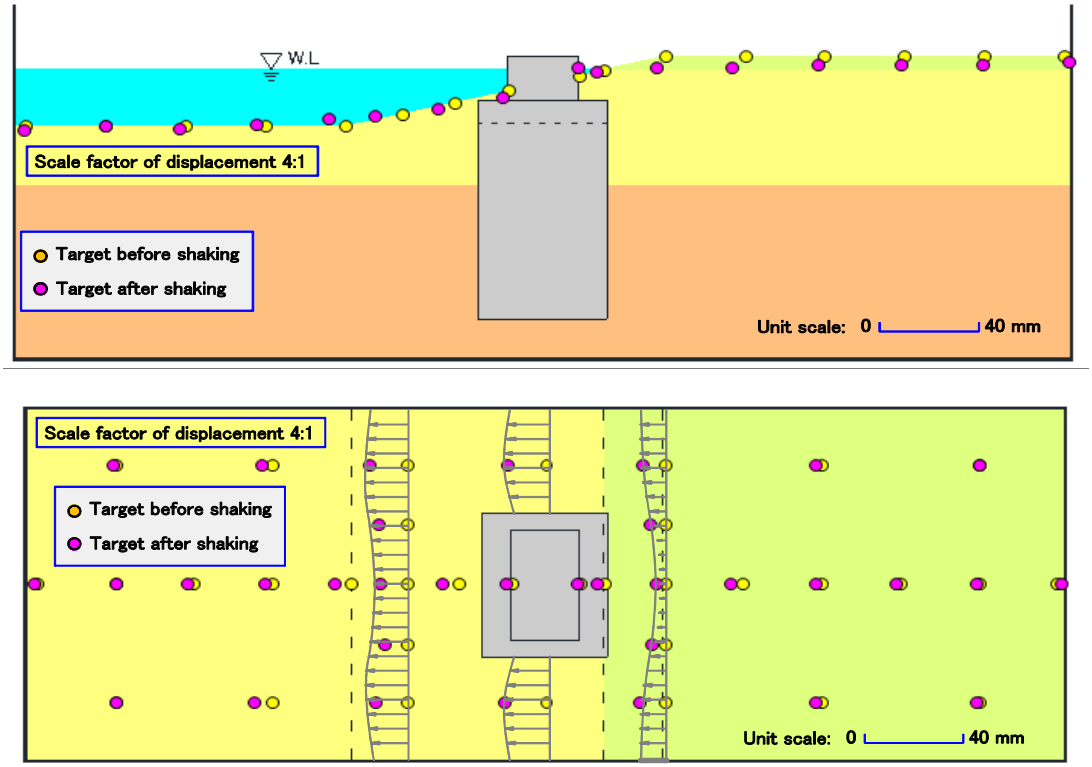

Fig.3.17 The measured displacement distribution of the ground surface movement in the slope model under 300 Gal

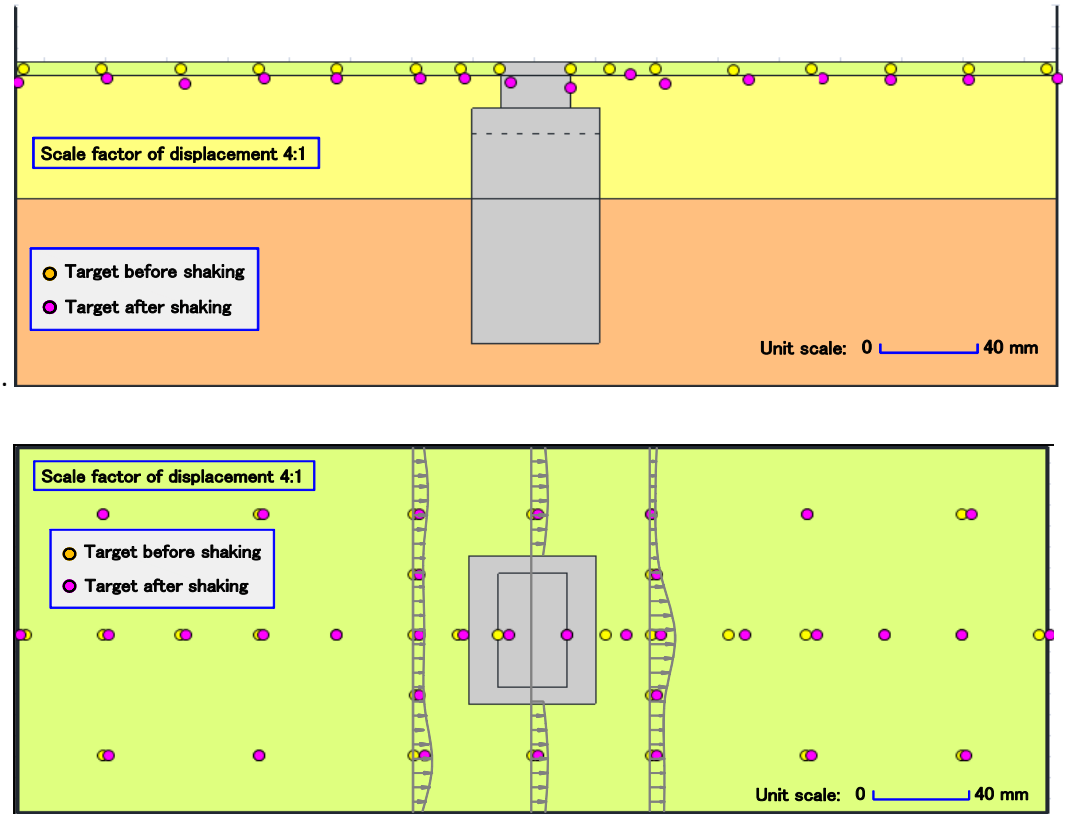

Fig.3.18 The measured displacement distribution of the ground surface movement in the flat model under 300 Gal

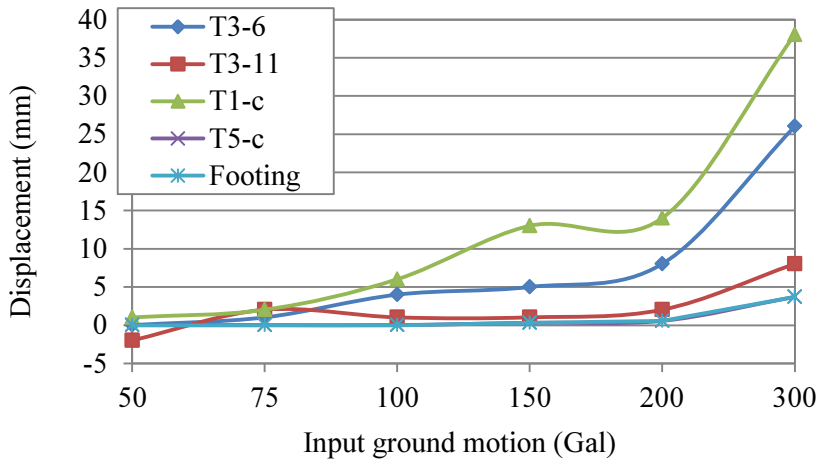

Fig.3.19 Measured residual displacement at T1-c, T3-6, T3-11, T5-c and the footing in the slope model from 50 to 300 Gal

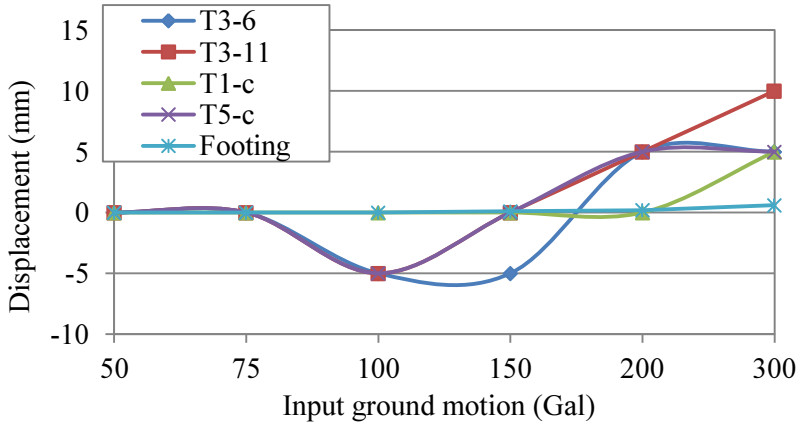

Fig.3.20 Measured residual displacement at T1-c, T3-6, T3-11, T5-c and the footing in the flat model from 50 to 300 Gal.

Fig.3.20 presents the horizontal residual displacement values of points near the foundation in the 50-300 Gal cases for the flat model. The figure illustrates that from 50 to 150 Gal, there was a slight difference in the displacement among points, including points T3-6, T3-11, T1-c, and T5-c of the front, back, and two sides of the foundation, respectively. The movement of the ground was from T3-6 to T3-11 to the right side of the foundation. The movement was in the opposite direction from 150 to 300 Gal.

The observed result of residual displacement in the ground shows that:

1) From 50 to 100 Gal input ground motions the residual displacements in two models were almost the same. However, from the higher input the displacement became larger in the slope model.

2) In the slope model when soil was liquefied there was a large movement on the slope ground so the foundation must prevent the movement from the soil flow more than in the flat model.

3.5 Behavior of the Superstructure

3.5.1 Horizontal acceleration responses

Fig.3.21 presents the time histories of the horizontal acceleration of the superstructure and pile cap in the flat model in cases of 100, 200 and 300 Gal input ground motion. It is observed that during shaking from 100 to 300 Gal the acceleration at AH3 of pile cap was larger than that at AH4 of superstructure. Moreover, the figure shows that the increase of acceleration of superstructure and pile cap was due to the increase of input ground motion.

The comparison of acceleration time histories between AH3 of pile cap and AH4 of superstructure is shown in **Fig.3.22**. It is seen that most of horizontal accelerations of pile cap were almost out of phase with that of superstructure during shaking. Moreover, when input ground motion increase from 100 to 300 Gal the ratio line axis of hysteresis loops rotated in the clockwise direction and around the line ratio 1:1.5. It means that the acceleration of pile cap at AH3 was greater than that of superstructure at AH4 and reduced according to liquefaction of soil. This is because the reduction of soil strength due to the liquefaction occurred. Furthermore, the hysteresis loop became fatter from 200 to 300 Gal. The number of cases which the acceleration of superstructure and foundation was the same phase occurred more during liquefaction and nonlinear properties of soil performed more significantly.

Time histories of the acceleration of the superstructure and pile cap in the slope model in cases of 100, 200 and 300 Gal are shown in **Fig.3.23**. Similar to the flat model, the acceleration at AH3 of pile cap was also larger than that at AH4 of superstructure and their difference reduced when liquefaction occurred. The comparison between them was displayed in the hysteresis loops, as shown in **Fig.3.24**. It also had the same trend as the flat model is that the acceleration of superstructure was almost out of phase with that of pile cap during shaking. However, the axis of the hysteresis loop in the case of 300 Gal in the slope model almost approached to the ratio line 1:1. It means that the difference of acceleration values became smaller and was not significant.

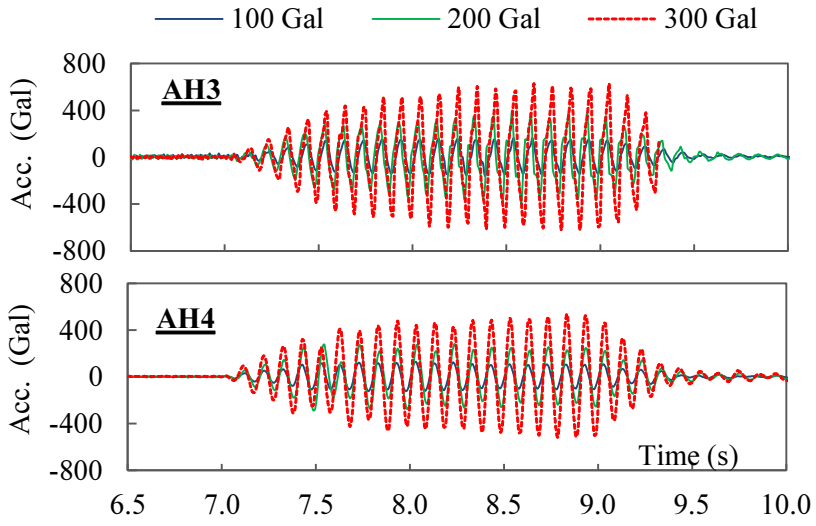

Fig.3.21 Time histories of acceleration of pile cap and superstructure from 100 to 300 Gal

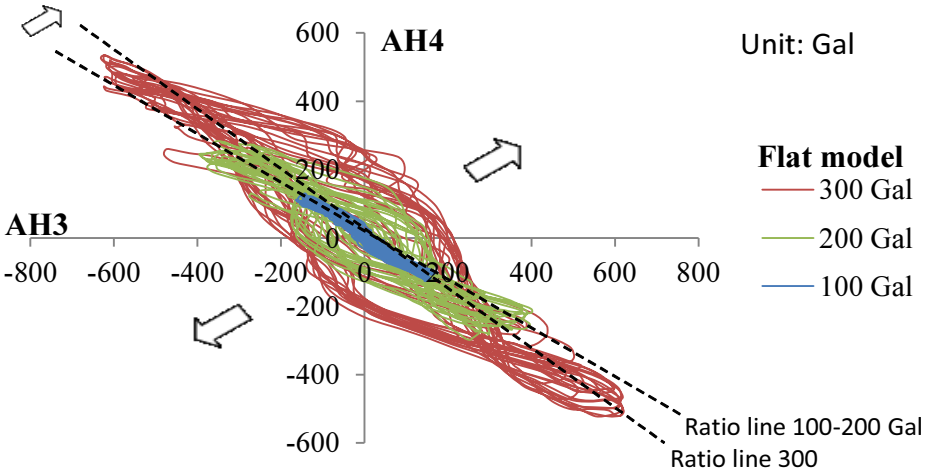

Fig.3.22 Comparison of acceleration time histories between AH03 of pile cap and AH04 of superstructure in the flat model

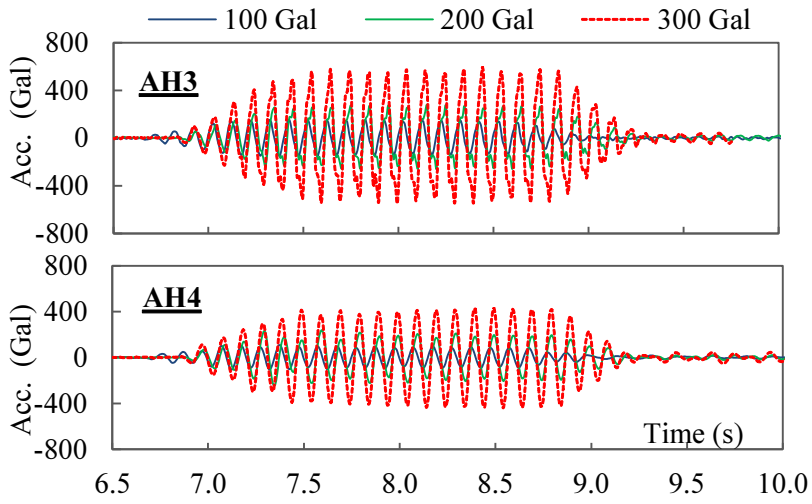

Fig.3.23 Time histories of acceleration between AH03 and AH04 in the slope model

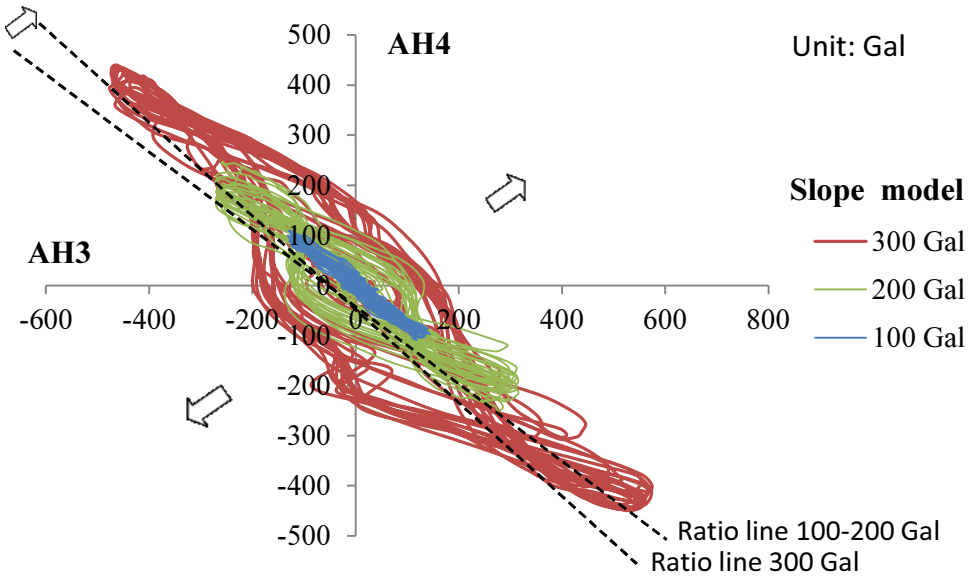

Fig.3.24 Comparison of acceleration time histories between AH03 of pile cap and AH04 of superstructure in the slope model

3.5.2 Displacement responses

Fig.3.25 presents the time histories of the horizontal and vertical displacements at DH1 of the pile cap and at DH2 superstructure from 100 to 300 Gal in the flat model. Results from these figure show that as the input ground motion increased, most of the displacements also increased. The horizontal displacement quite quickly increased in case of 300 Gal and the residual horizontal displacement appeared in cases of 200 and 300 Gal. In case of 100 Gal the difference of vertical displacement between DV1 and DV2 was not significant because there was no inclination of foundation.

However, in higher input ground motion of 200 and 300 Gal the displacement values at DV1 were almost positive, while these values at DV2 were negative. It means that the foundation inclined.

The comparison of horizontal displacement time histories between DH1 and DH2 in the flat model is shown in **Fig.3.26**. It shows that in case of 100 Gal most of displacement at DH1 was much smaller than that at DH2 and the difference was really significant, moreover DH1 was also out of phase with DH2, the loop was quite symmetric. However, when the input ground motion increased to 200 and 300 Gal the loop moved down and widely extended to the area where the DH1 was the same phase with DH2. It means that the superstructure and pile cap almost moved in horizontal direction together during liquefaction and their difference significantly reduced

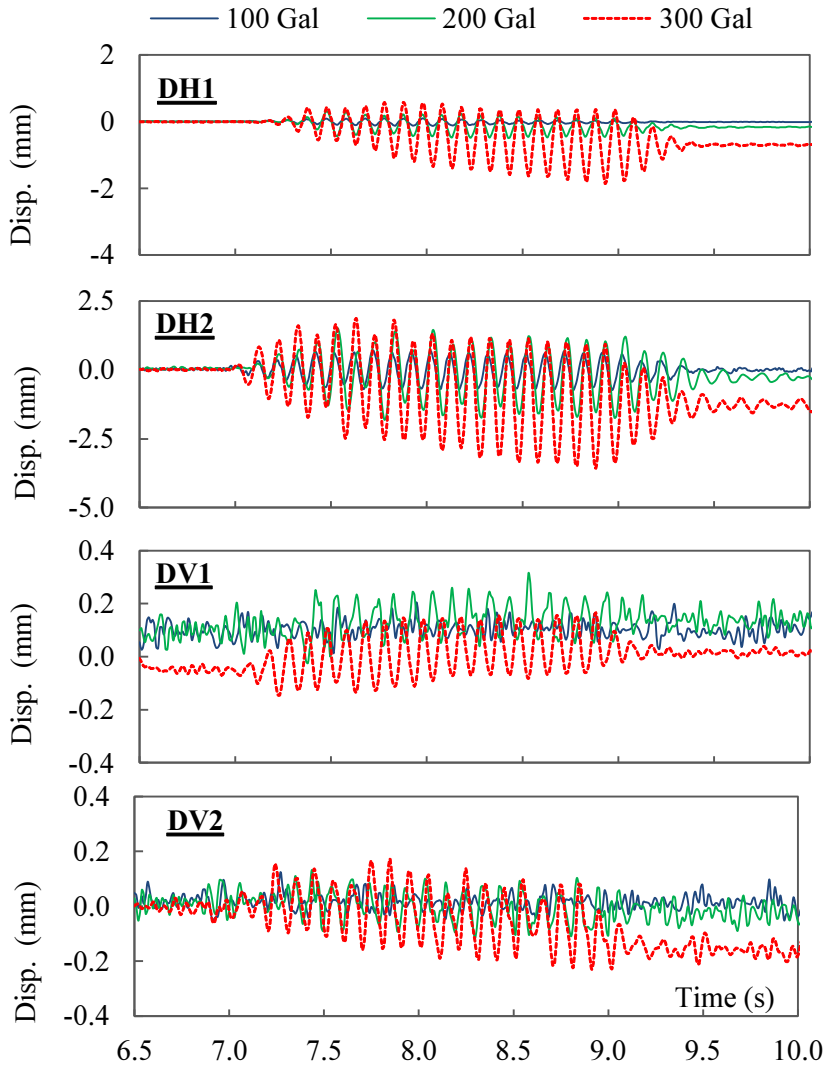

Fig.3.25 Time histories of displacement of superstructure and pile cap in the flat model

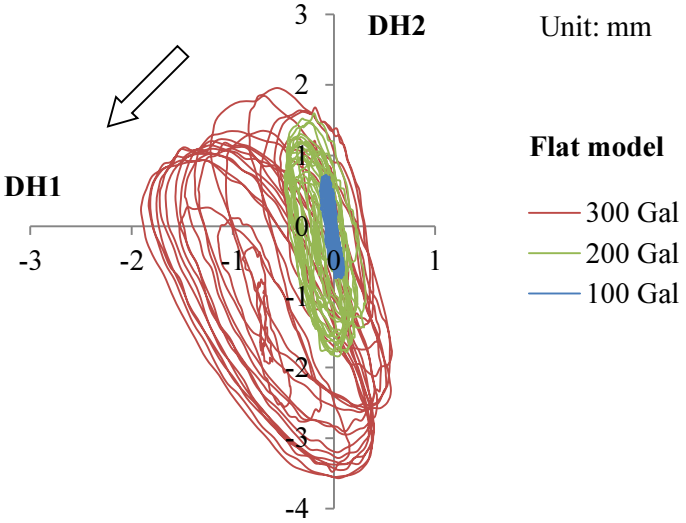

Fig.3.26 Comparison of displacement between DH2 of superstructure and DH1 of pile cap in the flat model

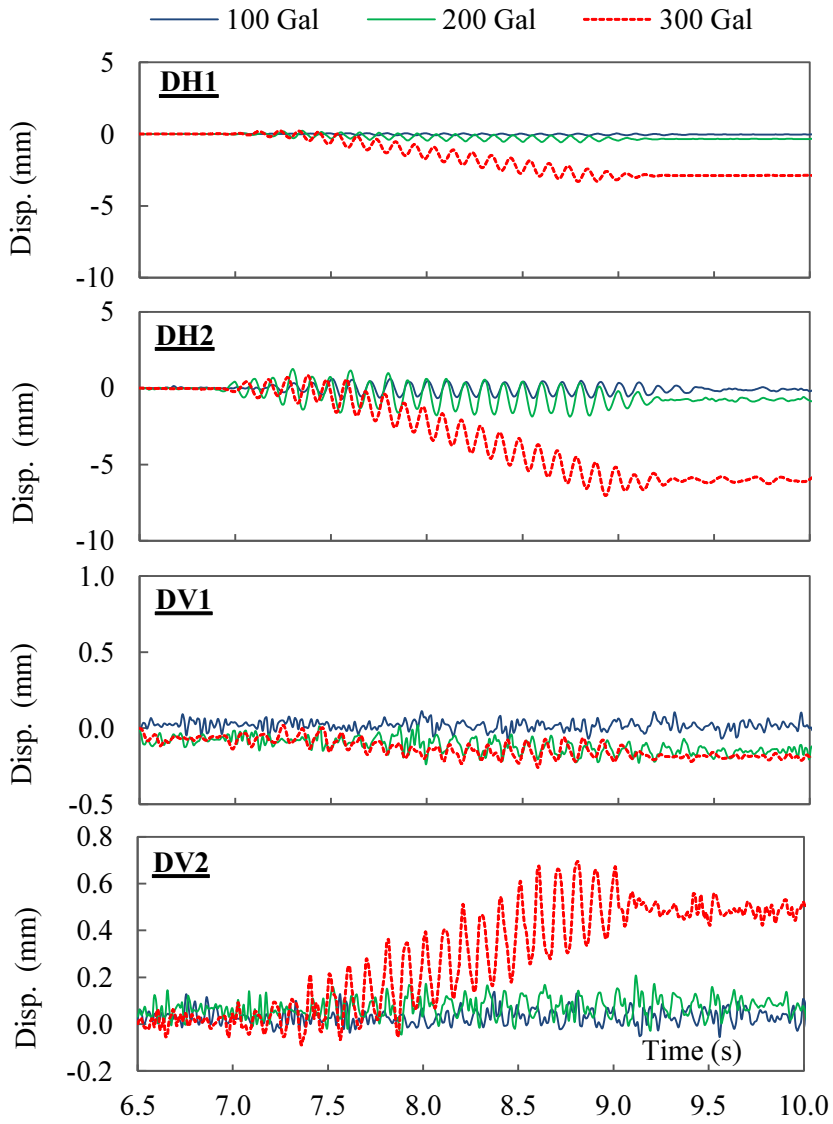

Fig.3.27 Time histories of displacement of superstructure and pile cap in the slope model

Fig.3.27 presents the time histories of the horizontal and vertical displacements at DH1 of the pile cap and at DH2 superstructure in the slope model from 100 to 300 Gal input ground motion. It is similar to the flat model but in the slope model the displacement greatly increased from 200 to 300 Gal, around 4 times for the horizontal displacement and 3.5 times for DV2 of vertical displacement. The vertical displacements at DV1 were almost negative, while that at DV2 were positive. It means that the foundation inclined and moved to the waterfront. The comparison of horizontal displacement time histories between DH1 and DH2 in the slope is shown in **Fig.3.28**. It is similar to phenomenon in the flat model, difference of difference between DH1 and DH2 was really large in case of 100 Gal and significantly reduced in case of higher input ground motion when liquefaction occurred. DH1 and DH2 had the same phase during liquefaction. Especially, because the

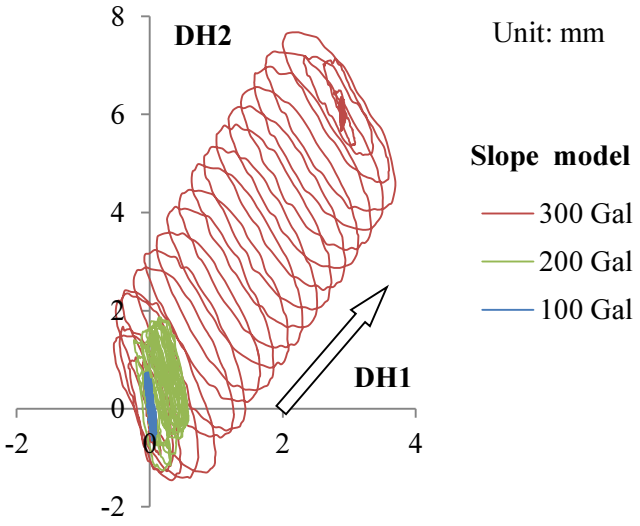

Fig.3.28 Comparison of displacement between DH2 of superstructure and DH1 of pile cap in the slope model

development of displacement in case of 300 Gal was greatly quick so its loop also quickly extended up.

3.5.3 Comparison

Cubrinovski et al. (2009) and Ramin Motamed et al. (2013) indicated that the displacement records are decomposed into cyclic and monotonic components. The cyclic component is generated by cyclic horizontal load and the monotonic one is caused by a residual movement of ground. As a result, in the consideration with both models in the slope model when the monotonic component of horizontal displacement increased then the cyclic one became smaller. The inclination of the foundation was determined by the following equation:

$$\alpha = \frac{DV2-DV1}{L}100 \qquad (3.5)$$

Where α is the inclination of the foundation (%); *DV1* and *DV2* are the residual values of vertical displacements at the top of the footing (mm); and *L* is the distance between *DV1* and *DV2* (266 mm).

Figs.3.29 and **3.30** show that from 50 to 100 Gal the maximum and residual displacements in both models was the same but the difference between them gradually increased. In case of 300 Gal the maximum displacement of superstructure and pile cap in the slope model two times larger than that in the flat model and 5 times for the residual displacement.

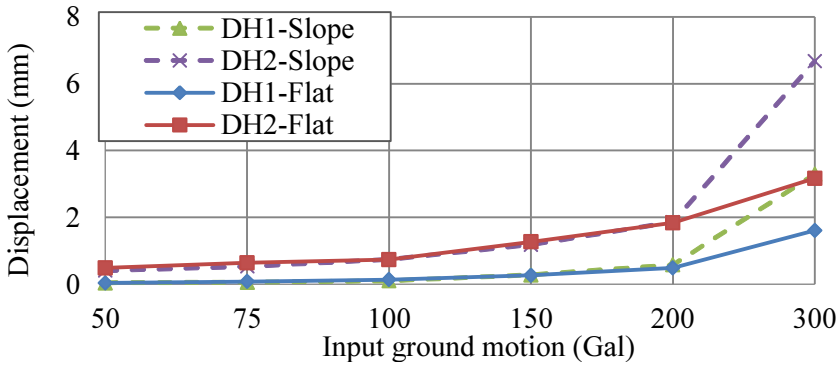

Fig.3.29 Comparison of displacement at DH1 and DH2 between the flat and slope models

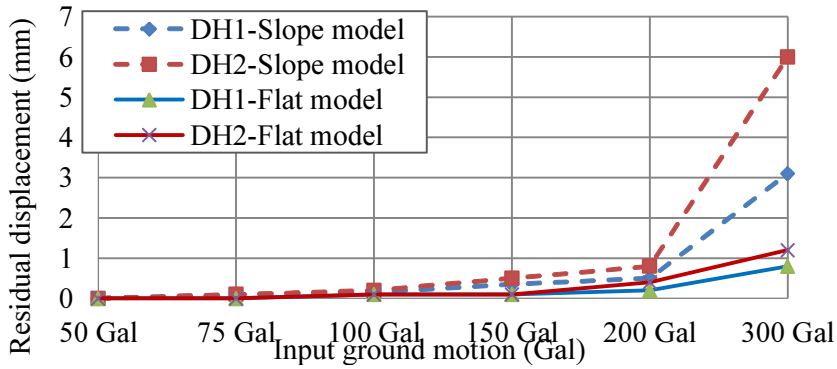

Fig.3.30 Residual displacement at DH1 and DH2 in the flat and slope models

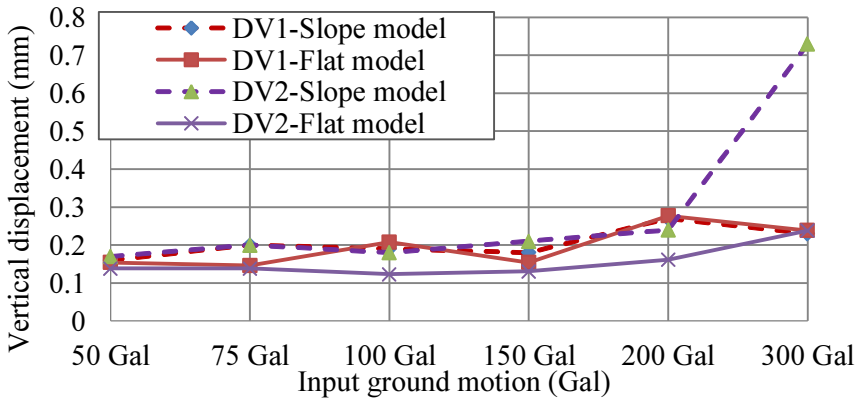

Fig.3.31 Vertical displacement at DH1 and DH2 in the flat and slope models

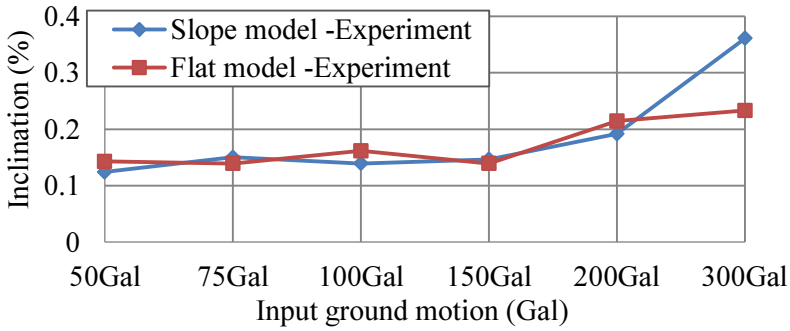

Fig.3.32 Inclination of foundation in the flat and slope models

Fig.3.31 shows that from 50 to 300 Gal the maximum vertical displacement at DV1 in both models was almost the same but at DV2 the displacement in the slope model was larger than that in the flat model, especially around 3 times in case of 300 Gal. **Fig.3.32** also show the foundation in the slope model inclined around 2 times larger than in the flat model.

3.5.4 Conclusion

The displacement, acceleration and comparison result of superstructure and pile cap in both models gives some findings as follows:

1) In lower input ground motion, the displacement of superstructure is out of phase with that of pile cap in both models. However, in the case of higher input their displacement responses are in the same phase.

2) The acceleration of superstructure is almost out phase with that of pile cap in both models during shaking.

3) From 50 to 100 Gal soil ground is not much liquefied acceleration, displacements of superstructure, pile cap and inclination of foundation in both model are almost the same. However, when liquefaction completely occurs then the responses in the slope is much larger than in the flat model.

3.6 Behavior of Foundation

3.6.1 Response strain

The maximum bending and axial strain distribution of the experiment along the foundation in both the flat and slope models from 50 to 300 Gal are shown in **Figs.3.33** and **3.34**, respectively. The bending strains dominated the axial strain when the input acceleration amplitude was less than 100 Gal. The distribution of the axial and bending strains was uniform along the foundation depth. When liquefaction occurred, the strain increased at the bottom of the foundation rather than at the upper location. Generally, **Figs.3.33** and **3.34** illustrate that the bending strains in both the experiment and ESA reach a maximum value near the bottom of the pile foundation at S2 in both models. This position was around the interface between the liquefaction and non-liquefaction layers. This is because during the shaking the foundation was embedded by the non-liquefaction layers and under the effect of the lateral ground movement the foundation was bended down.

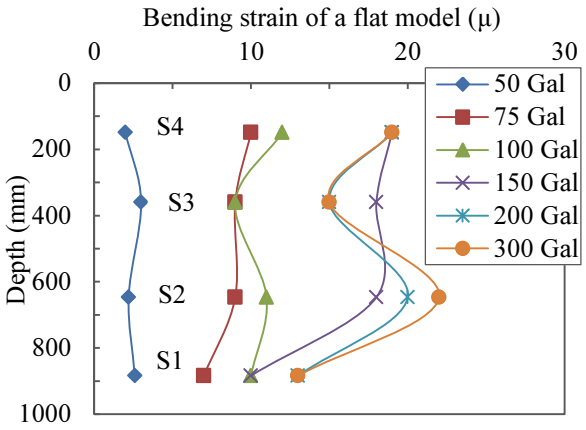

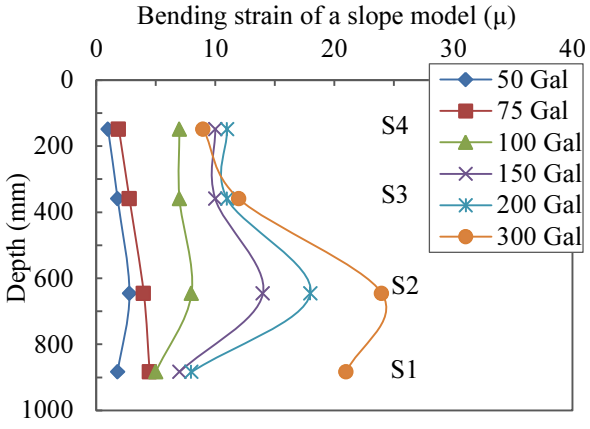

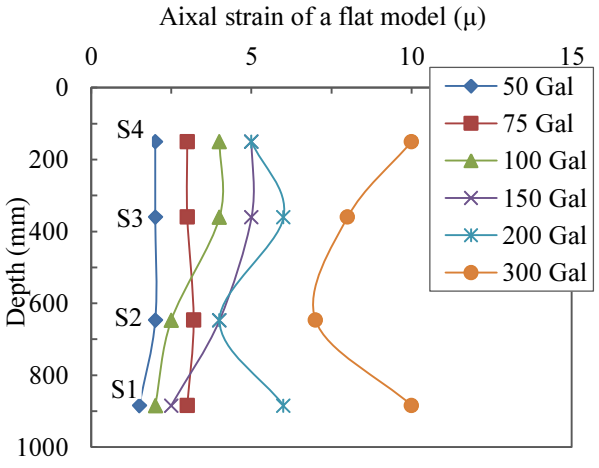

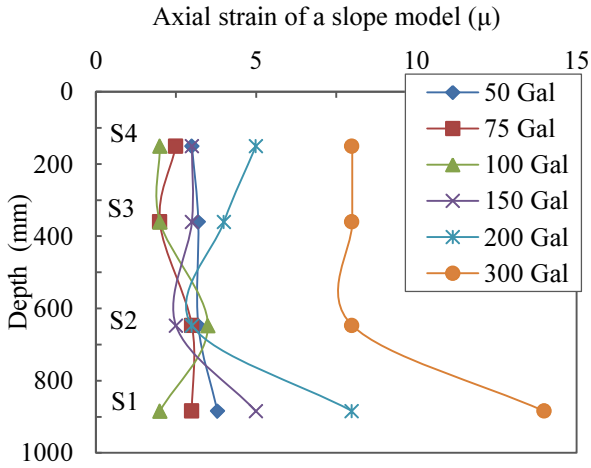

Fig.3.33 Bending and axial strain in experiment in the flat model.

Fig.3.34 Bending and axial strain in experiment in the slope model.

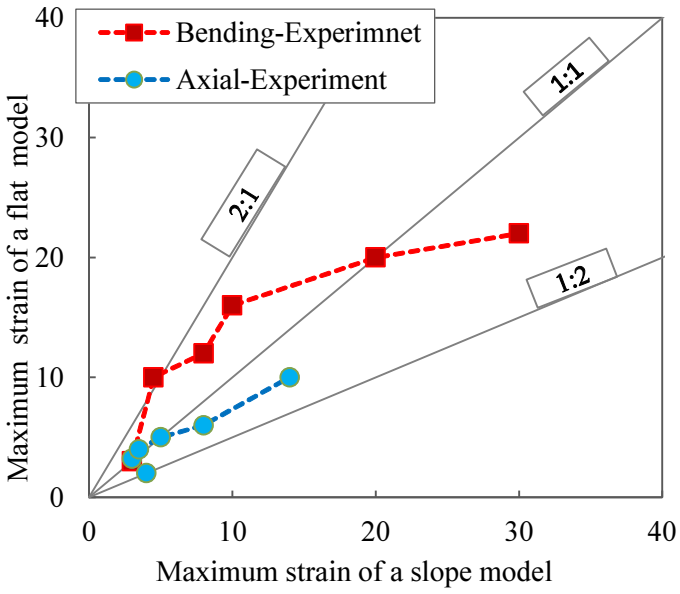

Fig.3.35 Comparison of bending strain along the front and back sides between the flat and slope models

3.6.2 Comparison and conclusion.

Fig.3.35 shows that the maximum bending strain in the slope model was less than that in flat model but in the case of 300 Gal the strain was 1.5 times larger than that in flat model. The maximum axial strain in the slope model was larger than that in the flat model during shaking.

3.7 Remarking Conclusions

Vibration test using the shaking table test was conducted on both the flat and slope models to investigate the dynamic behavior of SPSP foundation and effect of ground slope on the foundation. There are some main findings as follows:

(1) The dynamic response of foundation and ground consists of pore water pressures, displacements, accelerations and strains increased were in accordance with the increase in the input acceleration in both the flat and slope models in the vibration test. The lateral movement on the foundation became large when liquefaction occurred, and residual displacement at the top of foundation was observed for both models. The residual displacement in the slope model was considerably larger than that in the flat model

(2) In the slope model, the foundation moved down the slope and inclined in the shaking table test and quickly generated the high acceleration in slope model, the immigration of pore water pressure became more complicated at the bottom of slope. The movement of the slope at the foundation that was inserted into non-liquefaction layer was smaller than that of the free field.

(3) In the lower input ground motion from 50 to 100 Gal the difference of acceleration, displacement and inclination between two models was not much significant. However, in the higher input ground motions from 200 to 300 Gal the, soil was liquefied the displacement response of the pile cap and superstructure and inclination and strain of foundation in the slope model was almost larger than that in the flat model then during liquefaction. Therefore, the lateral movement of liquefaction layer due to slope may partially affect to the foundation when liquefaction occurred.

(4) The slope ground also made a declination of acceleration of superstructure and pile cap during liquefaction.

(5) In lower input ground motion, the displacement of superstructure was out of phase with that of ground foundation in both models. However, in the case of higher input motion as the soil was liquefied the displacement of superstructure was in phase with that of foundation. Meanwhile, the acceleration of superstructure was almost out of phases with that of foundation in both models during shaking. This phenomenon would be investigated and explained in the Chapter 3.

References

1) Iai, S.(1988), Similitude for shaking table tests on soil-structure-fluid model in 1G gravitational field, Report of the Port and Harbor Research Institute, Vol.27, No.3, pp.3-24.

2) Japan Port and Harbor Association (1989). Technical Standards for Port and Harbor Facilities. Ports and

3) Tatsuoka, F., Muramatsu, M. and Sasaki, T. (1982): Cyclic undrained stress-strain behavior of dense sands by torsional simple shear test, Soils and Foundations, 22(2), pp. 55-70.

4) Tatsuoka, F. Ochi, K., Fujii, S. and Okamoto, M. (1986). Cyclic undrained triaxial and torsional shear strength of sands for different sample preparation methods, Soils and Foundations, 26(3): pp. 23-41.

5) Tashiro, S., Kotake, N., Miyoshi, T. and Kiyomiya, O. (2009). Shaking table test of sheet pile quay wall back-filled with ground anchor for seismic reinforcement. National Conference of Japan Geotechnical Engineering Vol. 44, 1073-1074.

6) Wilson, Daniel W., Boulanger, Ross W., and Kutter, Bruce L. (2000). "Observed seismic lateral resistance of liquefying sand," J. Geotech. and Geoenviron. Eng., 126(10), pp. 898-906.

7) Yang, Z., and Elgamal, A. (2002). Influence of Permeability on Liquefaction-Induced Shear Deformation. Journal of Engineering Mechanics, ASCE, 128(7), pp. 720-729.

8) Abdoun, T. H., Dobry, R., O'Rouke, T. D., and Chaudhuri, D. (1996): Centrifuge modeling of seismically-induced lateral deformation during liquefaction and its effects on a pile foundation. Sixth Japan – U. S. Workshop on Earthquake Resistant Design of Lifeline Facilities and Countermeasures Against Soil Liquefaction, Report NCEER-96-0012, SUNY, Buffalo, NY, pp. 525 - 539.

9) Adachi, N., Miyamoto, Y., and Koyamada, K. (1998): Shaking table test and lateral loading test for pile foundation in saturated sand. Proc. Intl. Conf. Centrifuge '98, (T. Kimura, O. Kusakabe, and J. Takemura, eds.), Tokyo, Japan, Sept. 23-25, Vol. 1, pp. 289-294.

10) Girard, J., and Taylor, R. (1994): Blade geometry and soil permeability effects on thin blade plow resistance in dense, saturated, cohesionless soils—Phase II report. Rep. TM-2026-OCN, Naval Facilities Engineering Service Center, Port Hueneme, Calif.

11) Seed H. B., Alba P. D., Chan C. K. (1976): Sand Liquefaction in Large Scale Simple shear tests. Journal of Geotechnical Engineering Division, American Society of Civil Engineers, Vol. 102, No. GT9, pp. 909-927.

12) Behra K.C., Saran, S., Mittal R. K. (2005): Liquefaction Studies on Sand and Sand-Silt

Mixture", IGC, 397-400.

13) Tzou-Shin , U. Ming-Huei, W. Ming-Horn, H. (2005): A Large Biaxial Shear Box for Shaking Table Test on Saturated Sand. Geotechnical Testing Journal, Paper ID GTJ12649 Vol. 29, No. 1 www.astm.org, pp1-8.

14) Eiji , Y. Fardin, J. (1995): Behavior of saturated sand models under principal Stress axes rotation in shake table test, Third International Conference on Recent Advances in Geotechnical Earthquake Engineering & Soil Dynamics St. Louis, Missouri, Vol. I, pp.169-174.

15) Prasad S. K., Towhata I., Chandradhara G. P., Nanjundaswamy P. (2004): Shaking table tests in earthquake geotechnical engineering, Special Section: Geotechnics and Earthquake Hazards, Current Science, VOL. 87, NO. 10, pp. 1398-1404.

16) Pathak S. R., Dalvi R. S. & Katdare A. D. (2010): Earthquake Induced Liquefaction using Shake Table Test. Fifth International Conference on Recent trends in Geotechnical earthquake Engineering and Soil Dynamics, San Diego, California.

Chapter 4

Numerical Method in the JRA 2002 Specification Approach

4.1 Introduction

As discussed in the previous Chapter, the difference of dynamic responses of pier foundation and ground between the flat and slope models is greatly larger when liquefaction occurs. The effect of ground slope on the behavior of the foundation is really significant. Therefore, the simple numerical method based on the specification JRA was conducted on the test models to investigate the seismic response of foundation and to clearly examine the effect of the ground slope on the foundation

The simulation method using a total stress analysis (TSA) was carried out in this research. It is an equivalent linear and the effect of pore water pressure buildup is not considered. Because this method is a simple calculation in the practical engineering approach, so it is really suitable to application of the specification in a design work. In the specification JRA 2002, the verification of liquefaction is simply calculated by reducing the strength or shear modulus of soil based on the liquefaction condition of ground. Therefore, the total stress analysis using a reduction factor was easily conducted to capture the seismic response of foundation.

The 2D simulation method also conducted on both the flat and slope models of vibration experiment. The behavior of superstructure, pier foundation and ground were simultaneously considered to investigate the interaction between the kinematic force and inertial force. The TDAP III program (developed by Taisei Corporation, Japan) was used to calculate. This is a program in analyzing the seismic response of structure.

4.2 Modeling Methodology

4.2.1 Numerical models

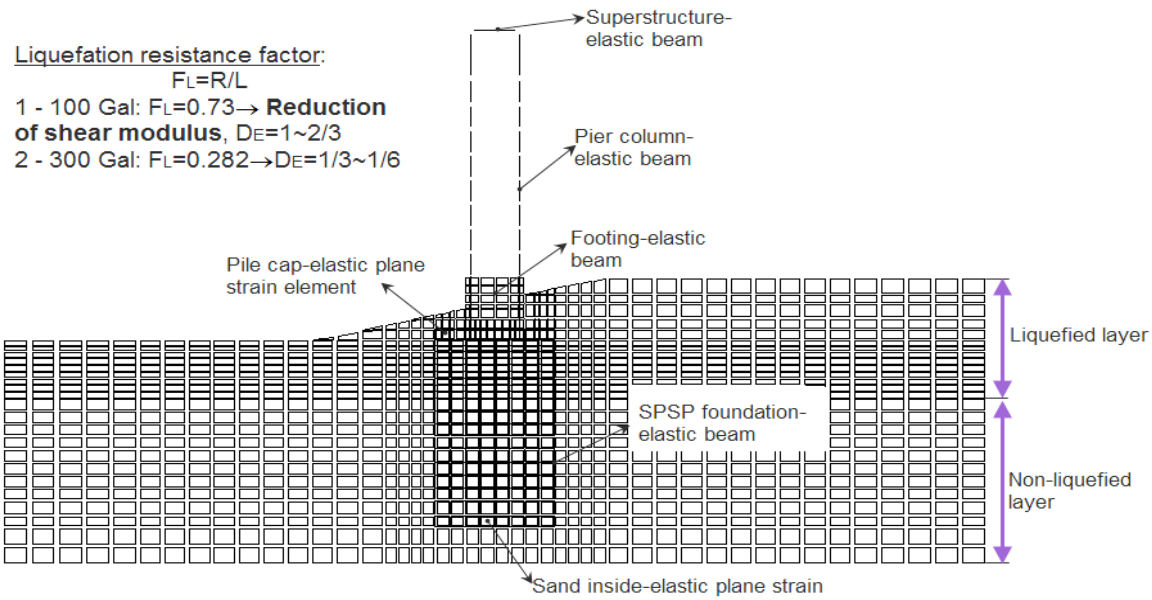

Fig.4.1 Numerical slope model in Total Stress Analysis (TSA).

The numerical model in the TSA for the slope model is shown in **Fig.4.1**. The foundation was divided into 9 parts with equal width in horizontal direction in plan, and each part was represented by a beam at its center. The connection between two piles was rigid. The piles, pier columns, and acrylic plate at the top of the pier were modeled as elastic beam elements. The steel footing plate and acrylic cap of the piles were modeled as plane strain elements. The soil inside and outside the foundation was modeled as plane strain elements in the TSA. Along the soil-pile interface, the piles and adjacent soil elements were connected by a few springs in the vertical and horizontal directions. The horizontal springs were modeled as cut-off tension springs.

4.2.2 Boundary condition

The boundary at the bottom of the model was fixed in the vertical and horizontal directions, and the lateral boundary at the two sides was fixed in the horizontal direction.

4.2.3 Rayleigh damping

The nonlinear dynamic analysis was conducted by a time-history direct integration method on these models. In the analysis, the self-weight analysis step was conducted first to calculate the initial stress and strain of the model before the calculation of the dynamic analysis. The damping ratio of structure and soil springs was assumed to be 0.03 and 0.1, respectively. Rayleigh's damping was used in this work shown in **Fig.4.2**, so the damping of models was re-calculated following the each time of reducing the shear modulus. This is

because the natural frequencies of pier foundation system change when liquefaction occurs. The damping ratio is very effective to dynamic response of model in the dynamic analysis.

4.2.4. Input ground motion

The input ground motion used in this total stress analysis was also an acceleration time history at the base of model which is similar to the input in the experiment.

4.3 Verification Procedure

4.3.1 Liquefaction condition calculation

Verification of liquefaction condition is one of the most important steps to determine the factor of shear modulus reduction. The reduction factor of liquefaction depends on the depth of liquefaction layer from the ground surface and the liquefaction factor F_L, and is stipulated in the specification JRA 2002, as shown in **Table 4.1.** In order to capture the reduction factor of shear modulus, the liquefaction factor F_L is firstly determined, as shown in **Eq.4.1**. The factor F_L depends on the level of earthquake (as represented by a shear stress ratio L and soil characteristics (as represented by a shear strength ratio R).

$$F_L = R/L \tag{4.1}$$

Where L : is a shear stress ratio during earthquake determined in **Eq. 4.2**; R : is a dynamic shear strength determined in **Eq.4.3**.

$$L = r_d k_{hg} \sigma_v / \sigma'_v \tag{4.2}$$

Where r_d : is a reduction factor of shear stress ratio in the vertical direction; k_{hg} : is a design seismic coefficient in the horizontal direction; σv : is a total overburden pressure and σv is an effective overburden pressure.

$$R = c_w R_L \tag{4.3}$$

Where c_w: is a modification factor based on the type of earthquake (an inland or a ocean earthquake); R_L: is a cyclic tri-axial strength at 20 cycles of load determined by **Eq.4.4**

$$R_L = \begin{cases} 0.0882\sqrt{\frac{N_a}{1.7}} & (N_a < 14) \\ 0.0882\sqrt{\frac{N_a}{1.7}} + 1.610^{-6}(N_a - 14)^{4.5} & (N_a > 14) \end{cases} \tag{4.4}$$

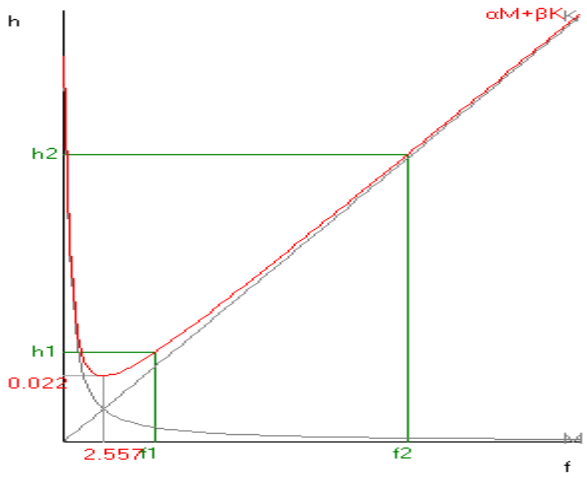

Fig.4.2 Rayleigh damping relationship

Table 4.1 Reduction factor of liquefaction

Range of F_L	Depth from Present Ground Surface x (m)	Dynamic shear strength ratio R			
		$R \leqq 0.3$		$0.3<R$	
		Verification for Seismic Motion Level 1	Verification for Seismic Motion Level 2	Verification for Seismic Motion Level 1	Verification for Seismic Motion Level 2
$F_L \leqq 1/3$	$0 \leqq x \leqq 10$	1/6	0	1/3	1/6
	$10 < x \leqq 20$	2/3	1/3	2/3	1/3
$1/3 < F_L \leqq 2/3$	$0 \leqq x \leqq 10$	2/3	1/3	1	2/3
	$10 < x \leqq 20$	1	2/3	1	2/3
$2/3 < F_L \leqq 1$	$0 \leqq x \leqq 10$	1	2/3	1	1
	$10 < x \leqq 20$	1	1	1	1

Note: Level 1 motions correspond to earthquakes with a high probability of occurrence during a bridge's service life, and

Level 2 motions correspond to earthquakes with a low probability of occurrence during a bridge's service life.

Based on the equations, table and similarity law, the reduction factor of shear modulus was determined for the flat model. Its range was from 1 to 1/2 in the 100 Gal input case and from 1/3 to 1/6 in the 300 Gal case. As to the slope model, the determination of overburden pressure was very complex because it is difficult to choose the overburden pressure of which the lower, higher or slope grounds using in the calculation of liquefaction condition. Therefore, in this research the reduction factor would be reduced step by step from 2/3 to1/100, as shown in **Table 4.2.**

Table 4.2 Analysis cases of shear modulus reduction of both models in TSA

Models	G_o	$2/3G_o$	$1/3G_o$	$1/6G_o$	$1/10G_o$	$1/100G_o$
Flat	○	○	○	○	×	×
Slope	○	○	○	○	○	○

4.3.2 Calculation procedure

The procedure of calculation using the total stress analysis consists of the following steps:

1) These reduction factors of shear modulus in the flat model were calculated by using the specification JRA-2002

2) The models with original shear modulus were performed in accordance with the non-liquefaction phenomenon. The natural frequencies and damping ratio were determined to calculate the Rayleigh's damping in the dynamic analysis.

3) To gradually reduce the shear modulus of liquefaction layer. The Rayleigh's damping was re-calculated.

4.4 Eigen Value Analysis

Eigen value analysis was conducted to verify the dynamic characteristics of two models by considering natural frequencies, mass and damping ratio. These parameters are very effective to the dynamic behavior of SPSP foundation during earthquakes. The difference of parameters would be used to explain the difference of seismic responses between two models during liquefaction

Table 4.3 summarizes the fundamental frequencies, mass ratios and mode damping of both models when liquefaction does not occur, and their modal mode of the first natural frequency and second natural frequency are presented in **Figs.4.3** and **4.4** for the flat and slope models, respectively. The first modal mode and frequency are almost controlled by the mass and flexural rigidity of pier column; while, the second mode and frequency are almost controlled by the mass and rigidity of SPSP foundation and soil ground. This table illustrates that both the first and second frequencies in the slope model were lower than those in the flat model. However, the difference between the frequencies in the two models was quite small. The mode damping of the slope model was almost identical to that of the flat model.

Table 4.3 Result of the eigenvalue analysis

Mode No	Flat model		Slope model	
	Frequency (Hz)	Mode damping (%)	Frequency (Hz)	Mode damping (%)
1	5.97	3.21	5.86	3.21
2	16.84	9.63	16.56	9.56

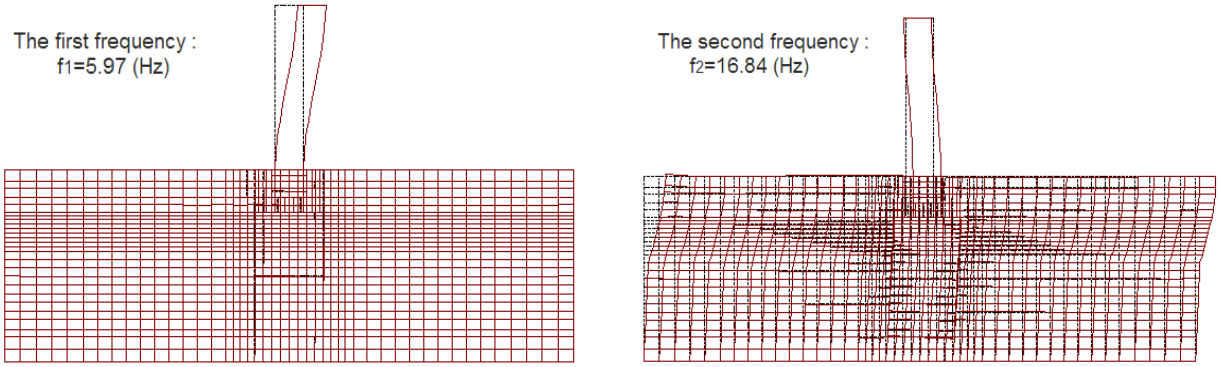

Fig.4.3 Fundamental natural frequencies of the flat model TSA.

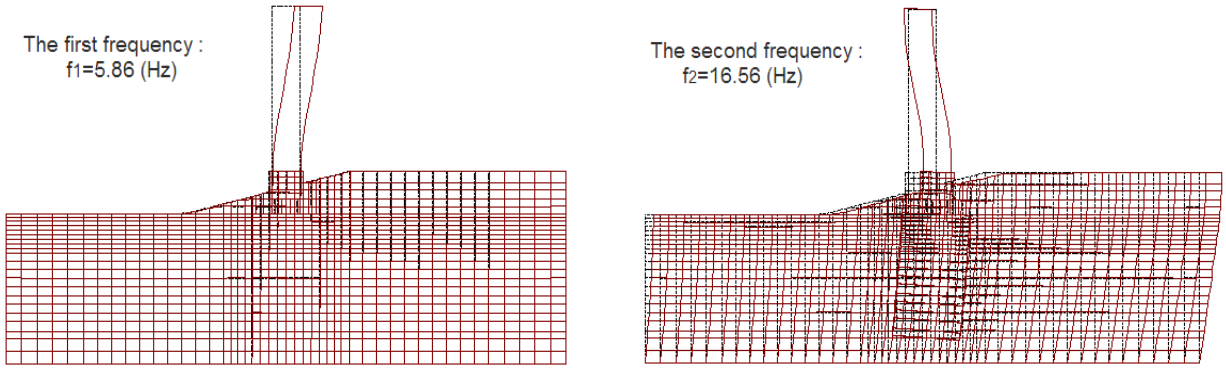

Fig.4.4 Fundamental natural frequencies of the slope model TSA.

Therefore, there was a slight difference in the dynamic characteristics of the two models in the initial state when liquefaction did not occur. This would explain the small difference of dynamic responses between two models during in the lower input ground motion from 50 to 100 Gal.

Eigen value analysis was continuously calculated in the cases of 2/3Go, 1/3Go and 1/6Go. **Fig.4.5a** presents that their first natural frequency was almost identical during shaking and liquefaction.

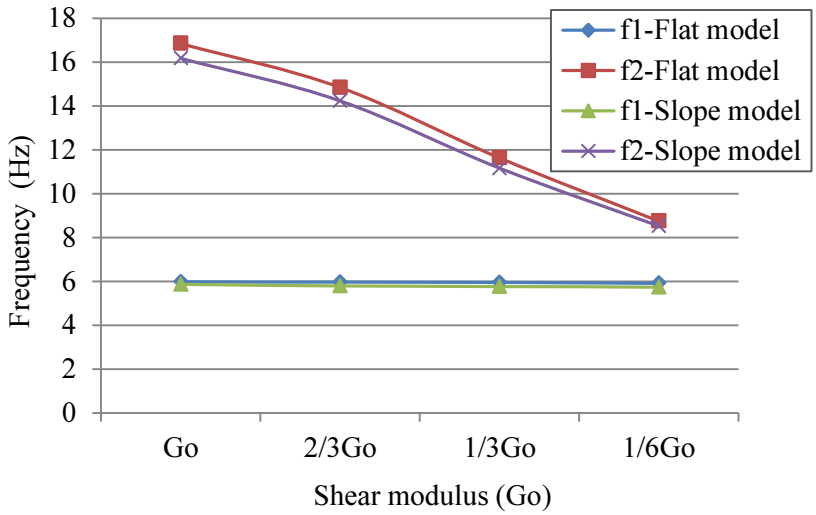

Fig.4.5a Fundamental natural frequencies of both models with a reduction of shear modulus

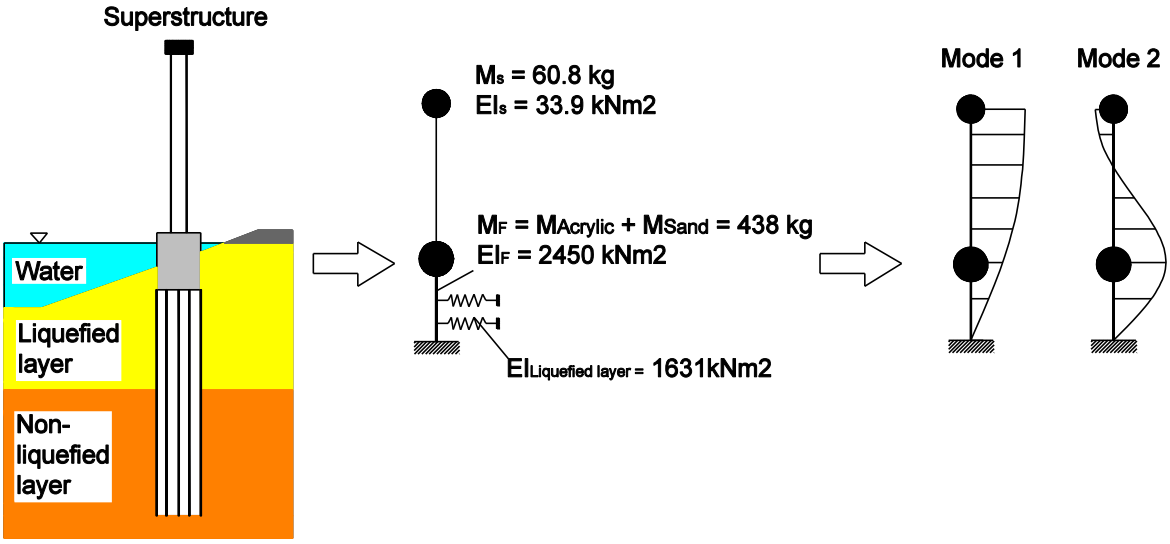

Fig.4.5b Double mass system of pier- SPSP foundation system and their modal modes

This is explained in **Fig.4.5b**. The figure shows that the pier foundation system is modeled as a double mass system with mass 1 of superstructure and mass 2 of foundation and embedded in the non-liquefaction layer. There are modal modes in this system, as shown **Fig.4.5b**. Because the stiffness of foundation is much larger than that of superstructure around 8 times and approximately 2 times than that of sand soil in the liquefaction layer so when the stiffness of soil reduces during liquefaction and significantly affects to the second natural frequency but is not significant to the first one. While, the second frequency significantly reduced. This is also because the mass ratio of second frequency was 76%, as shown in **Table 4.3** which includes the structure and soil ground

and in the first modal mode the participation mass ratio was 3% includes the structure. Therefore, the shear modulus reduction of ground affects to the second modal mode of pier foundation structures. Moreover, the difference of these frequencies between two models was quite little. However, it is significant because the dynamic responses of structure are very sensitive to fundamental frequencies.

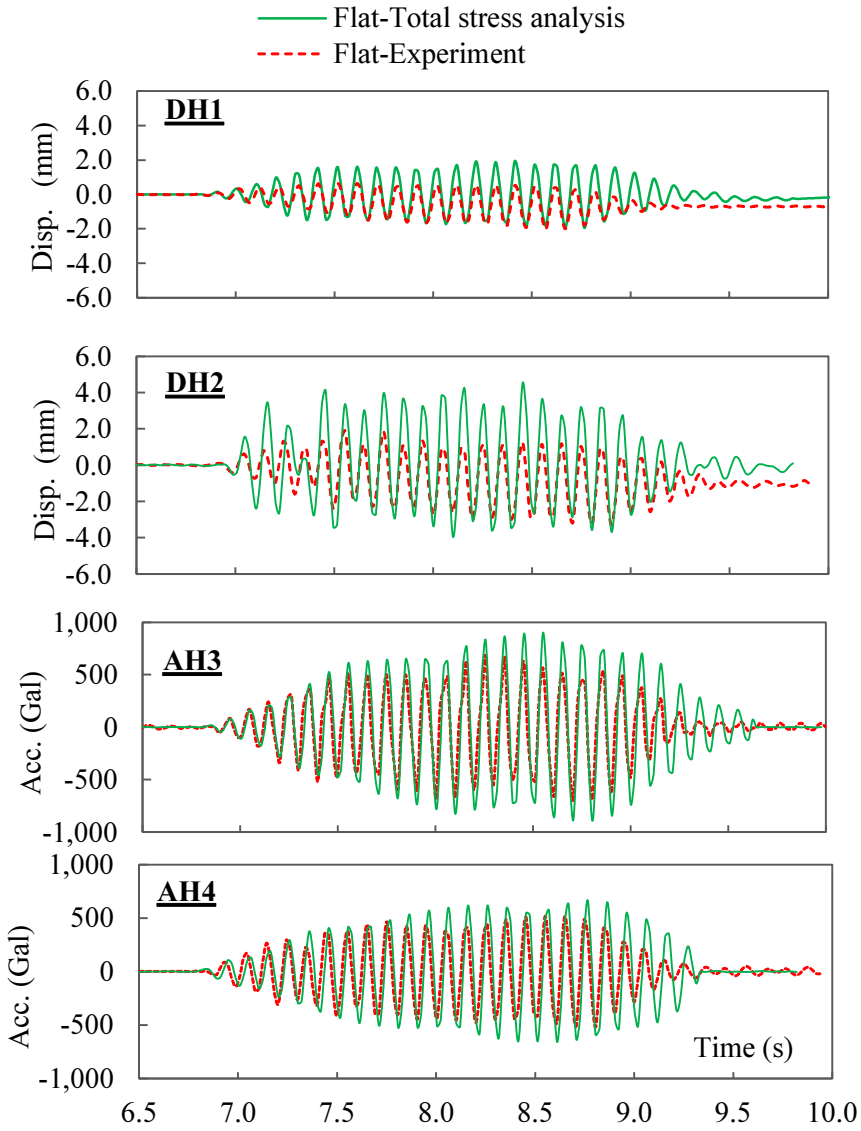

Fig.4.6 Horizontal displacement and acceleration time histories of 300 Gal of superstructure in case of 1/6Go in the flat model

4.5 Behavior of superstructure and pile cap

4.5.1 Flat model

Time histories of horizontal displacement and acceleration of superstructure and pile cap of 300 Gal in case of $1/6G_o$ are shown in **Fig.4.6**. It is observed that there was a good

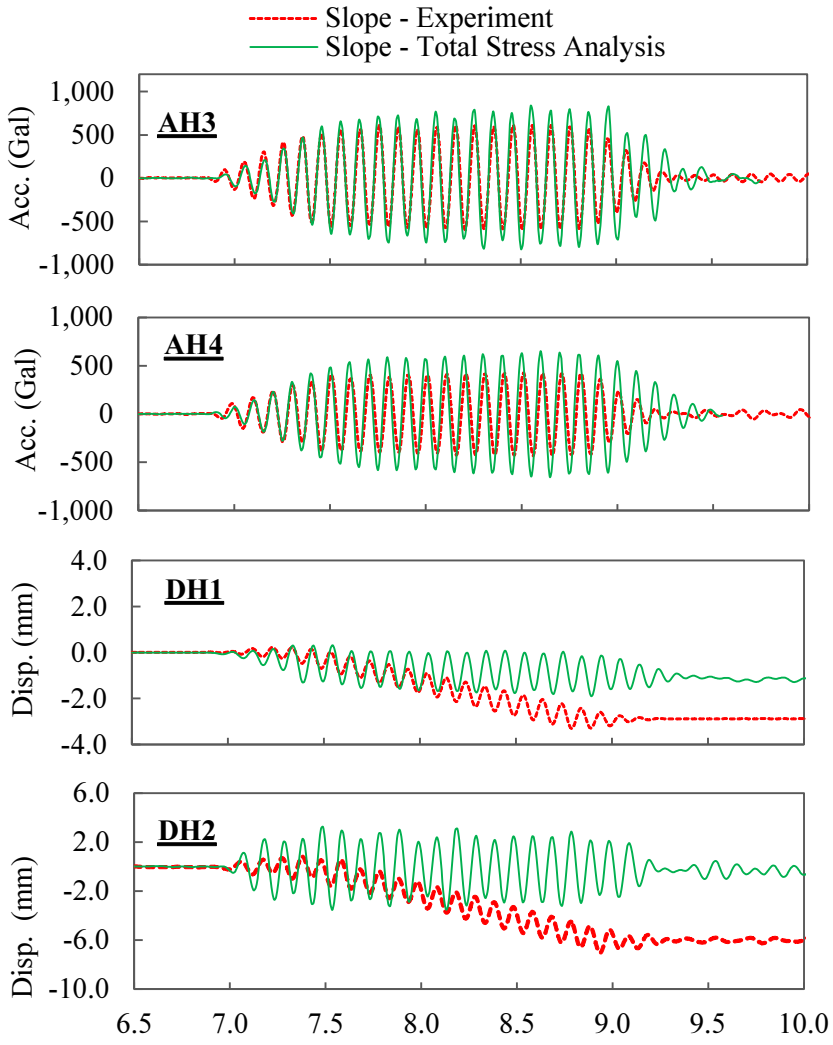

Fig.4.7 Horizontal displacement and acceleration time histories of 300 Gal of superstructure in case of 1/6Go in the slope model

agreement of the displacement and acceleration between TSA and the experiment. The residual displacement was not appeared in TSA because this is an equivalent linear method.

4.5.2 Slope model

The **Fig.4.7** shows time histories of horizontal displacement and acceleration of superstructure and pile cap of 300 Gal in case of $1/6G_o$ in the slope model. It is seen that the acceleration of TSA was larger than that in the experiment around 1.53 times for the superstructure and 1.37 times for the pile cap, while the displacement of TSA was less than around 0.67 times for the superstructure and 0.56 times for the pile cap. As a result, in case of $1/5G_o$ seismic response in TSA had not agreement with that in the experiment.

4.5.3 Comparison

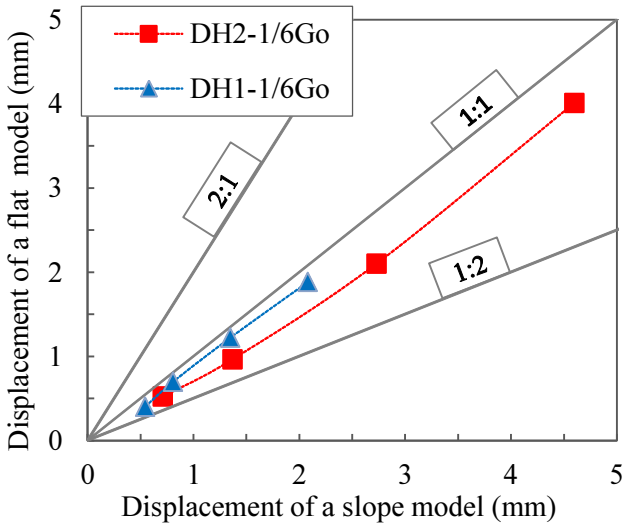

Fig.4.8 Comparison of horizontal displacement in case of $1/6G_o$ at DH1 and DH2

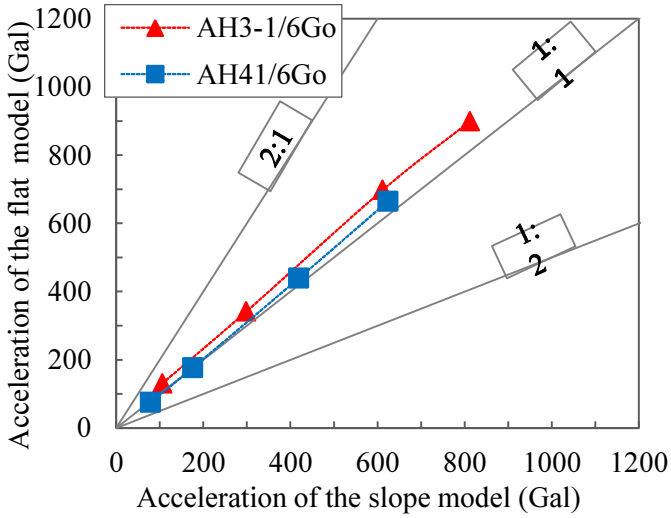

Fig.4.9 Comparison of horizontal acceleration in case of $1/6G_o$ at DH1 and DH2

The comparison of horizontal displacement at DH1 and DH2 in case of $1/6G_o$ between two models is shown in **Fig.4.8.** The entire comparison line of DH1 and DH2 was below the line ratio 1:1 toward the slope model. It means that the displacement of superstructure and pile cap in the slope model was larger than that in the flat model during shaking from 50 to 300 Gal. The comparison of horizontal acceleration at AH3 and AH4 in case of $1/6G_o$ between two models is shown in **Fig.4.9**. The comparison line of AH3 and AH4 was almost above the line ratio 1:1 toward the flat model. It means that the acceleration of superstructure and pile cap in the slope model was less than that in the flat model during shaking from 50 to 300 Gal. However, the difference of acceleration was quite small.

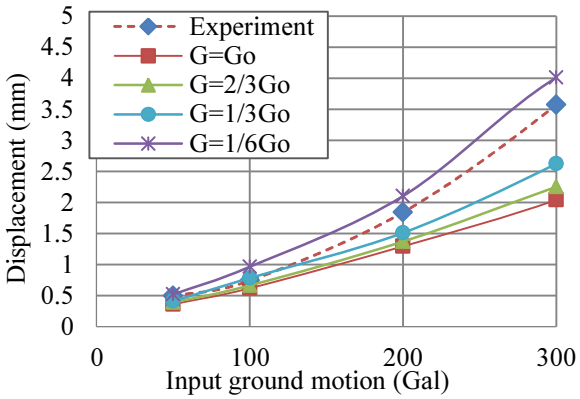

Fig.4.10 Displacement of superstructure in the flat model.

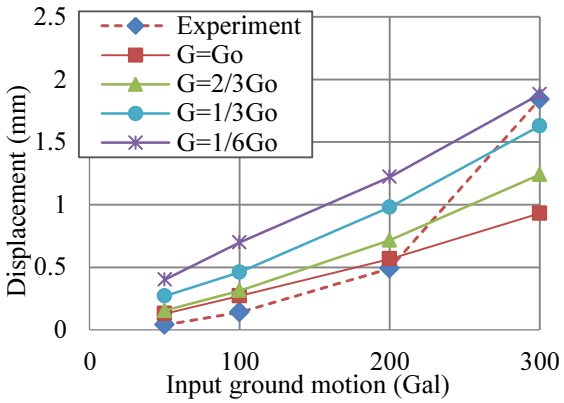

Fig.4.11 Displacement of pile cap in the flat model.

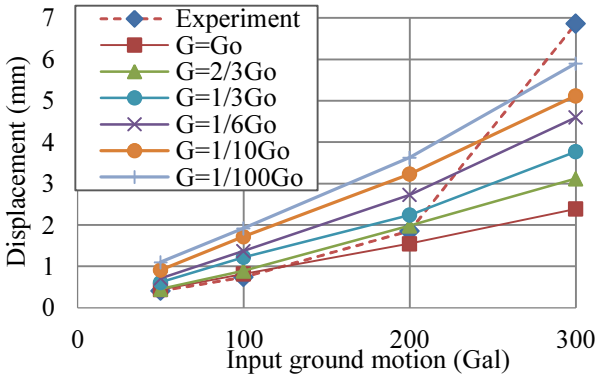

Fig.4.12 Displacement of superstructure in the slope model.

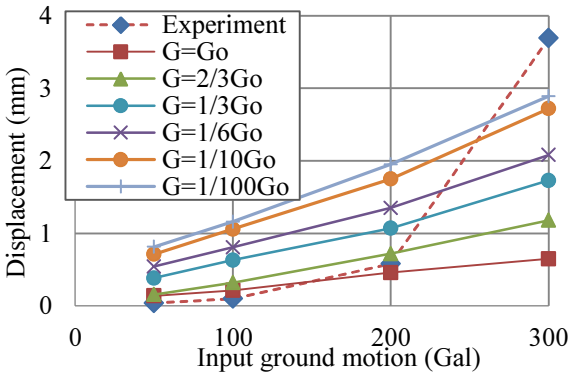

Fig.4.13 Displacement of pile cap in the slope model.

The maximum horizontal response displacement of the superstructure and pile cap in the flat model experiment illustrated in **Figs.4.10** and **4.11**, respectively, resembles the displacement in the TSA for the initial shear modulus G_o case. Next, from 150 Gal to 200 Gal, the displacement of the experiment was within the range of the displacement of $2/3G_o$ and $1/3G_o$ in the TSA case. Finally, in the 300 Gal case, the displacement of the experiment was in the range of $1/3G_o$ to $1/6G_o$. Clearly, the results suggest that in the flat model, the TSA method stipulated in JRA 2002 can suitably produce the response by reducing the shear modulus of the liquefaction sand layer.

As for the slope model **Figs.4.12** and **4.13** show that there was a similar resemblance in the displacement in cases from 50 to 200 Gal. However, in the 300 Gal case, the maximum displacement of the slope model was over the maximum displacement of the $1/100G_o$ case. The result indicates that in the case of high amplitude input ground motion, the TSA method may not produce a good agreement of response displacement with the experiment.

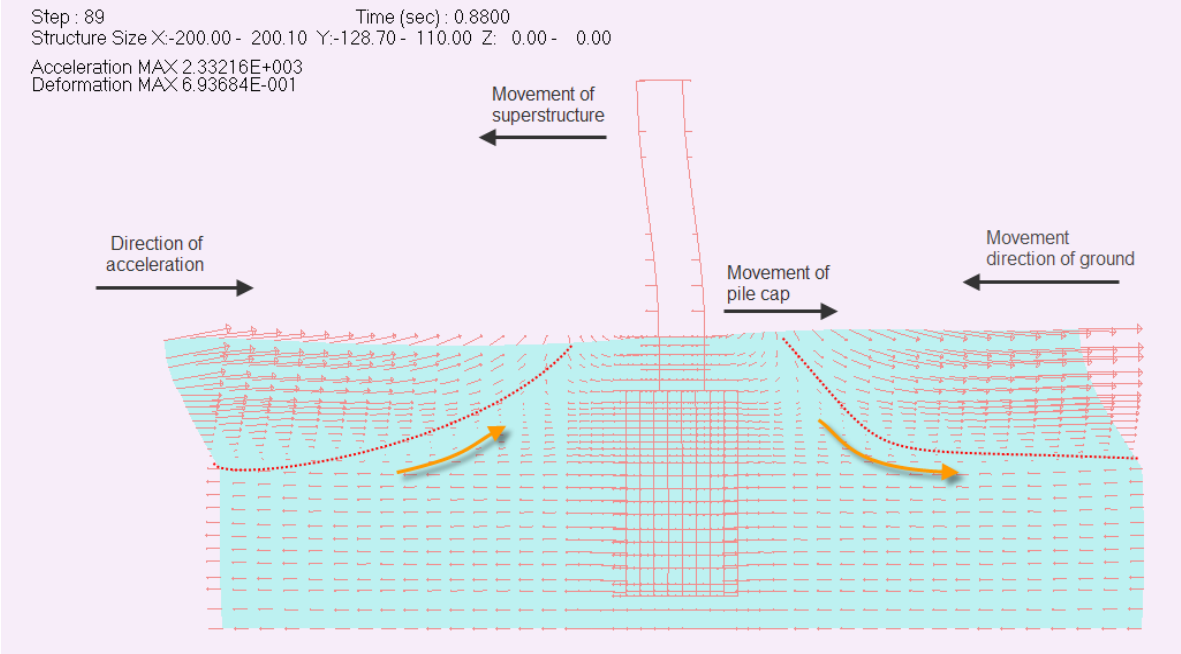

Fig.4.14 Behavior of ground in the flat model in case 300 Gal input ground motion

4.6 Behavior of Ground

4.6.1 Horizontal acceleration and displacement of ground

Tokimatsu et al. (2005) suggested that as the natural frequency of superstructure is less than that of ground, the kinematic force is out of phase with the inertial force. Inversely, if the natural frequency of superstructure is larger than that of ground, the kinematic force is in phase with the inertial force.

The frequency of soil ground was 22 Hz for a liquefaction layer and 32 Hz for a non-liquefaction layer, as determined by **Eq.4.5.** The determined frequency of ground was around 4 times larger than that of superstructure. As a result, this is in agreement with observations in the **Figs 4.14** and **4.15.** Therefore, the displacement and acceleration of superstructure was out of phase with that of foundation in the both models. This is in an agreement with the dynamic response result in the experiment

$$f = \frac{v_s}{4H} \tag{4.5}$$

Where *f*: is a frequency of soil layer; v_s*:* is a shear wave velocity of soil layer; *H:* is a height of the soil layer.

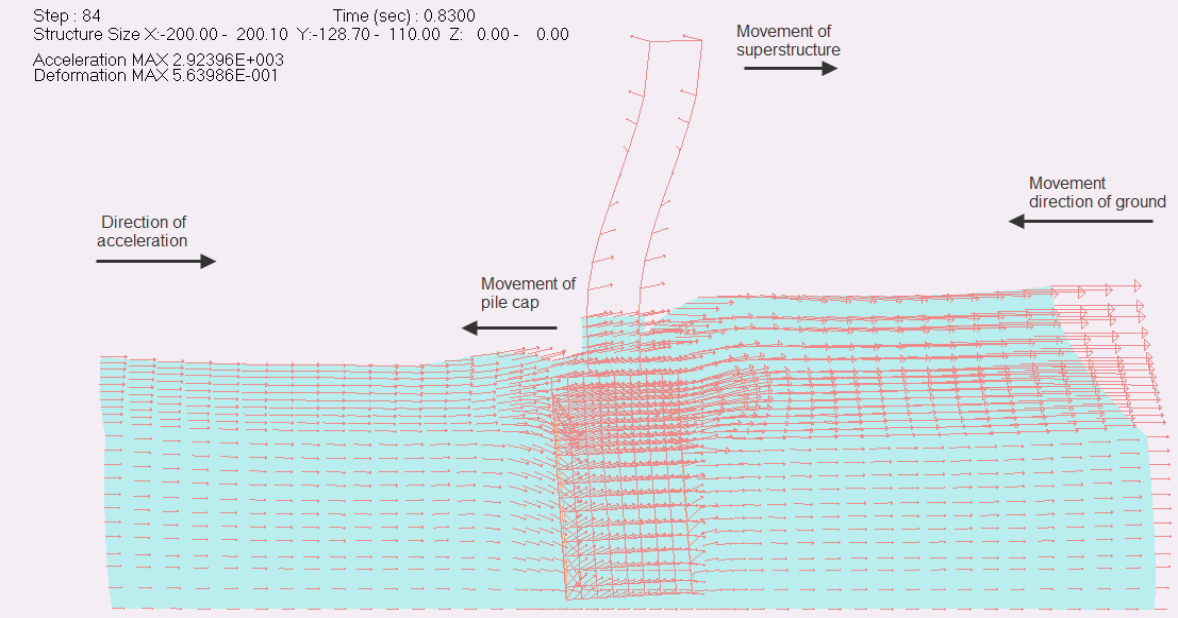

Fig.4.15 Behavior of ground in the slope model in case 300 Gal input ground motion

Figs.4.14 and **4.15** also show behavior of ground including the movement and horizontal acceleration in the ground under 300 Gal in the flat and slope modes, respectively. It seen that the acceleration increased from the bottom to surface of ground. The acceleration direction of soil surrounding the foundation in the slope model complexly changed during shaking, at the time of 0.83 s the acceleration direction of soil element on the front side of foundation moved down and that on the back side moved up. While, in the flat model the acceleration was almost in the horizontal direction. This phenomenon is shown in **Fig.4.14.**

The comparison of ground horizontal acceleration in the slope model from 50 to 300 Gal is shown in **Fig.4.16**. The increase of acceleration was in accordance with the increase of input ground motion. The **Fig.4.16** indicates that the difference at AH9 and AH13 of near field between TSA and the experiment was quite small from 50 to 300 Gal. While, the difference of acceleration between them at AH6 and AH16 of far field was small from 50 to 150 Gal but became much larger from 200 to 300 Gal. The larger difference is because the nonlinear properties of soil became more significant during liquefaction with a reduction of shear modulus but TSA did not consider the nonlinear in this study. Therefore, there was a good agreement in the near field and in the far field and TSA may not produce a good agreement in the far field.

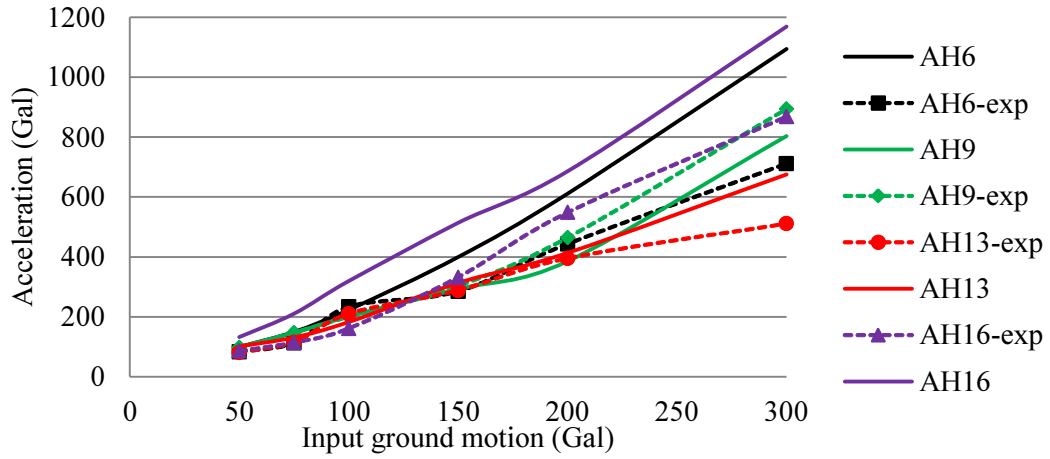

Fig.4.16 Horizontal acceleration of ground in the slope model in case 300 Gal input motion

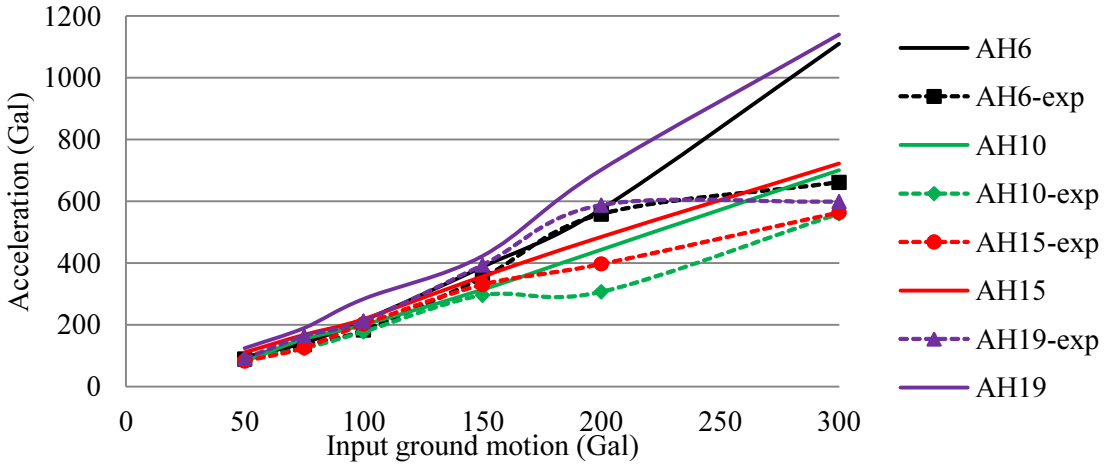

Fig.4.17 Horizontal acceleration of ground in the flat model in case 300 Gal input ground motion

The comparison of ground acceleration in the flat model in case of 300 Gal is shown in **Fig.4.17**. This figure also shows the same trends with the slope model. The increase of acceleration was in an accordance with an increase of input ground motion. There was a good agreement of acceleration in the near field between the total stress analysis (TSA) and the experiment; while, in the far field the difference between them was greatly significant. This is a limitation of TSA in performing the dynamic behavior of SPSP foundation during liquefaction or liquefaction induced lateral spreading.

4.6.2 Reaction stress

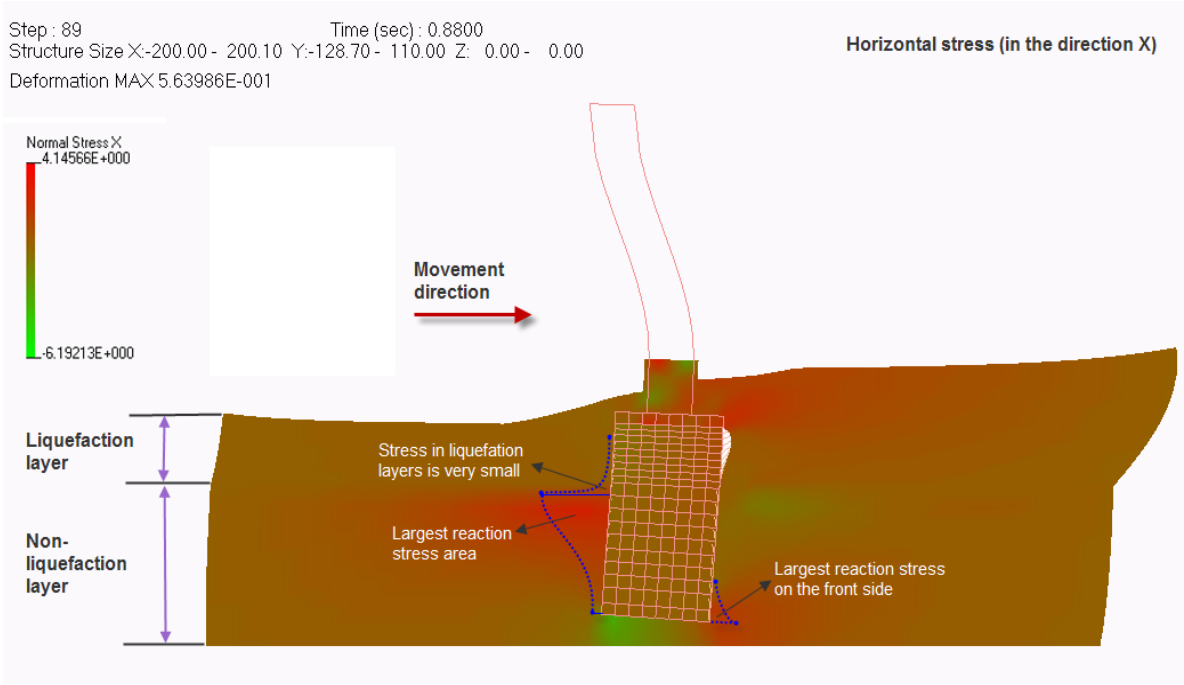

Fig.4.18 Distribution of horizontal reaction stress in the slope model in case of $1/6G_o$

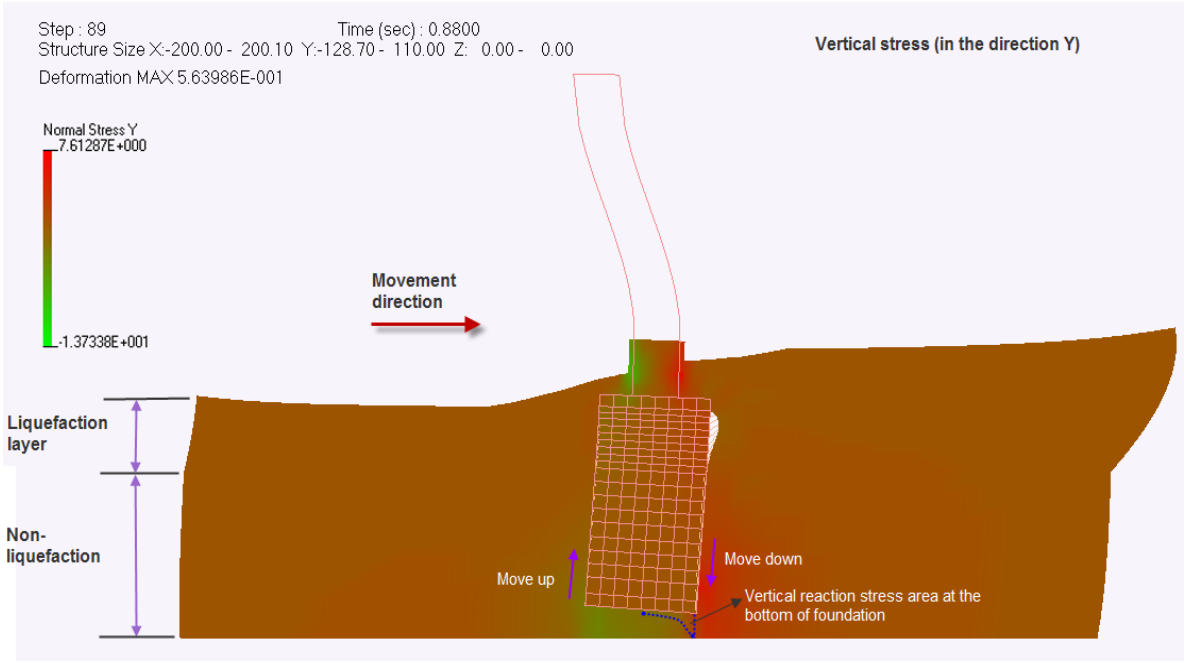

Fig.4.19 Distribution of vertical reaction stress in the slope model in case of $1/6G_o$

Fig.4.18 presents the distribution of horizontal reaction stress of ground in the slope model in case of 1/6Go. It is observed that the reaction stress in the liquefaction layer was very small; while, the reaction stress values in the non-liquefaction layer were largest at the back side of foundation bottom. The distribution of the stress became smaller in the deeper

layer. The maximum reaction stress also was observed at the font side of foundation bottom but its distribution became smaller in the deeper layer. Their distribution is shown in **Fig.4.18.**

The vertical stress at the bottom (in the direction Y) shows that the largest compressive reaction stress was observed at the front bottom of foundation, its distribution is shown in the **Fig.4.19**. This figure also shows that the soil on the back side of foundation moved up, while, the soil on the front side moved down. It means that the foundation inclined following to the movement of ground.

4.7. Conclusions

The numerical method using the total stress analysis in consideration of specification JRA 2002 by reducing the soil shear modulus in the liquefaction verification was conducted on two models. There are some main findings as follows:

(1) The second natural frequency of models is significantly affected by a reduction of soil shear modulus in the liquefaction verification. The difference of dynamic characteristic between the flat and slope models is also significant in the second frequency.

(2) The displacement response of the slope of the superstructure and pile cap in the slope model is larger than that in the flat model, while its acceleration response becomes smaller. However, the total stress analysis provides smaller responses of displacement than that in experiment.

(3) Total stress analysis using the linear reduction of shear modulus produces a good agreement of horizontal acceleration with the experiment in the near field but in the far field there is not an agreement between them. The acceleration behavior of soil around the foundation in the slope model is really complex in the movement direction because of the soil movement in the slope ground.

(4) The result of the TSA indicates that the dynamic response displacement of the TSA with a reduction of shear modulus agrees reasonably well with that of the experiment in the flat model. However, the TSA method cannot provide a reasonable response displacement for the slope model even for case reduced the shear modulus until 1/100 G_o. This is because the displacement of the ground was estimated to critical side when the sand was liquefied.

(5) The horizontal reaction stress is smaller in the liquefaction layer when shear modulus of soil increases. It means that reaction stress in the liquefaction layer increases when the liquefaction occurs.

Reference

1) JRA (2002): Specifications for highway bridges. Japan Road Association, Preliminary English Version, *Public Works Research Institute (PWRI) and Civil Engineering Research Laboratory (CRL)*, Japan.
2) Kurimoto, O. Takeshi, F. Yuzuru, Y. (2001). Seismic response of pile-supported structure considering nonlinearity of superstructure and pile, and liquefaction of surrounding ground , *The second UJNR Workshop on SSI*, Tsukuba, Japan.
3) Trung, N.T. Kiyomiya, O. An, T.X. (11/2012). Verification of influence on seismic performance of SPSP foundation under the 2011 pacific coast p of Tohoku earthquake. *Proceedings of the 1th International Symposium on Earthquake engineering of JAEE*, Tokyo, Japan.
4) An T.X., Kiyomiya O. (9/2012). Trung N.T. Seismic Performance of Steel Pipe Sheet Pile Foundation on Soft Ground. *Proceedings of the 15th of World Conference in Earthquake Engineering,* Lisbon, Portugal.
5) An T.X., Kiyomiya O. Hung T. V. and Kochi R. (2011). Nonlinear dynamic analysis of soil-steel pipe pile sheet-structure interaction under seismic excitation, *Proceedings of the 35th International Symposium on Bridge and Structural Engineering*, jointly organized by IABSE-IASS, London, UK
6) Wolf, J.P. (1985). Dynamic Soil-Structure interaction, Prentice-Hall, Inc., Englewood Cliffs, New Jersey.
7) Mylonakis G., and Gazetas G. (2000). Seismic soil–structure interaction: beneficial or detrimental , *Journal of Earthquake Engineering*, Vol. 4, Issue 3, pp.277–301.
8) Mylonakis G., Gazetas G., Nikolaou S. and Michaelides O. (2000). The role of soil on the collapse of 18 piers ofthe Hanshin Expressway in the Kobe Earthquake, *12th World Conference on Earthquake Engineering*, New Zealand.
9) Tuladhar R., Mutsuyoshi H. and Maki T. (2008). Seismic Behavior of concrete bridge pier considering soil-pile-structure interaction, *The 14th World Conference on Earthquake Engineering*, No. 02-0075, October, Beijing, China, pp.12-17.
10) Boris J., Sashi K., and Feng X. (2004). Influence of soil-foundation-structure interaction on seismic response of the I-880 Viaduct, *International Journal for Engineering Structures*, Vol. 26, Issue 3, pp.391-402 Khalil L.,
11) Sadek M., and Shahrour I. (2007). Influence of the soil–structure interaction on the fundamental period of buildings, *Earthquake Engineering and Structural Dynamics, Vol. 36*, pp.2445–2453.
12) Tokimatsu, K., Suzuki, H. and Sato, M. (2004): Influence of inertial and Kinematic components on pile response during earthquakes. *Proc., 11th International Conference on Soil Dynamics*

and Earthquake Engineering, pp.768-775.

13) Tokimatsu, K., Suzuki, H and Suzuki, Y (2001): Back-calculated p-y relation of liquefied soils from large shaking table tests", *Proceedings of the 4th International Conference on Recent Advances in Geotechnical Earthquake Engineering and Soil Dynamics and Symposium*, in Honor of Professor W.D.Liam Finn, San Diego, California.

14) Tokimatsu, K (1999): "Performance of pile foundations in laterally spreading soils", *Proceedings of the 2nd International Conference on Earthquake Geotechnical Engineering*, Lisbon, Portugal, June 21-25, Vol 3, pp. 957-964.

This page intentionally left blank

Chapter 5

Dynamic Effective Stress Analysis

5.1 Introduction

The numerical method using the TSA based on the specification JRA 2002 mentioned in the chapter 3 is a linear equivalent approach. This method may predict rough seismic responses of pier foundation system but it is difficult to completely perform the behavior of foundation and ground in the consideration with pore water pressure buildup of ground. Therefore, another advantaged numerical method using an effective stress analysis (ESA) was also considered in the study.

The effective stress analysis is one of the most advanced numerical analyses in geotechnical engineering. It allows simulating a complex dynamic behavior of soils during liquefaction with generation and dissipation of pore water pressures in the long term. Recently, two theory models of soil elements suggested by Iai et al. (1992, 2010) adopted in seismic design work for the evaluation of liquefaction problems including assessment of liquefaction-induce lateral spreading. The first model is a Multi-spring model in the un-drain condition and another is a Glass cocktail model in the drain condition. The FLIP program (developed by Port and Airport Research, Institute, Yokosuka, Japan) was used in this analysis. The 2D numerical model was applied to both the flat and slope models of vibration test. The liquefaction parameters were also determined from soil characteristics of ground of test model. The numerical result of analysis would be compared and evaluated with a seismic response of experiment.

5.2 Adopted Theory Models of Soil

5.2.1 Multi-spring model

The soil was modeled as plane strain elements using two liquefaction models of the loose sand. The first model is called a multi-spring model and is shown in **Fig.5.1**. The multi-spring model is a strain-space multiple-mechanism model. This model approach was firstly

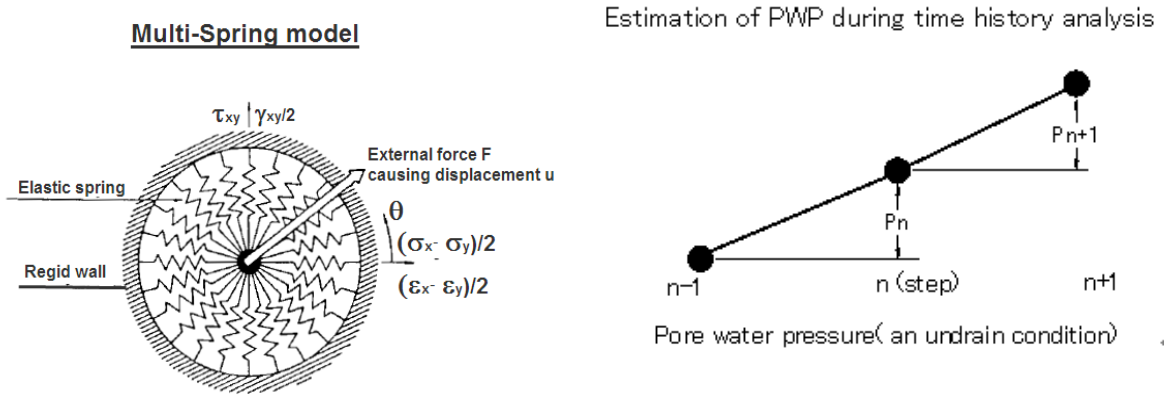

Fig.5.1 Multi-spring model in effective stress analysis

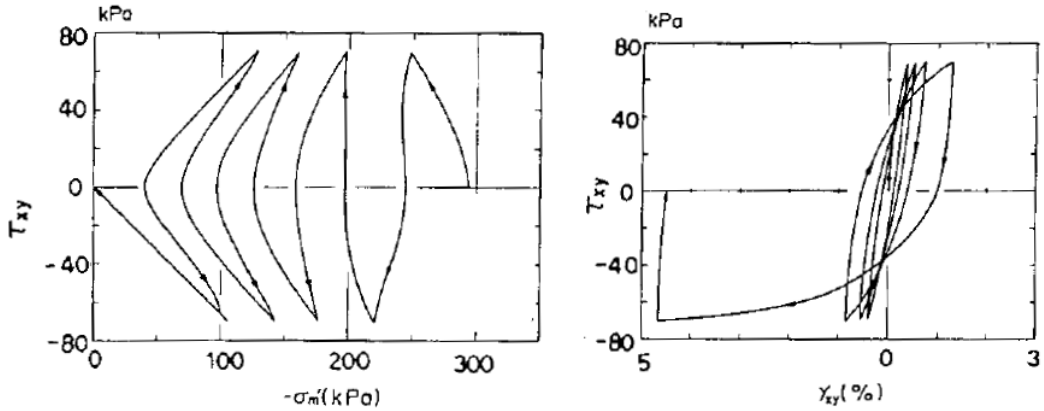

Fig.5.2 Calculation result of stress and strain by a Multi-spring model (Iai et al. 1992)

proposed by Towhata and Ishihara et al. (1985). It postulated that the actual shear force mechanism was associated with multiple inelastic springs that were defined by the relationship between the stress and strain. Towhata and Ishihara (1985) and Miura et al. (1986) proposed two assumptions. Firstly, the rotation of principal stress axes results in the increase of pore water pressure in the un-drained condition. Secondly, the direction of strain does not coincide with that of principal stress. The multi-spring model considers the effects of rotation on the behavior of cohesion-less soil. The result of calculating the multi-spring model is shown in **Fig.5.2**.

5.2.2 Glass cocktail model

The second model is a Cocktail glass model improved from a strain-space multiple-mechanism model in the drained condition suggested by Iai et al. (2011), as shown in **Fig. 5.3**. There are two main assumptions in this model. Firstly, the volumetric strain ε_d is decomposed in a dilative component ε_d^d and contractive component ε_d^c, as shown in **Eq.**

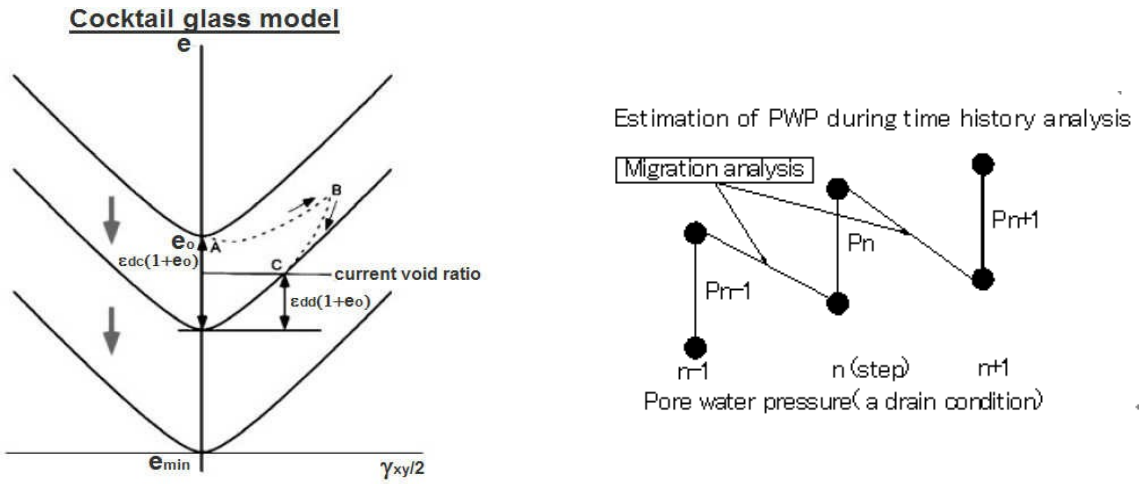

Fig.5.3 Cocktail glass model in effective stress analysis

5.1. The dilative component affects to a dissipation of pore water pressure in the steady state and horizontal displacement response. The contractive component can lead the failure of soil or an increase of magnitude of response of soil movement while the dilative component can limit the magnitude. The motivation of the division is due to the dilatancy at the minimum void ratio of cohesion-less soil is impossible to produce a contraction and during the cyclic shear volumetric strain is contractive if cohesion-less soil accumulates non-reversible damages. The curve of the relationship between the volumetric strain and shear strain is similar to a cocktail glass; hence, it is called a cocktail glass model. The second is a relationship between relative velocity and coefficient of permeability determined as follows:

$$\varepsilon_d = \varepsilon_d^c + \varepsilon_d^d \tag{5.1}$$

Where ε_d is a volumetric strain of dilatancy; ε_d^c is a contractive component; ε_d^c is a dilative component. This assumption influences the rate of pore water development and dissipation.

Ozutsumi et al. (2000) presented a migration of water was obtained by multi dimension equation of consolidation by Biot:

$$\{k(\theta)h_i\}_i - \left(\frac{\partial \delta_{i,i}}{\partial t}\right) S_r - C(\psi)\left(\frac{\partial h}{\partial t}\right) = 0 \tag{5.2}$$

Where $k(\theta)$ is a coefficient of permeability; ψ is a pressure head; $C(\psi) = n\left(\frac{\partial S_r}{\partial \psi}\right)$ is a relative water content; n is a porosity; S_r is a degree of saturation; h is a hydraulic gradient : δ is a displacement. k is determined by the sand size and the void ratio in the test vessel.

5.3 Modeling Methodology

5.3.1 Numerical models

The numerical models in the ESA for the slope and flat models are shown in **Figs.5.5** and **5.6,** respectively. The foundation was divided into 5 parts with equal width in horizontal direction in plan, and each part was represented by a beam at its center. The connection between two piles was rigid. The piles, pier columns, and acrylic plate at the top of the pier were modeled as elastic beam elements. The steel footing plate and acrylic cap of the piles were modeled as plane strain elements. The soil was modeled as plane strain elements using two liquefaction models of the loose sand. The first model is a multi-spring model and second model is a glass cocktail model, as described the above part. Along the soil-pile interface, the piles and adjacent soil elements were connected by joint elements in the vertical and horizontal directions. The horizontal joints were modeled as cut-off tension springs. The joint elements in the FLIP program have the same behavior characteristic with the spring element in the TDAP III program. The **Table 5.1** and **Fig.5.4** show the joint properties in the numerical models. The hydrodynamic pressure acting along the slope surface of the revetment was considered using fluid elements.

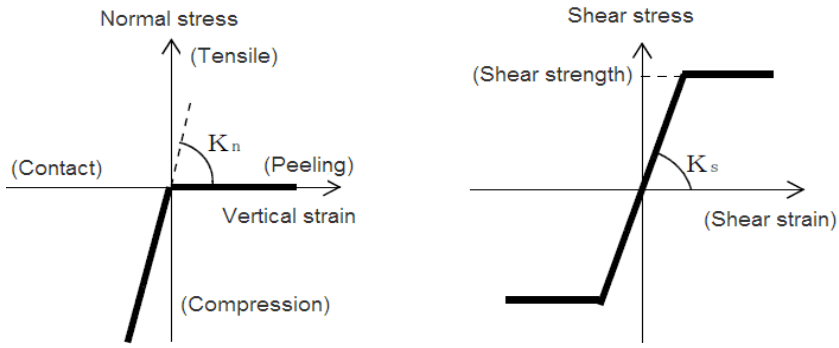

Fig.5.4 Joint property of interface element between soil and the foundation

Table 5.1 Joint parameters of soil-foundation interaction in the numerical model

Position	Width m	Rigidity normal direction, K_n kPa	Rigidity tangent direction, K_s kPa	Adhesion c_J kPa	Friction angle f_J
Footing	0.466	1,000,000	1,000,000	0	26.6
Surface and sides	0.608	1,000,000	1,000,000	0	26.6
Bottom of foundation	0.608	1,000,000	1,000,000	0	26.6

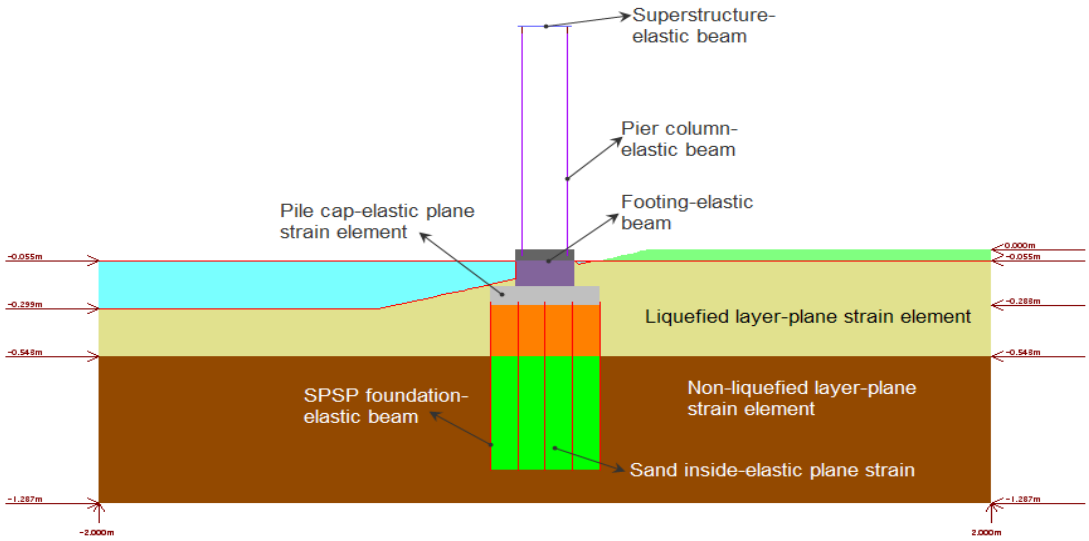

Fig.5.5 Numerical slope model in Effective Stress Analysis (ESA)

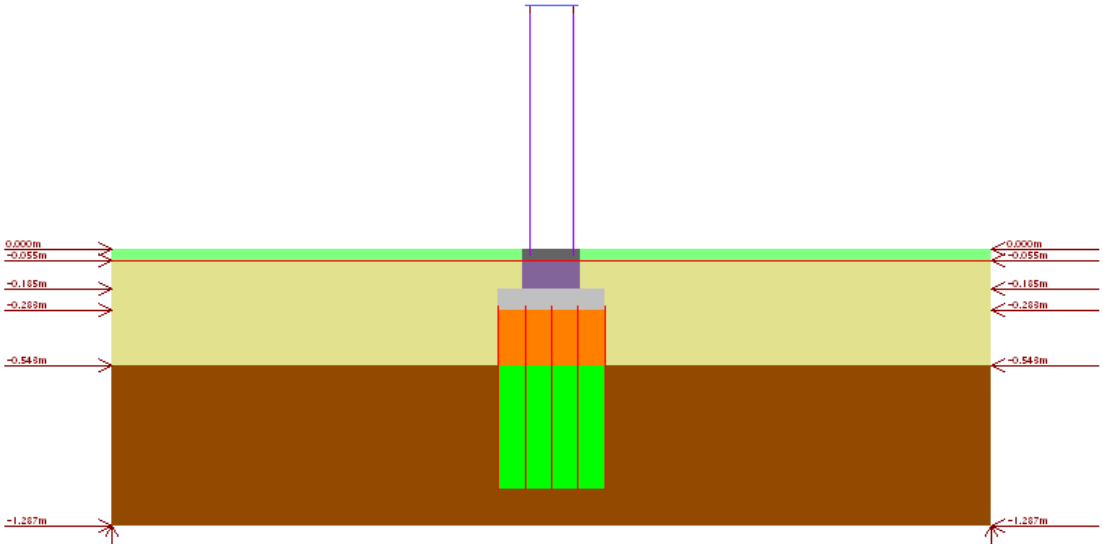

Fig.5.6 Numerical flat model in Effective Stress Analysis (ESA)

5.3.2 Boundary condition

The boundary at the bottom of the model was fixed in the vertical and horizontal directions, and the lateral boundary at the two sides was fixed in the horizontal direction. It is similar to the boundary in TSA. In both of the analyses, the self-weight analysis step was conducted first to calculate the initial stress and strain of the model before the calculation of the dynamic analysis. v

5.3.3 Rayleigh damping

The numerical integration was performed using the Wilson-θ method with θ = 1.4. A Rayleigh damping method with parameters α = 0 and β = 0.002 was used to ensure the

numerical stability of the analysis. There are some methods to determine the Rayleigh damping β, one of them was mentioned in the research. The factor was determined by **Eq.5.3**.

$$\beta = \frac{h}{\pi f} \tag{5.3}$$

Where h: is a damping ratio of the soil ground, value of 0.1 was used in this calculation; f: is the average of typical frequency of ground, as determined by **Eq.5.4**

$$f = \frac{\sum v_{si} H_i}{\sum H_i^2} \tag{5.4}$$

Where H_i: is the height of ith soil layer and v_{si}: is a shear wave velocity of ith soil layer.

5.4 Verification Procedure

5.4.1 Determination of liquefaction parameter of soil element

5.4.1.1 Liquefaction front

The **Fig.5.6** shows that the liquefaction front is an envelope of stress points of shear work moves from the initial to the failure lines, in which shear work is an effective mean stress ratio. The shear work is accumulated by cyclic shear under un-drained condition. The transformation line suggested by Ishihara et al. (1975) and performs the dilative zone in the stress space from contractive zone. The correlation between the liquefaction front and shear work as follows:

$$S_o = 1 - 0.6\left(\frac{w}{w_1}\right)^{p_1} \qquad (if\ w < w_1) \tag{5.5}$$

$$S_o = (0.4 - S_1)\left(\frac{w_1}{w}\right)^{p_2} \qquad (if\ w > w_1) \tag{5.6}$$

Where S_1, w_1, p_1 and p_2 are parameters of cohesion-less soil represented for the cyclic mobility.

S_o is a parameter to be defined by the function of shear work; m_1 is an inclination of the failure line, defined by the shear resistance angle; m_2 is an inclination of the transformation phase line, defined by the transformation angle; m_3 is an inclination of auxiliary line as determined to ensure the smooth transition.

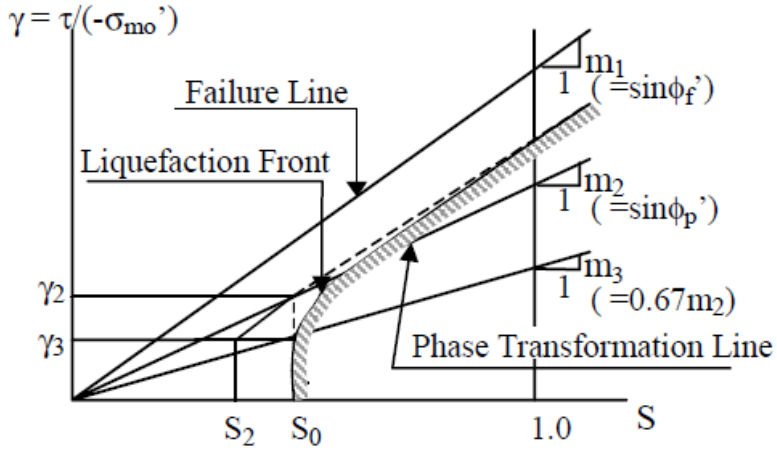

Fig.5.7 Liquefaction front and relationship between shear stress ratio and shear work.

5.4.1.2 Multi-spring model parameters

Parameter S_1 is recommended to take a value of 0.005 so that S_o never will be zero. The c_1 is used to specify the threshold level and depends on the fine content (%) (Percentage by mas of fine soil passing through the 75μm meshes F_c and equivalent SPT N value, as shown in **Fig.5.7.** The parameter p_2 is determined by **Eq.5.7** and ranges from 0.6 to 1.5. There larger p_2 is, the faster the shear strain amplitude increase.

$$p_2 = -0.016N_a + 1.215 \tag{5.7}$$

Because w_1 is not influenced by variation of p_1 so value of p_1 firstly determined with ranges from 0.4 to 0.7. Generally, the larger the p_1 and the larger w_1, the more slowly generation of pore water pressure. The value of w_1 is determined by **Fig.5.8**. The influence of stress (or strain) history on cyclic deformation-strength characteristics of soil in the liquefaction layer is shown in **Fig.5.9**. The figure shows relationship between stress and strain of liquefaction layer in both the indoor three axial vibration test and ESA. **Fig.5.10** shows the relation between the shear stress and mean effective stress in the sand model.

4.4.1.3. Glass cocktail model parameters

The liquefaction parameters of the soil layers for cocktail glass models were determined using the shear modulus and relative density of the sand, among other parameters, which are summarized in **Table 5.2**. The parameter r_K is to determine the difference of bulk modulus for drained and un-drained conditions. The power index l_K is allowed to take the value larger than or equal to unity to simulate the liquefaction where the contractive component of dilatancy captures the volumetric strain, it ranges from 1 to 5%. The

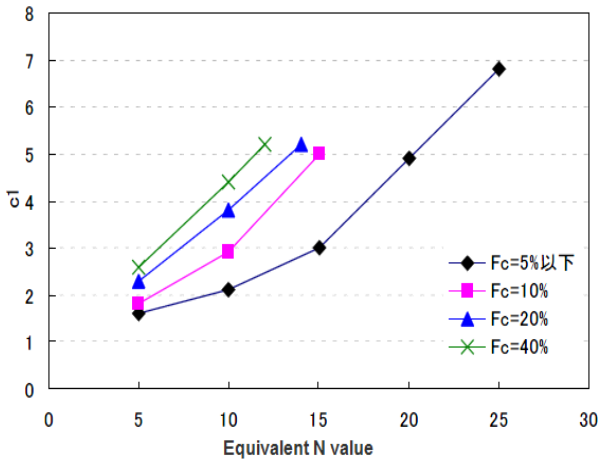

Fig.5.8 Determination of threshold limit of dilatancy

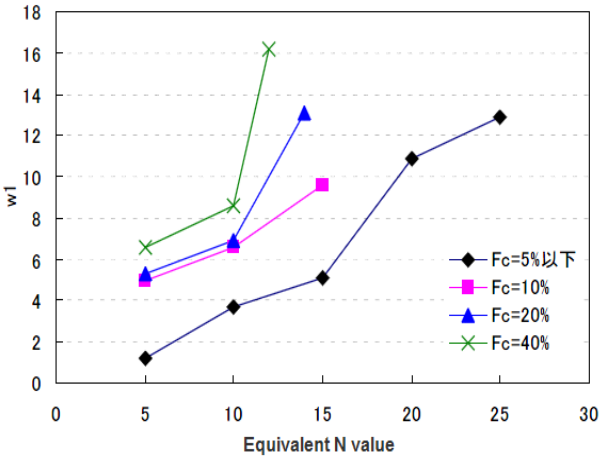

Fig.5.9 Determination of initial phase of cumulative dilatancy

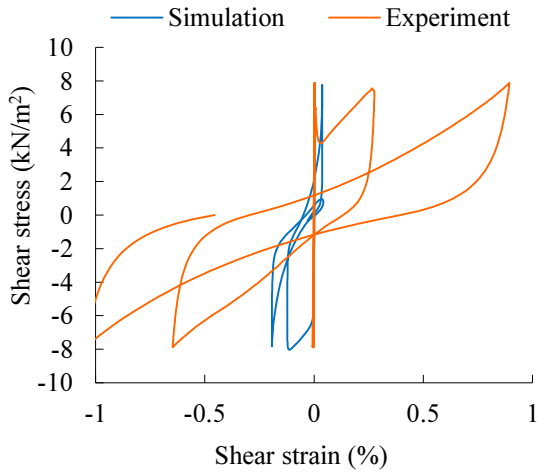

Fig.5.10 Stress-strain curves from liquefaction parameters

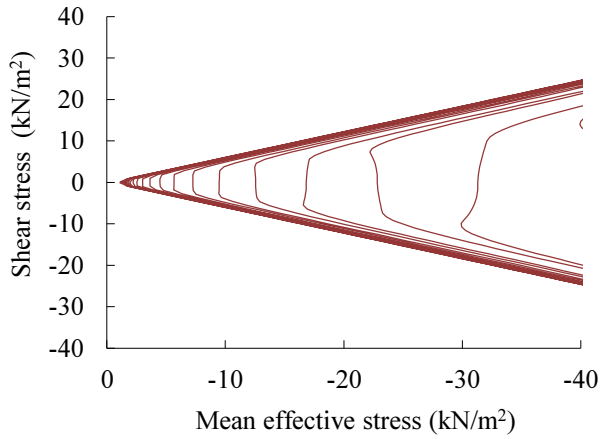

Fig.5.11 Effective stress paths from liquefaction parameters

coefficient of permeability for sand using the cocktail glass model was determined by the Kozeny-Carman et al. (2003) as follows:

$$k = C\frac{g}{\mu_w \rho_w}\frac{e^3}{S^2 D_R^2(1+e)} \tag{5.8}$$

Where k is a coefficient of permeability; C is a constant; μ_w is a dynamic viscosity of water; ρ_w is a density of water; D_R is a specific weight of sand; S is a specific surface; and e is a void ratio.

Table 5.2 List of soil parameters

Parameter		Symbol	Liquefaction layer
Parameters for Muti-Spring model	Phase transformation angle	ϕ_p(degree)	28
	Overall cumulative dilatancy	w_1	8.2
	Initial phase of cumulative dilatancy	p_1	0.45
	Final phase of cumulative dilatancy	p_2	1.07
	Threshold limit for dilatancy	c_1	4.48
	Ultimate limit of dilatancy	S_1	0.005
Parameters for Cocktail glass model	Reduction factor of bulk modulus for liquefaction analysis	r_K	0.5
	Power index of bulk modulus for liquefaction analysis	l_K	2
	Parameter controlling dilative and contractive components	$r_{\varepsilon d}$	0.5
	Parameter controlling contractive component	$r^c_{\varepsilon d}$	2
	Parameter controlling initial phase of contractive component	q_1	1
	Parameter controlling final phase of contractive component	q_2	1
	Limit of contractive component	ε^{cm}_d	0.5
	Small positive number to avoid zero confining pressure	S_1	0.005
	Parameter controlling elastic range for contractive component	c_1	4.48

5.4.2 Calculation procedure

The procedure of calculation using the effective stress analysis consists of the following steps: 1) these reduction factors of shear modulus in the flat model were calculated by using the specification JRA-2002; 2) To perform the behavior of foundation and ground in the un-drained condition by a multi-spring model; 3) To perform the behavior of foundation and ground in the drained condition by a glass cocktail model; 4) Evaluation of dynamic response between two models and the experiment.

5.5 Dynamic Response Result

5.5.1 Excess pore water pressure

The time histories of the EPWP at points W4 and W8 of ESA and the experiment under the 300 Gal input ground motion are shown in **Fig.5.12** for the flat model. The results of the EPWP among the experiment, multi-spring model, and cocktail glass model are fairly different from each other. The liquefaction starting time was at 7.5 s, whereas the EPWP dissipation, maximum EPWP ratio, and vibration components differed considerably. The EPWP ratio gradually decreased after the vibration stopped in the vibration test; this phenomenon can be explained using the cocktail glass model. The cocktail glass model displayed a cyclic component of the EPWP, but the reasoning behind this component is not clear. As soil was liquefied the liquefaction time in both numerical models was around 2 s. It is in the same trend with the experiment.

The time histories of the EPWP at points W4 and W8 of ESA and the experiment under the 300 Gal input ground motion are shown in **Fig.5.13** for the slope model. The cyclic components of EPWP were observed in both the both the glass cocktail model and vibration test

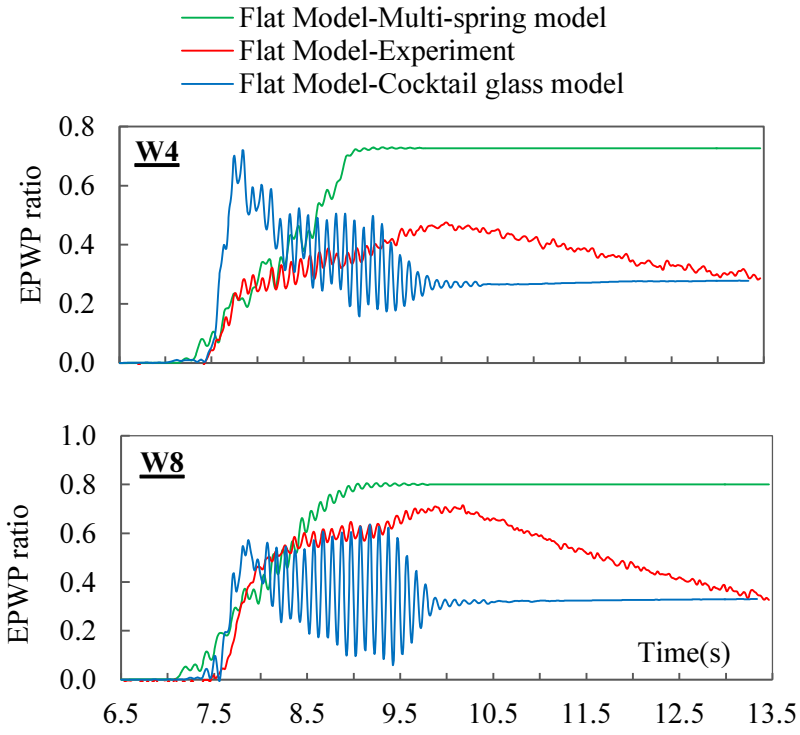

Fig.5.12 Time history of EPWP ratio at W4 and W8 in the flat model under 300 Gal.

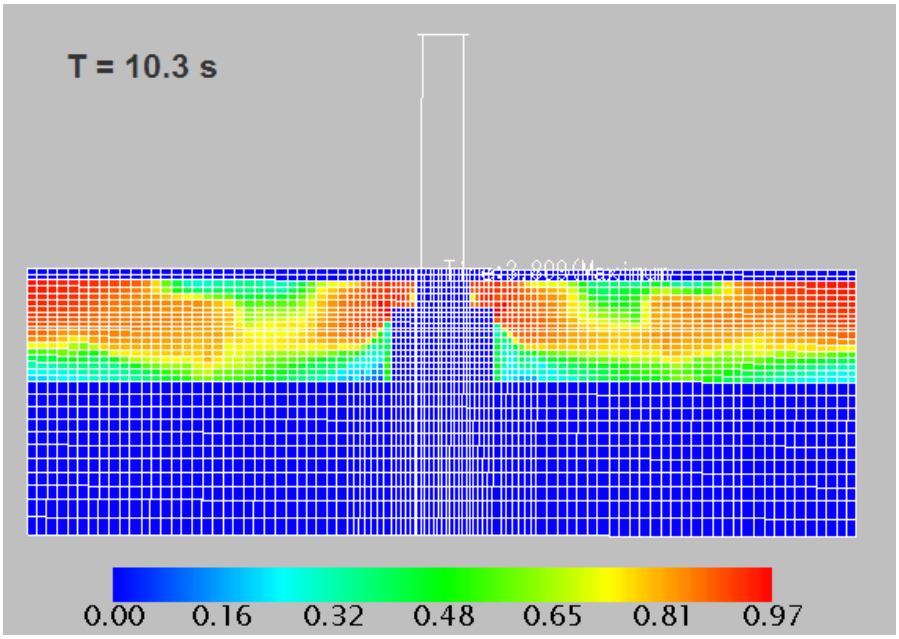

Fig.5.13 EPWP ratio distribution in flat model under 300 Gal.

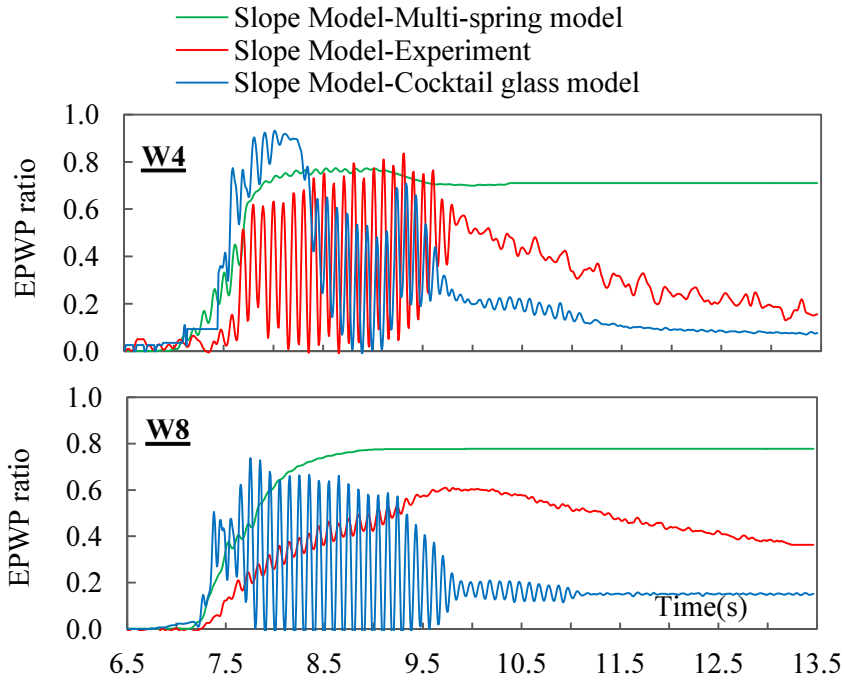

Fig.5.14 Time history of EPWP ratio at W4 and W8 in the slope model under 300 Gal

The EPWP ratio distribution of the ground under 300 Gal is shown in **Fig.5.14** for flat model. The EPWP ratio reached approximately 1.0 at the surface liquefied layer after 10.3 s. However, the EPWP was not uniform at the surface layer in the multi-spring model. The EPWP ratio gradually decreased after the vibration stopped in the experiment; this phenomenon can be explained using the cocktail glass model. EPWP ratio was almost same between the experiment and the cocktail model after 12 s. However, the generation and

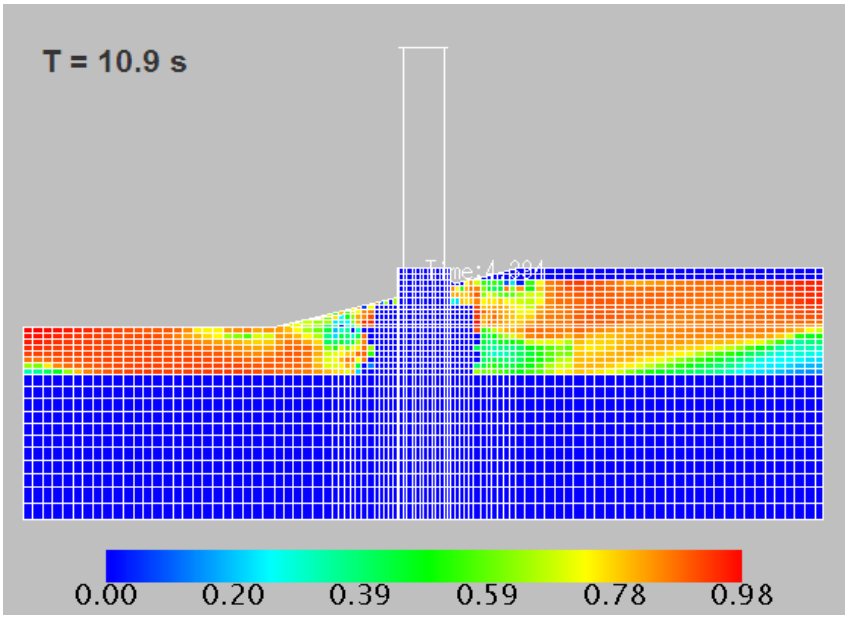

Fig.5.15 EPWP ratio distribution in slope model under 300 Gal.

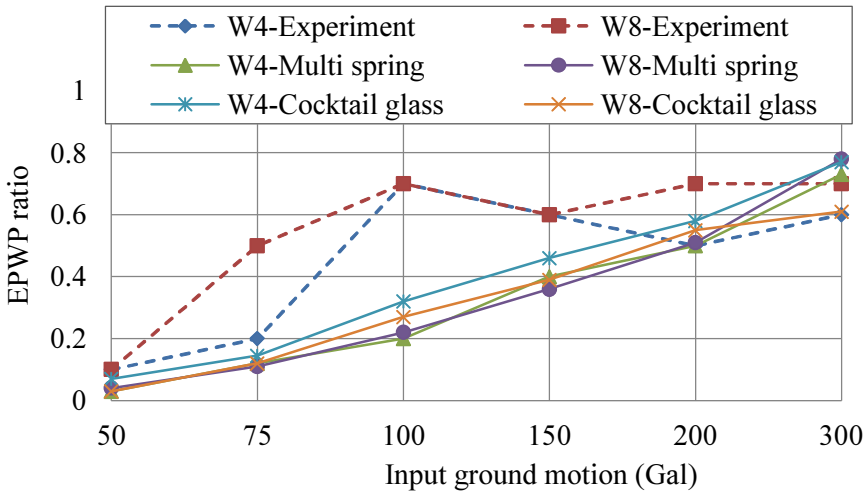

Fig.5.16 EPWP ratio in the flat models from 50 to 300 Gal

dissipation of EPWP in the model occurs very quickly during vibration time of 2 s. The cocktail glass model displayed a vibration component of the EPWP. We assumed that the quick dissipation of EPWP was due to large value of coefficient of permeability of the test sand and low value of water viscosity. These items are limitation of 1-G vibration model test.

It is also assumed that the vibration component was due to unstable calculation of by double integrations of the constitutive equation. The EPWP ratio distribution of the ground in the slope model under 300 Gal is shown in **Fig.5.15**. The EPWP ratio also reached approximately 1.0 at the surface liquefied layer after 10.9 s. However, the EPWP was almost uniform at the surface layer in the multi-spring model.

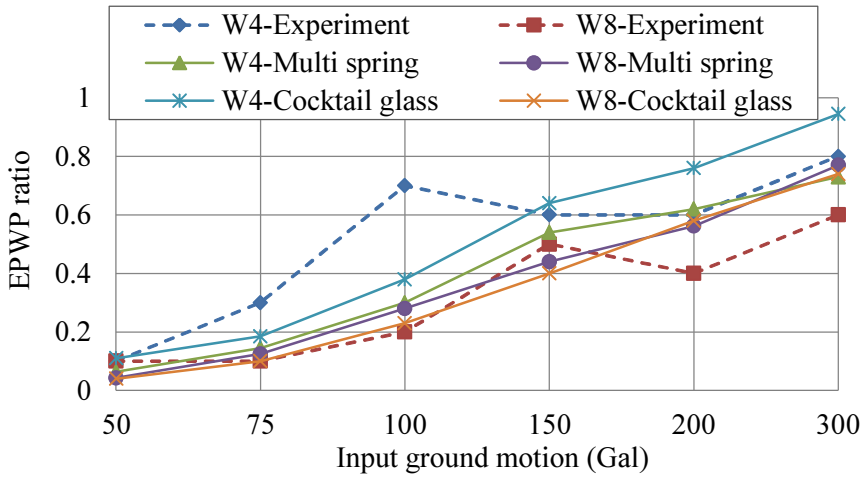

Fig.5.17 EPWP ratio in the slope model from 50 to 300 Gal

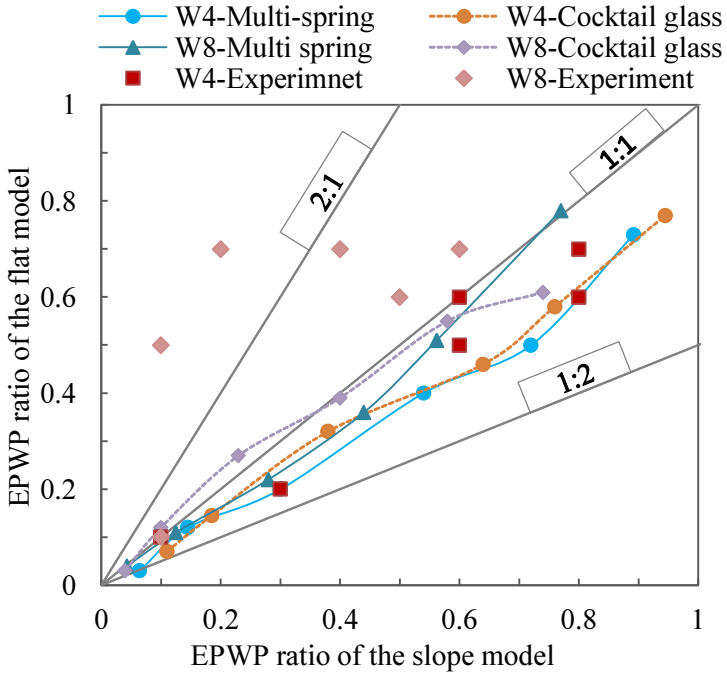

Fig.5.18 Comparison of EPWP ratio at W4 and W8 between the flat and slope models.

The EPWP ratios from the 50-300 Gal input ground motions are shown in **Figs.5.16** and **5.17** for the flat and slope models, respectively. The EPWP ratio increased due to the increase in input ground motion in the multi-spring model. It seen that the difference between the slope and flat models was quite small during shaking.

Fig.5.18 compares the EPWP at W4 and W8 between the slope and flat models obtained by the experiment and ESA from 50 to 300 Gal. There are six red points in **Fig.5.18**, and their values gradually increase. The EPWP ratio of the slope model at W4 was 1.1÷1.25 times higher than that of the flat model in both the experiment and ESA.

While, at W8 the EPWP ratios of ESA using both the multi spring and cocktail models were nearly identical between two models but in the experiment the ratios of flat model were larger than that of slope model. Regarding as the EPWP response of two numerical models in the effective stress analysis and experiment, there are some findings as follows:

1) The increase of EPWP ratio in both models was in accordance with an increase of input ground motion.

2) The liquefaction start time and EPWP ratios were almost identical for both models. However, in the slope model, the liquefaction area ratio was larger than that in the flat model.

3) The difference of EPWP ratio between the Multi-spring, Cocktail-glass models and experiment was little. However, the dissipation and vibration component of EPWP were explained in the Cocktail glass model

5.5.2 Displacement and acceleration of superstructure and pile cap

5.5.2.1 Horizontal acceleration

Fig.5.19 presents the time histories of the horizontal acceleration of the superstructure and pile cap of the flat model under the 300 Gal input ground motion in both ESA and the experiment. For the superstructure, the acceleration at AH4 of the experiment was nearly identical to that of the ESA. The acceleration of the experiment was larger for the pile cap at AH3, with a difference between the values of 10-12%.

Fig.5.20 presents the time histories of the horizontal acceleration of the superstructure and pile cap for the 300 Gal input ground motion for the slope model. The accelerations of the superstructure and pile cap of the experiment were also larger than that of the ESA.

Figs.5.21 and **5.22** illustrates that the acceleration of AH4 and AH3 from 50 to 300 Gal in the vibration test was in good agreement with that of the ESA for both models. Moreover, the accelerations of the superstructure and pile cap display a similar trend in both the Multi-spring and Cocktail glass models. The difference of acceleration was minimal in the 50-100 Gal cases but in the 100-300 Gal cases the acceleration in the slope model was less than that in the flat model 5-10%.

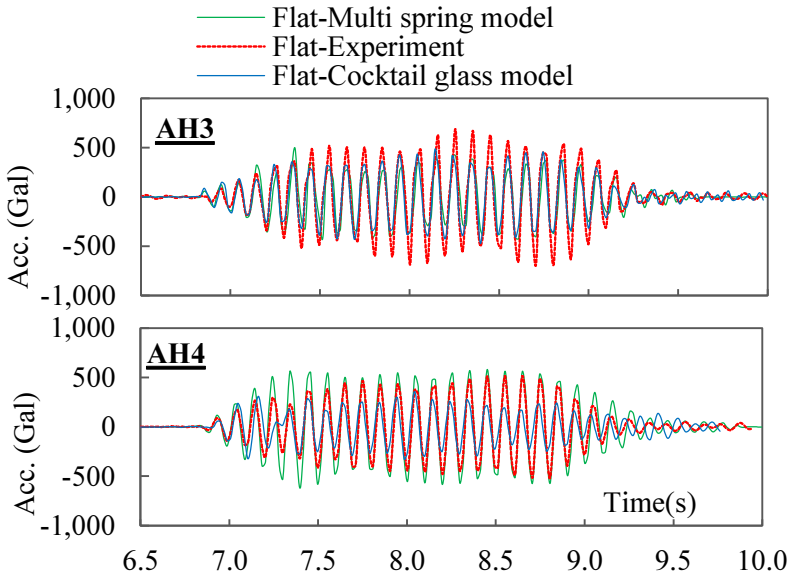

Fig.5.19 Time history of acceleration at AH3 and AH4 in the flat model under 300 Gal

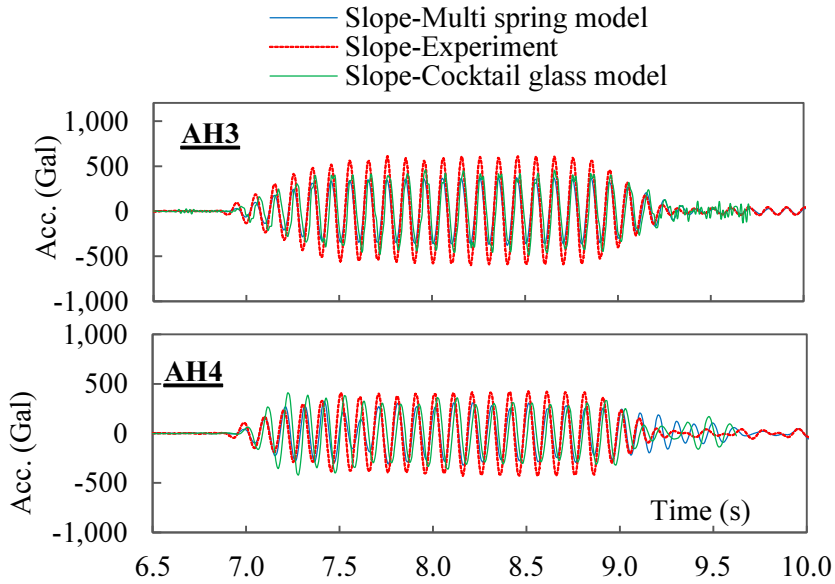

Fig.5.20 Time history of acceleration at AH3 and AH4 in the slope model under 300 Gal

Fig.5.23 presents a comparison of the maximum horizontal accelerations of the superstructure and pile cap in the experiment and ESA under the 50-300 Gal input ground motion in both models. The accelerations are nearly identical between the flat and slope models. The difference in acceleration was minimal in the 50-100 Gal cases but little larger in the 100-300 Gal cases. The numerical result of two models shows some conclusions as

1) The increase of acceleration in both models was in accordance with an increase of input ground motion.

2) Both the Multi-spring model in a undrain condition and a Cocktail model in a drain condition performed a good acceleration response of superstructure and pile cap in two

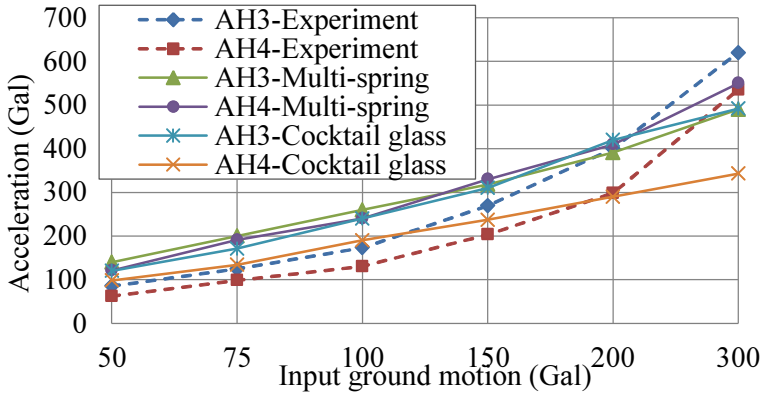

Fig.5.21 Maximum acceleration of AH4 and AH3 in the flat model from 50 to 300 Gal

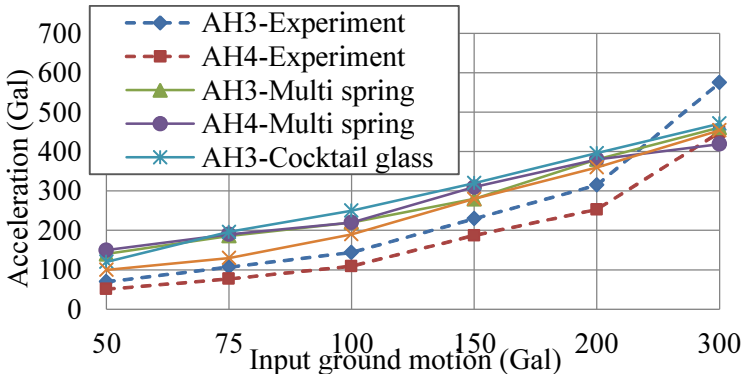

Fig.5.22 Maximum horizontal acceleration of the superstructure at AH4 and pile cap at AH3 in the slope model from 50 to 300 Gal

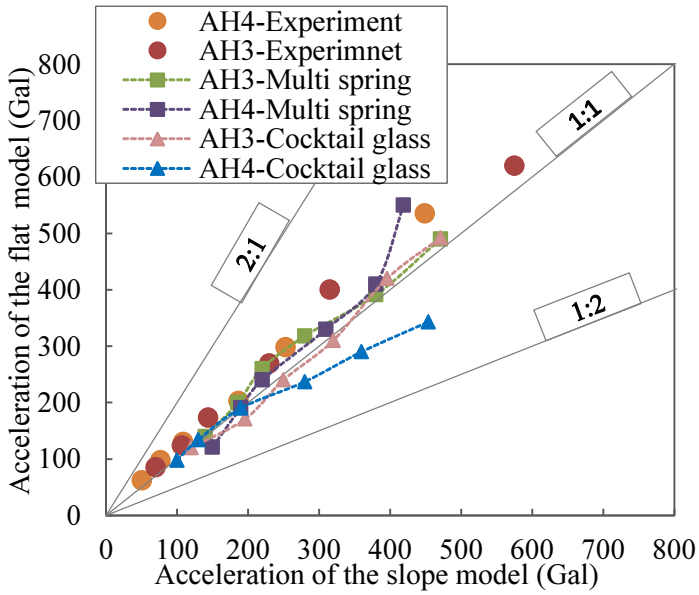

Fig.5.23 Comparison of acceleration at AH3 and AH4 between the flat and slope models

models. Moreover, they were in the similar trends with the experiment: in the lower input ground motion the difference of acceleration between two models is minimal; however, in the higher input motion the acceleration response in the slope model was smaller.

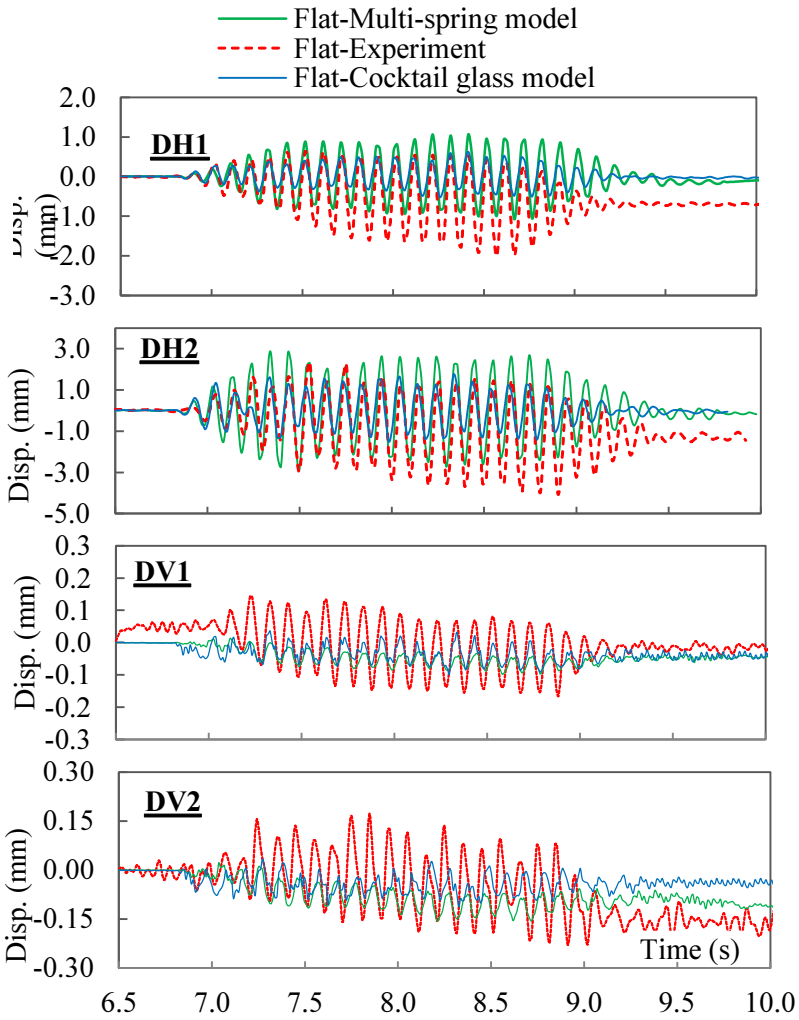

Fig.5.24 Displacement of superstructure and pile cap in the flat model under 300 Gal

5.5.2.2 Horizontal and vertical displacement

Fig.5.24 presents the time histories of the horizontal and vertical displacements of the pile cap and superstructure in the flat model in both the experiment and ESA. The displacements at DH1 and DH2 in the experiment were larger than those in the ESA. The displacements in the ESA-cocktail-glass model were considerably smaller than the displacements in other cases. The residual displacement was observed in the experiment. However, a small residual displacement was calculated by the ESA. **Fig.5.25** presents the time histories of the horizontal and vertical displacements at the pile cap and superstructure in the slope model under the 300 Gal. The residual displacement calculated in the ESA and the difference of the maximum displacement between the ESA and experiment were rather large. The displacement of DV1 exhibited a downward trend and that of DV2 exhibited an upward trend. This result of vertical displacement indicates that the foundation rotated and inclined toward the left. The vertical displacement at DV1 and DV2 in the 300 Gal case in

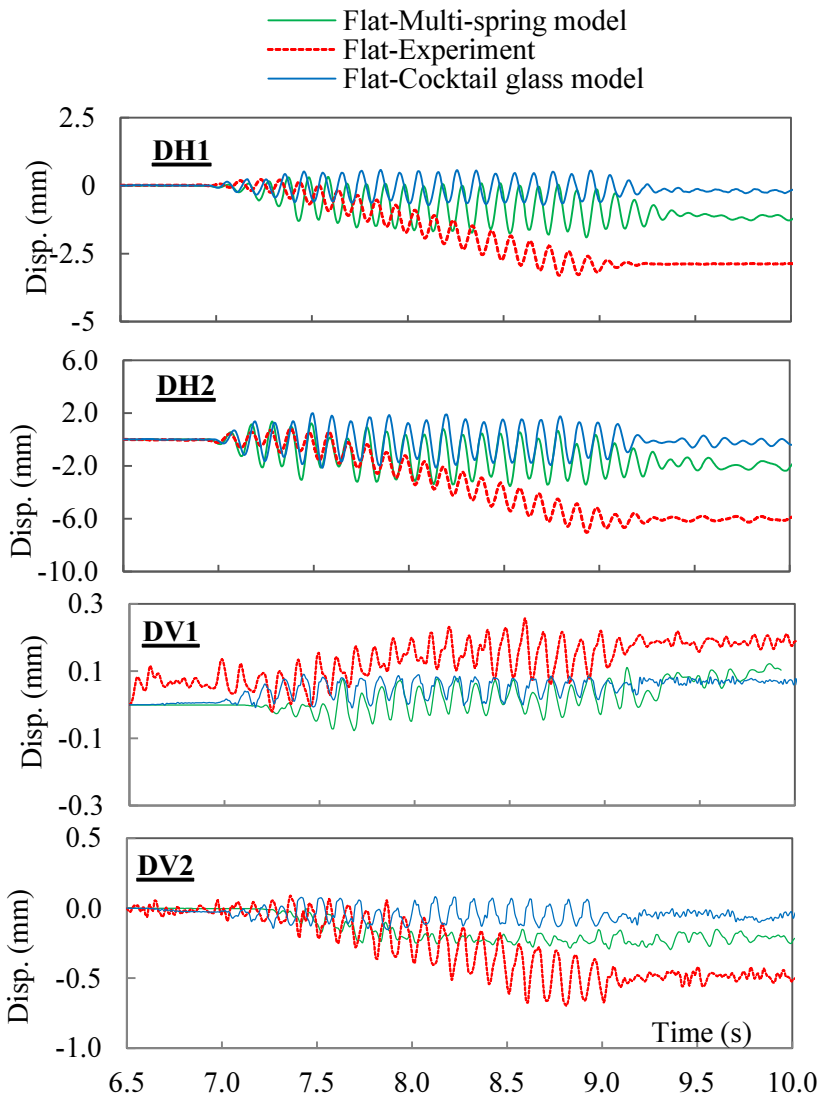

Fig.5.25 Horizontal and vertical response of superstructure and pile cap in the slope model under 300 Gal

the experiment was approximately 1.5 times less than that in the ESA-multi-spring and the displacements in the ESA-cocktail-glass were smallest.

The maximum and residual displacements during shaking from 50 to 300 Gal are shown in **Figs.5.26** and **5.27** for the flat model, respectively. There was a remarkable agreement between the experiment and ESA-multi-spring for the maximum and residual displacement between 50 to 150 Gals; however, the displacements in the ESA-multi-spring were considerably less than those in the experiment for the 150-300 Gal cases. Based on the JRA-2002, the allowable displacement of 4.9 mm for the top of the foundation was calculated by multiplying the width of the foundation by 1%. Thus, when liquefaction occurred, the maximum horizontal displacements of the pile cap under the 300 Gal input ground motion was approximately 0.35 times less than the allowable displacement for the experiment and 0.2 times less than that for the ESA-multi-spring. Moreover, the maximum

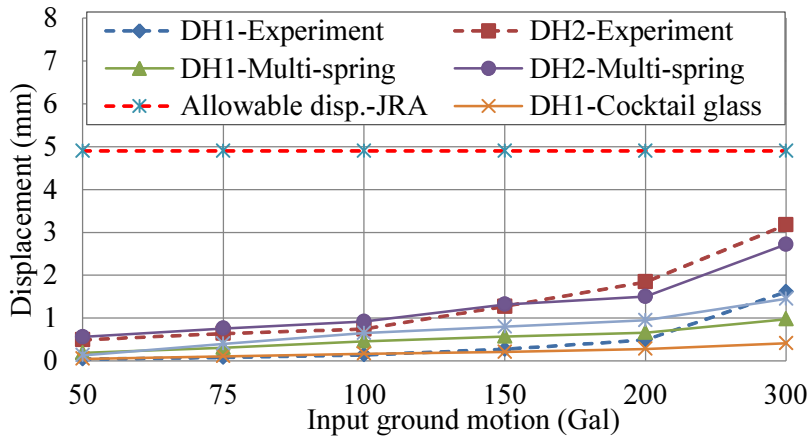

Fig.5.26 Maximum horizontal displacement of the superstructure DH2 and pile cap DH1 in the flat model from 50 to 300 Gal

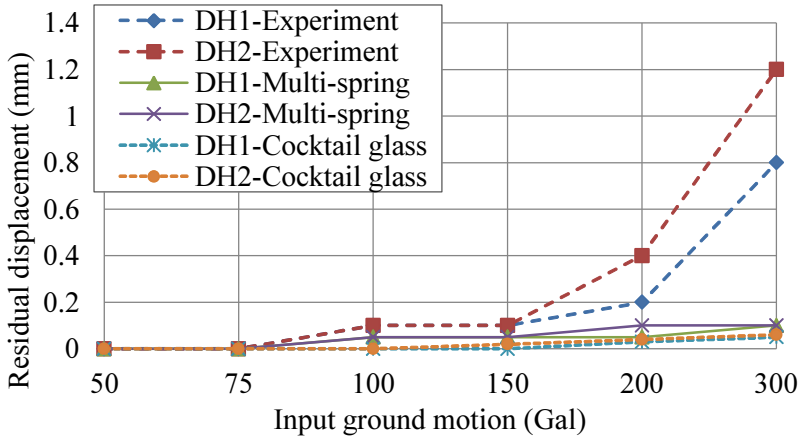

Fig.5.27 Residual horizontal displacement of the superstructure DH2 and pile cap DH1 in the flat model from 50 to 300 Gal.

displacements in the ESA-cocktail- glass were approximately 2 times less than that in the experiment, while, the residual displacements were very small and not significant during shaking.

The maximum and residual horizontal displacements during shaking from 50 to 300 Gal in the slope model are shown in **Figs.5.28** and **5.29** for the slope model, respectively. Compared with the allowable displacement of the pile cap, the maximum displacement at the pile cap was approximately 0.7 times less than that in the experiment, 0.4 times less than that in the ESA-multi-spring and 0.15 times for ESA-cocktail- glass. The maximum horizontal displacement at the pile cap satisfied the allowable design value. Moreover, from 50 to 150 Gal there was a good agreement of the maximum and residual displacement between the experiment and ESA-multi-spring; however, in the 300 Gal case, the displacements in both the ESA-multi-spring and cocktail-glass was much less than that in the experiment

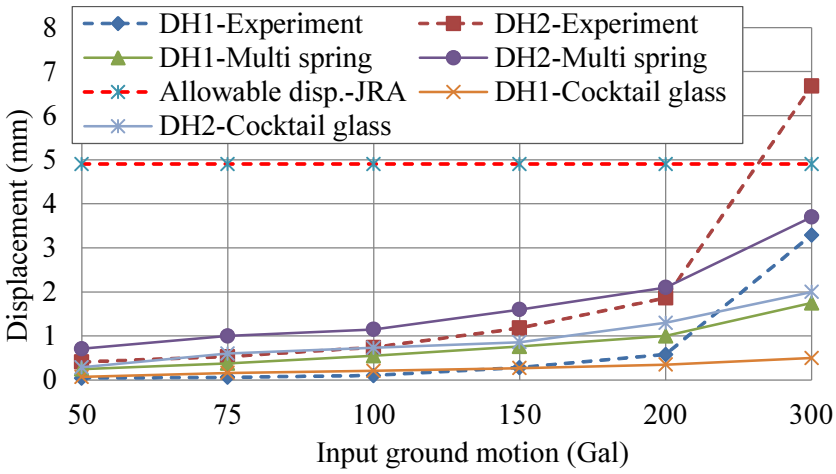

Fig.5.28 Maximum horizontal displacement of the superstructure DH2 and pile cap DH1 in slope model from 50 to 300 Gal.

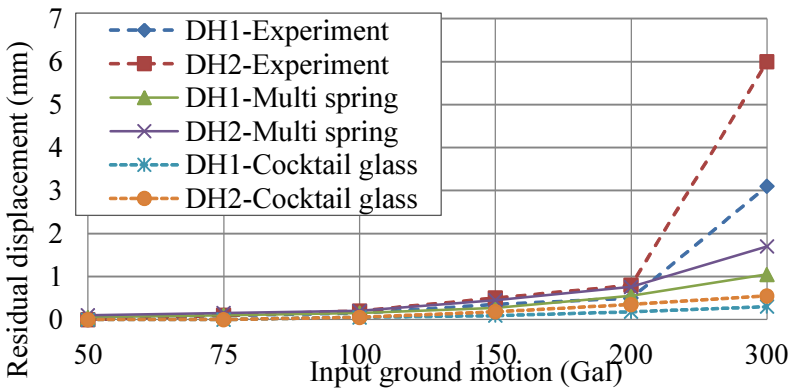

Fig.5.29 Residual horizontal displacement of the superstructure DH2 and pile cap DH1 in the slope model from 50 to 300 Gal

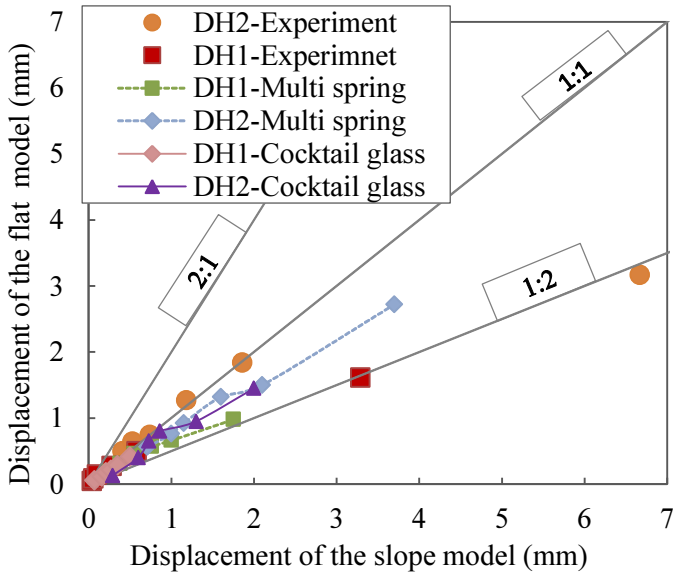

Fig.5.30 Comparison of maximum horizontal displacement at DH1 and DH2 between the flat and slope models.

Figs.5.26 and **5.28** show almost constant displacements from 50 to 150 Gal. This is because in the lower input ground motion, the inclination of foundation was small so the maximum vertical displacement increased a little and. However, in the higher input motion, the inclination became larger, the residual displacement component increased more significantly. The difference of maximum vertical displacement was also more significant.

Fig.5.30 illustrates that when the range of the maximum displacement is 0-1 cm in the 50-100 Gal cases, the difference in the displacement of the superstructure and pile cap between the flat and slope models was minimal, and their ratio was approximately 1:1. The range of the displacement increased for the 100-300 Gal cases, and the difference progressively increased; the displacement ratio approached 1:2, indicating that the displacement of the slope model became approximately twice that of the flat model in this experiment. The ESA had the same trend with the vibration test. However, the differences of displacement between two models were smaller. **Fig.5.31** presents the maximum vertical displacements in the flat model during shaking under the 50-300 Gal input ground motion. There was a remarkable agreement between the experiment and ESA-multi-spring. Moreover, there was a slight difference in the displacement value between DV1 and DV2 in both the experiment and ESA-multi-spring. The settlement of the foundation in the flat model was almost even. The displacements in the ESA-cocktail-glass were much smaller than other cases. **Fig.5.32** presents the maximum vertical displacements in the slope model during shaking under the 50-300 Gal input ground motion. There was a slight difference in the displacement value between DV1 and DV2 from the 50 to 200 Gal input ground motion in both the experiment and ESA-multi-spring. However, the difference between the values became larger, and the displacement at DV2 was approximately three times larger than that at DV1 for both the experiment and ESA-multi-spring in the 300 Gal case. The displacements in the ESA-cocktail-glass were also much smaller than other cases. Based on **Eq.5.9,** the inclination in this case was 0.23% in the experiment. The inclined settlement of the foundation model occurred in the slope. The inclination of the foundation was determined by the following equation:

$$\alpha = \frac{DV2-DV1}{L}100 \tag{5.9}$$

Where α is the inclination of the foundation (%); *DV1* and DV2 are the residual values of vertical displacements at the top of the footing (mm); and L is the distance between *DV1* and *DV2* (266 mm).

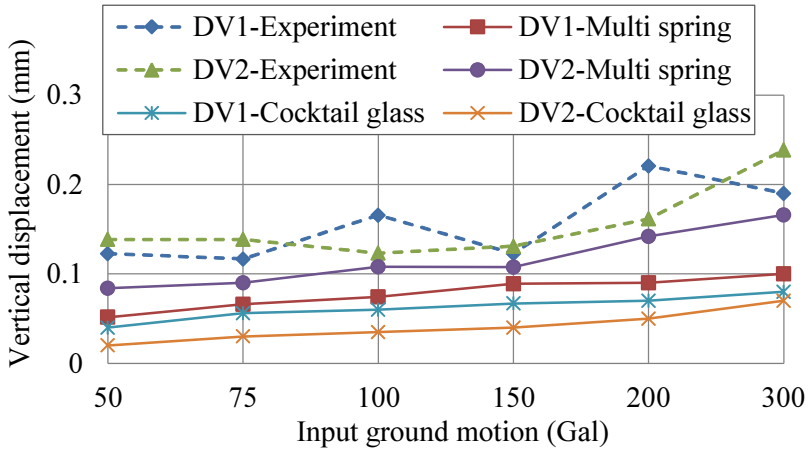

Fig.5.31 Maximum vertical displacement of the pile cap at DV1 and DV2 in the flat model from 50 to 300 Gal

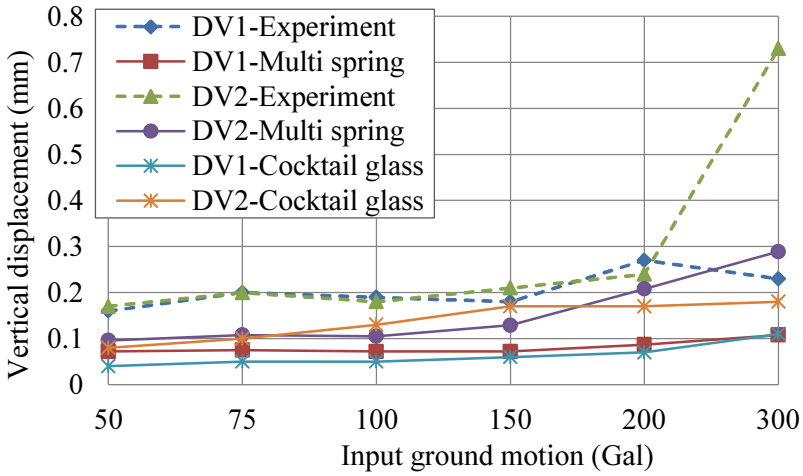

Fig.5.32 Maximum vertical displacement of the pile cap at DV1 and DV2 in the slope model from 50 to 300 Gal

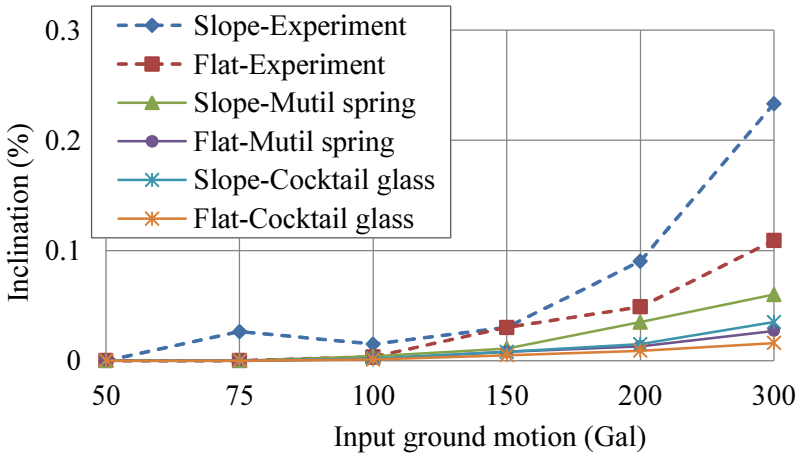

Fig.5.33 Comparison of the inclination of foundation between the flat and slope models from 50 to 300 Gal

Fig.5.33 presents the inclination of the foundation in the experiment and ESA under the 50-300 Gal input ground motion in both models. In both the experiment and ESA-multi-spring, the difference in the inclination between the two models was minimal for the 50-150 Gal cases. However, in the 300 Gal case, the inclination in the slope model was approximately 0.2 and 0.05 times less than the allowable inclination (1%) for the experiment and ESA-multi-spring, respectively. While, in the flat model, the inclination was approximately 0.11 times less than the allowable value for the experiment and 0.03 times less for the ESA-multi-spring. The inclinations in ESA- cocktail-glass were very small in the both models.

Regarding to the displacement responses of two models in the effective stress analysis, there are some conclusions as follows:

1) The displacement response increased in an accordance with an increase of input ground motion.

2) The effective stress analysis using both the Multi-spring and Cocktail-glass models displayed that the displacement of superstructure and pile cap and inclination responses of foundation in the slope model were larger than that in the flat model. However, the residual displacement and inclination were not in a good agreement with the experiment; Furthermore, these responses in the Cocktail-glass model were less than that in the Multi-spring model.

3) The ESA and experiment were in the same trend: in the lower input ground motion from 50 to 100 Gal, the displacement response of superstructure and pile cap between two models were almost identical; however, in the higher input the liquefaction phenomenon started a development the response in the slope model became larger. It means that the effect of slope became more significant

5.5.3 Behavior of ground

5.5.3.1 Horizontal acceleration

Fig.5.34 presents the time histories of the horizontal accelerations at points AH8, AH10, and AH19 in the flat model. In the non-liquefaction layer, the acceleration at AH8 of ESA using the multi-spring model corresponded well with that of the experiment, and the acceleration did not exhibit any amplitude variations during the shaking period. Meanwhile, the acceleration at the near-field AH10 and far-field AH19 of the liquefaction layer varied

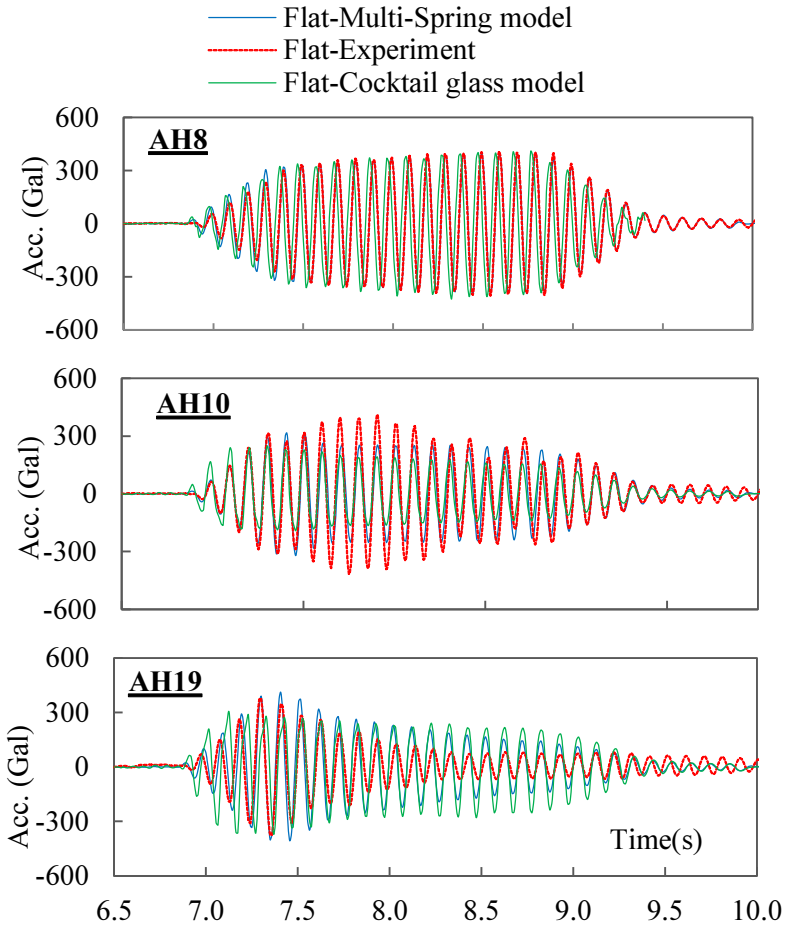

Fig.5.34 Time history of acceleration at AH8, AH10, AH19 in flat model under 300 Gal.

significantly starting at 7.5 s, and this amplitude gradually reduced between 7.5 and 10 s, as shown in **Fig.5.34**.

The horizontal accelerations at points AH7, AH9, and AH16 in the slope model are shown in **Fig.5.35**. These points are at the same position, corresponding to points AH8, AH10, and AH19 in the flat model. Similar to the acceleration behavior in the flat model, the acceleration amplitude in the liquefaction layer at points AH9 and AH16 decreased and did not appear in the non-liquefaction layer at AH7.

However, **Fig**.**5.35** illustrates that the amplitude of the acceleration toward the water at AH9 and AH16 became larger compared to that of the acceleration toward the land in the vibration test. The instability of the slope ground generated the high acceleration in the direction of the water. However, the calculation did not provide the same result as the vibration test. It means that the effective stress analysis using both multi-spring and cocktail glass models cannot explain the performance of acceleration during liquefaction, as shown at AH9 and AH16 in the ground.

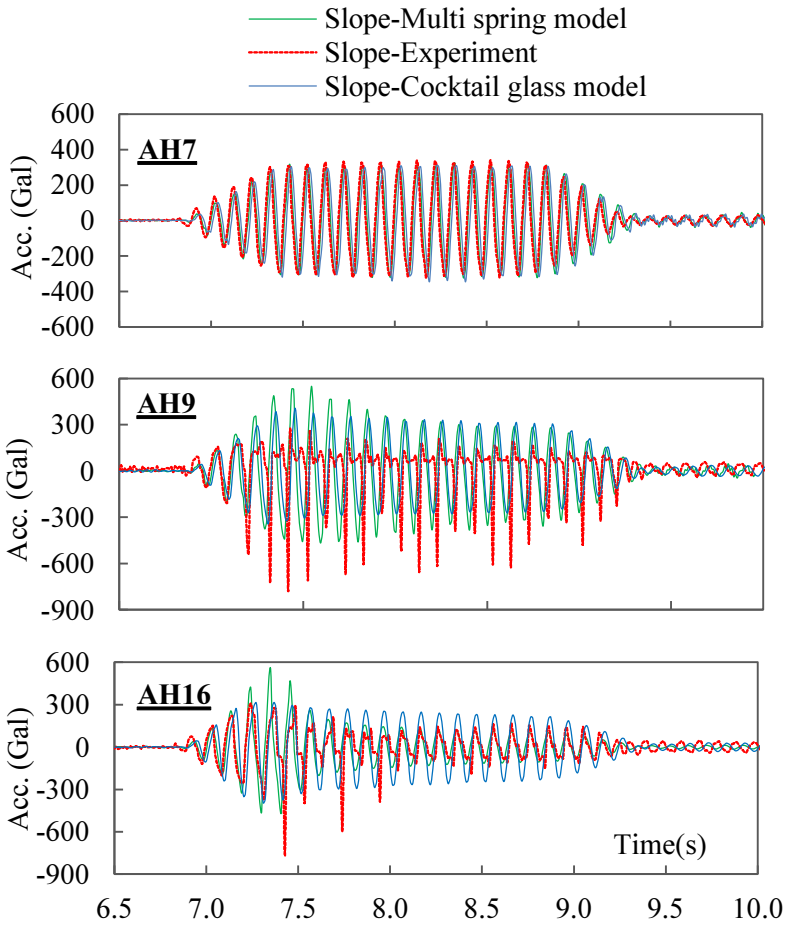

Fig.5.35 Time history of acceleration at AH7, AH9, AH16 in slope model under 300 Gal.

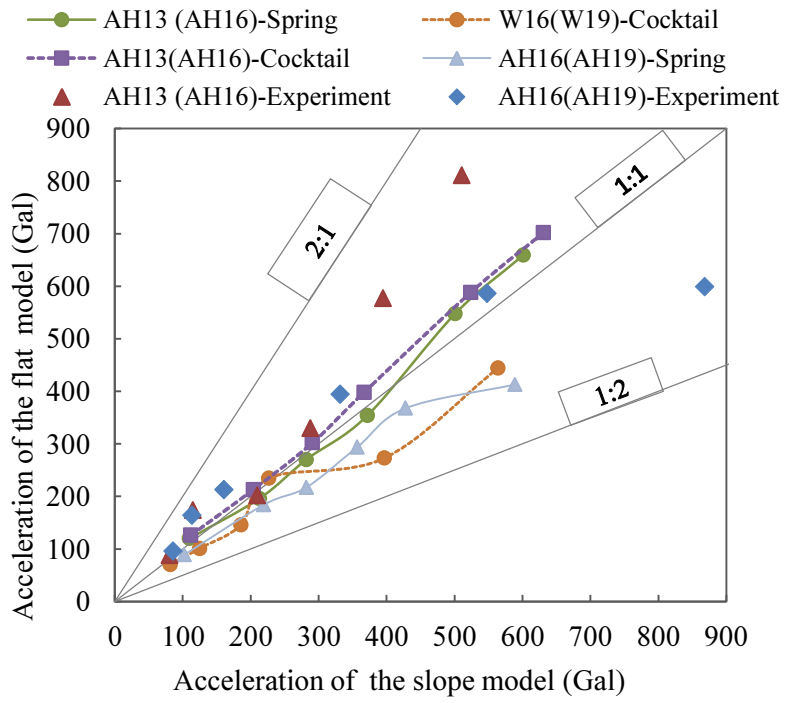

Fig.5.36 Comparison of acceleration at AH13, 16 in the flat model and AH16, 19 in the slope model.

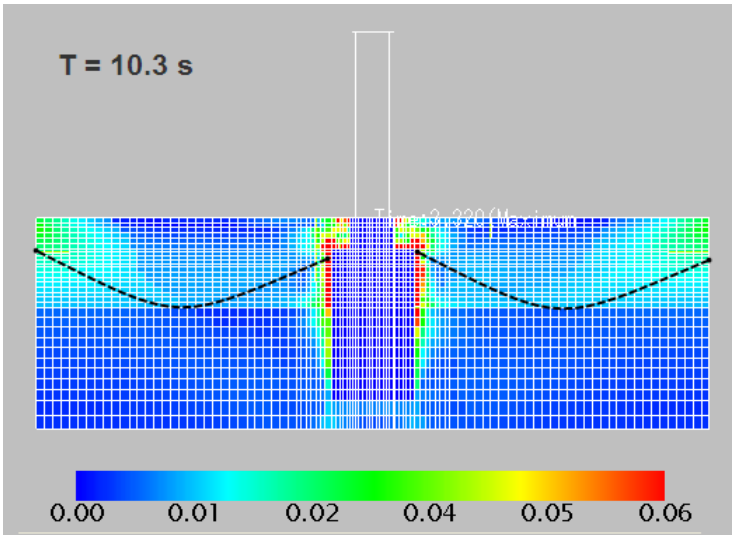

Fig.5.37 Maximum shear strain distribution in the flat model under 300 Gal

Fig.5.36 presents comparison of the horizontal accelerations at AH13, AH16 in the slope model and at AH16, AH19 in the flat model. The difference of the acceleration in the near field between AH13 in slope model and AH16 in the flat model was minimal in the 50-150 Gal cases in both the experiment and ESA. However, the acceleration ratio steadily approached 2:1 in the 150-300 Gal cases. The acceleration at AH 13 in the flat model became approximately 1.5 times that of the slope model in the experiment under 300 Gal. While, in the far field the acceleration at AH19 in the flat model was less than that at AH16 in the slope model approximately 1.5 times in both the experiment and ESA. The ESA using multi-spring and cocktail-glass models had the same trend in the acceleration development in the experiment.

5.5.3.2 Shear strain

Fig.5.37 presents the maximum shear strain distribution of the surface layer using the ESA-multi-spring. Large strain values were calculated in the area around the foundation in both the liquefaction and non-liquefaction layers. The strains were also quite large in the far field. Moreover, the maximum strains in the range 0.008-0.01 in the liquefaction layer distribution are presented by the black dashed line shown in **Fig.5.37**; the distribution had a symmetric pattern. **Fig.5.38** presents the maximum shear strains in the area around the foundation and on the down- and up-slope areas. The maximum strain distribution in the range 0.04-0.07 in the liquefaction layer is presented by the black dashed line in **Fig.5.38**; however, the distribution had an asymmetric pattern. The strain of the soil elements on the front of the foundation was larger than that on the back of the foundation.

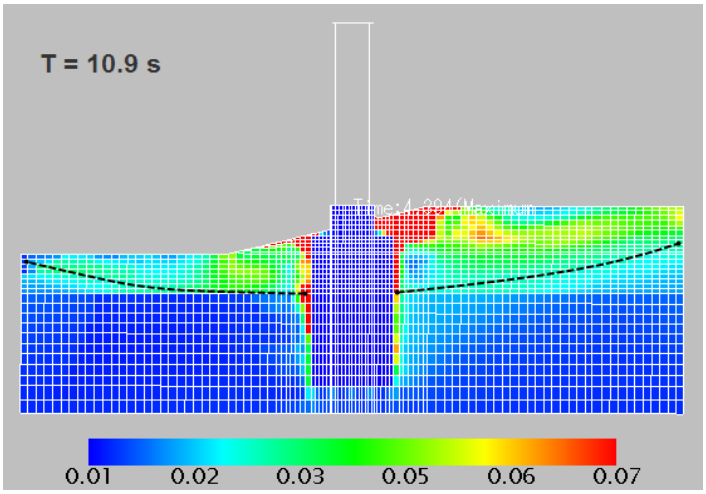

Fig.5.38 Maximum shear strain distribution in the slope model under 300 Gal.

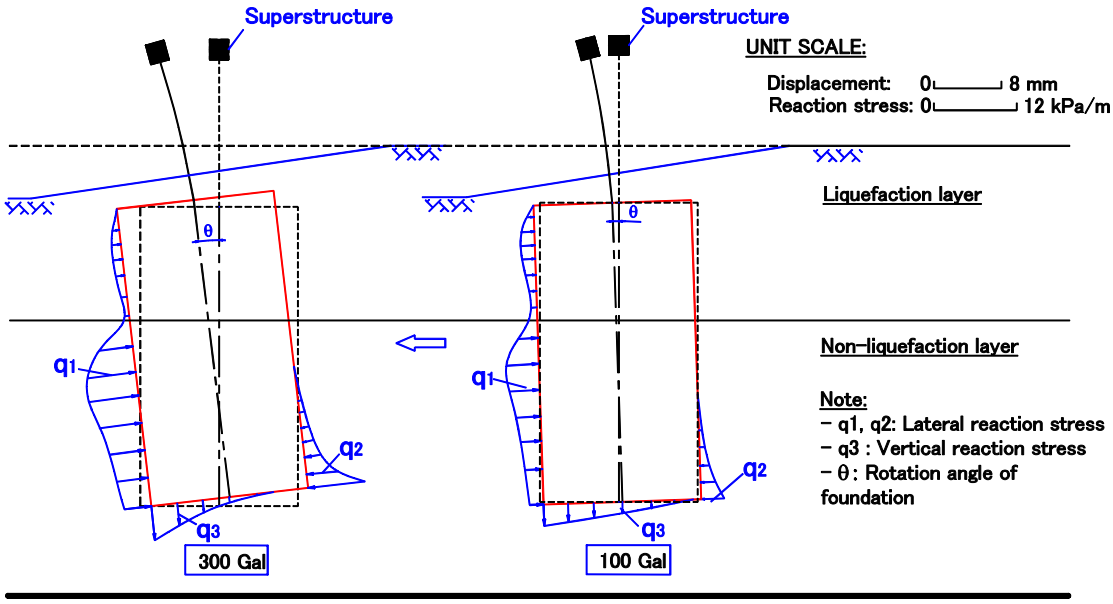

Fig.5.39 Ground reaction stress distribution of the SPSP foundation in the slope model

Fig.5.39 presents the distribution of the reaction stresses along the foundation obtained by the ESA-multi-spring in the slope model. The reaction stress became small in the liquefied layer but large in the un-liquefied layer after liquefaction as to both the flat and the slope models. For the slope model, the reaction stress was small at both the front wall and the back wall. The other hand, the reaction stress at the back wall was large even though the sand was liquefied for the slope model. This reaction stress at the back wall pushed the foundation to move forward and rotated around the tip of the foundation. The reaction stress of the bottom was nearly zero on the back side of the foundation, except for the area at the rear of the bottom due to the rotation of the foundation and cut off tension under 300 Gal case. The foundation resisted the movement due to the un-liquefied sand

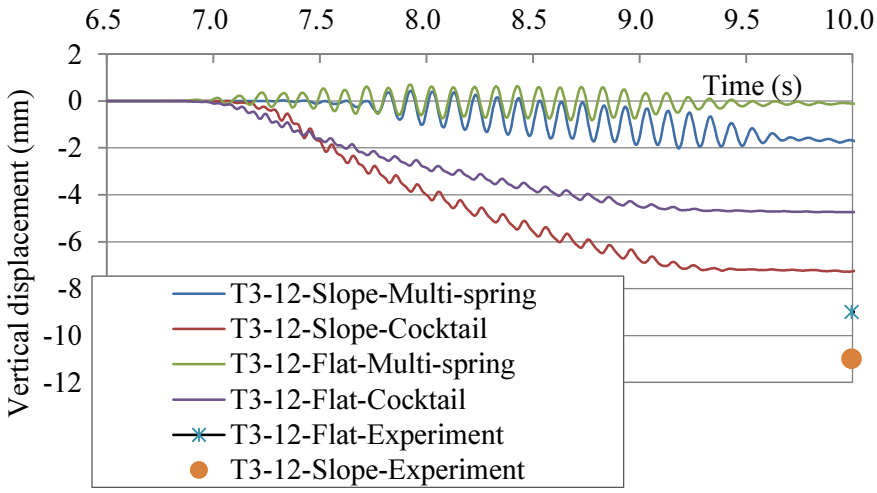

Fig.5.40 Vertical displacement on ground in the slope and flat models under 300 Gal

5.5.3.3. Vertical displacement of ground

The T3-12 point in the near field of foundation located in the landward of slope model was chosen to perform a vertical displacement response of ground in both models. The **Fig.5.40** shows the maximum vertical displacement in both experiment and ESA for both models. This figure presents that the displacement of the multi-spring model was approximately four times less than that of the cocktail glass models. The effective stress analysis using the cocktail glass model corresponded more closely with the results of the experiment than did the ESA using the multi-spring model with regard to the vertical displacement.

5.5.3.4 Conclusions

1) Both the multi-spring and cocktail-glass models performed a good acceleration behavior of ground compared with the experiment. When liquefaction phenomenon occurred with the inclination of acceleration amplitude also started in accordance with a generation of pore water pressure.

2) The reaction stress became small in the liquefied layer but large in the un-liquefied layer after liquefaction as to both the flat and the slope models. During the liquefaction the strain values of ground in the slope model was larger than that in the flat model. This may be because of instability of slope ground.

3) The vertical displacement of ground in the Cocktail glass model (a drained model) was in a better agreement with the result of vibration test than that in the Multi-spring model (an un-drained model).

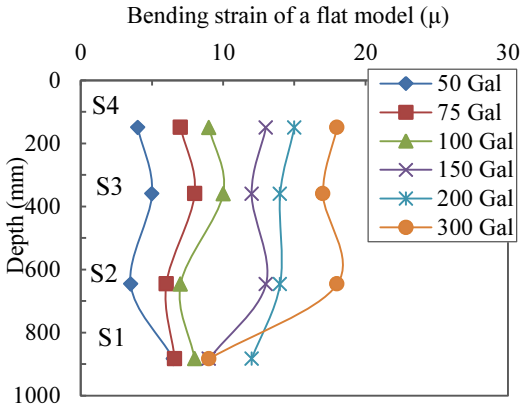

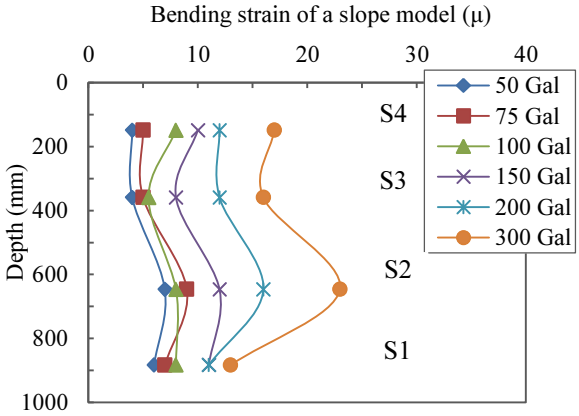

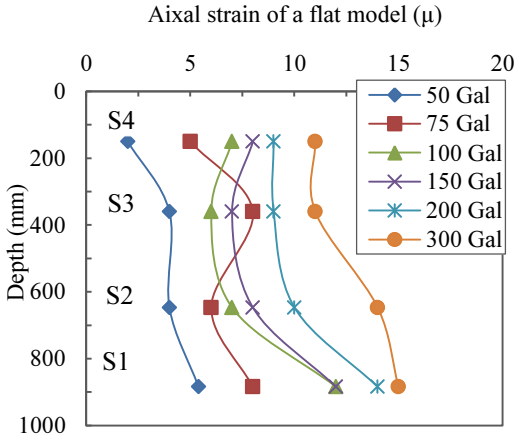

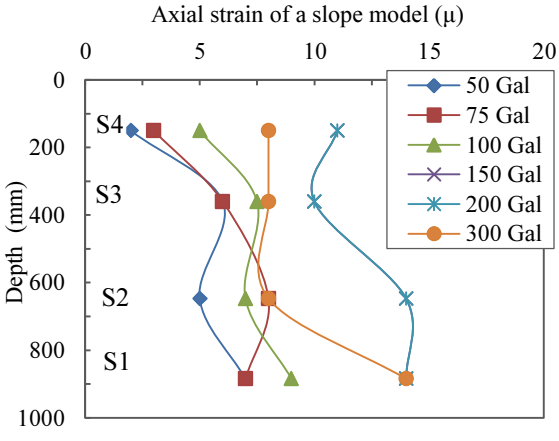

Fig.5.41 Bending and axial strain in ESA in the flat model.

Fig.5.42 Bending and axial strain in ESA in the slope model.

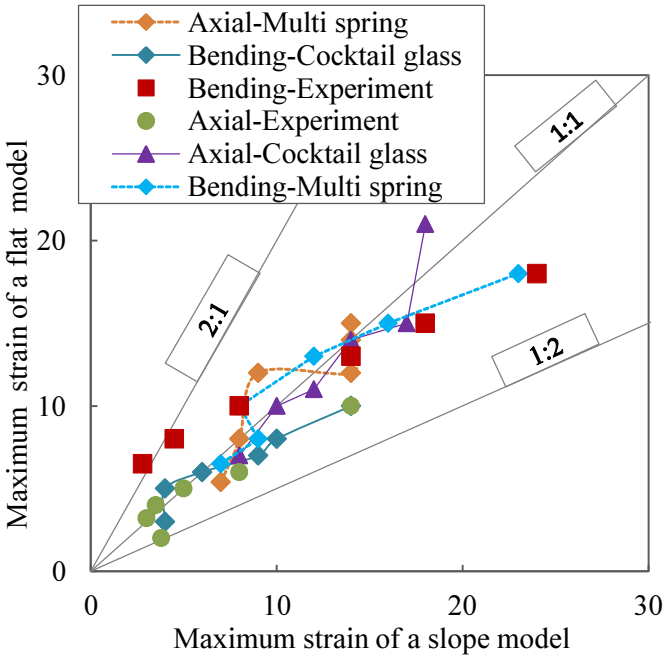

Fig.5.43 Comparison of maximum strain along the front and back sides between the flat and slope models

5.5.4 Behavior of foundation

The maximum bending and axial strain distribution of ESA along the foundation in both the flat and slope models from 50 to 300 Gal are shown in **Figs.5.41** and **5.42**, respectively. The bending strains dominated the axial strain when the input acceleration amplitude was less than 100 Gal. The distribution of the axial and bending strains was uniform along the foundation depth. When liquefaction occurred, the strain increased at the bottom of the foundation rather than at the upper location. Generally, **Figs.5.41**, and **5.42** illustrate that the bending strains in both the experiment and ESA reach a maximum value near the bottom of the pile foundation at S2 in both models.

Fig.5.43 presents a comparison of the maximum bending strain and axial strain of the pile foundation between the two models from 50 to 300 Gal in both the experiment and ESA. The maximum bending strain of the flat model in the experiment was almost larger than that of the slope model in the 50-150 Gal cases. However, when the liquefaction process was complete, the strain of the slope model became 1.5 times larger than that of the flat model in the 300 Gal case. For the ESA using both multi spring and cock tail models from 50 to 200 Gal, the difference in the bending strain between the two models was minimal, and in case of 300 Gal the strain of the slope model was larger than that of the flat model approximately 1.3 times. The result of the experiment also illustrates that the maximum axial strain in the slope model was approximately 1.5 times larger than that in the flat model. While, the axial strain difference in the ESA between two models was small. Moreover, ESA-multi-spring had the same trend as the experiment; however, the strain in the slope model was slightly larger than that in the flat model.

The strain responses in two numerical models illustrated some conclusions as follows:

1) The maximum bending strain observed at the locations around contact area between liquefied and non-liquefied layer near the bottom of foundation when liquefaction occurred.

2) The experiment and ESA were in the same trends : in the lower input ground motion the strain values almost were constant; however, when in the higher input ground the soil liquefied the strain in two models increased in a accordance with an increase of input ground motion.

3) Generally, the strain response of foundation in the slope model was larger than that in the flat model.

5.6 Conclusions

The numerical analysis using an effective stress analysis was conducted on the both the flat and slope models to performed the dynamic behavior of SPSP foundation. The undrain model (Multi-spring model) and drain model (Cocktail glass model) were used in this study. Based on these results, there are main findings as follows:

(1) The effective stress analysis partially performed the dynamic behavior of the flat and slope models with regard to the strain, pore water pressure, acceleration responses. It also displayed the difference of dynamic responses between two models. However, the calculated value of residual displacement, inclination of foundation, etc. was not in an agreement with the vibration test.

(2) The displacement, acceleration, inclination and strain response increased due to the increase in the input acceleration in the flat and slope models.

(3) Both multi-spring and cocktail-glass models were in the same trend with the vibration test is that: in the lower input ground motion, the difference of response between two models was minimal; however, in the higher input ground when the liquefaction of soil developed the response of displacements, strains, inclination in the slope model were larger than that in the slope model; whereas the acceleration in the slope model was smaller. It means that he lateral movement of liquefaction layer due to slope may partially affect to the foundation when liquefaction occurred.

(4) The bending and axial strains along the foundation axial were nearly uniform before the liquefaction of sand occurred. When liquefaction occurred, the strains in the non-liquefaction layer became larger instead of the strains in the liquefied layer. The reaction stress of the slope model was small in the liquefied layer. The reaction force at the front wall was small in the liquefied layer for the slope model. However, the reaction at the back wall was large to move the foundation to front direction. The foundation resisted the movement due to the non-liquefaction layer.

(5) The cocktail glass model that considers the dilative component of the sand and seepage of water can be used to estimate the dissipation of the pore water pressure and vertical displacement. However, the response displacement using the cocktail glass model is smaller than that using the multi-spring model. The cocktail model can explain the dissipation of the pore water pressure in the vibration test; however the

calculation result had the vibration component and was not stable. Methods of determining the parameters in the ESA using both the multi-spring model and the cocktail glass model to coincide the test results should be examined in future studies.

References

1) Iai, S. (1988), "A model that does not break out in the two-dimensional effective stress analysis for liquefaction,", Proc., 43rd Annual Conf. of JSCE, 3, pp418-419 (in Japanese)

2) Iai, S., Matsunaga, Y. and Kameoka, T. (1990), "Parameter identification for a cyclic mobility model," Report of the Port and Harbour Research Institute, Vol.29, No.4, pp.57-83.

3) Iai, S., Matsunaga,Y. and Kameoka,T. (1990): Strain space plasticity model for cyclic mobility, Report of Port and Harbor Research Institute, Vol.29,No.4,pp.27-56.

4) Iai, S., Matsunaga, Y. and Kameoka, T. (1992a), "Strain space plasticity model for cyclic mobility," Soils and Foundations, Vol.32, No.2, pp.1-15

5) Iai, S., Matsunaga, Y. and Kameoka, T. (1992b), "Analysis of un-drained cyclic behavior of sand under anisotropic consolidation," Soils and Foundations, Vol.32, No.2, pp.16-20

6) Towhata,I. And Ishihara,K. (1985): Modeling soil behavior under principal stress axes rotation, Proc. 5th International conference on numerical method in geomechanics, Nagoya, pp.523-530.

7) Ishihara,K., Yoshida,N. and Tsujino,S. (1985): Modeling of stress-strain relations of soils in cyclic loading, Proc. of 5th International Conf. on Num. Methods in Geomechanics , Nagoya, Vol.1,pp.373-380.

8) Ozutsumi,O. and Iai,S. (2001): Adjustment Method of the Hysteresis Damping for Multiple Shear Spring Model, Proc. of 4th International Conf. on Recent Advances in Geotech. Earthquake Eng. and Soil Dynamics.

9) Osamu Ozutsumi: Study on numerical analysis method of earthquake damage prediction for ground-structure system on liquefied layer, doctoral dissertation, Kyoto university,Dec.2003(in Japanese).

10) Robert, P. Chapuis., Aubertin, M.: Predicting the coefficient of permeability of soil using Kozeny-Carman equation. Technical report. EPM-RT-2003-3, 2003.

11) Yoneda, M.: On the longitudinal motion of girder of cable stayed bridges and simplified method of estimating natural frequency corresponding to this motion. Journal of Structural Mechanics and Earthquake Engineering, JSCE, I-4, 1990 (in Japanese).

12) Uzuoka, R., Cubrinovski, M., Zhang, F., Yashima, A., and Oka, F. (2006). "Accuracy of prediction with effective stress analysis for liquefaction-induced earth pressure on a pile group." New Zealand Workshop on Geotechnical Earthquake Engineering, pp.120-132.

13) Nguyen Thanh Trung. Osamu Kiyomiya. Tongxiang An. Makoto Yoshida (7/2013): Shaking table test on steel pipe sheet pile foundation in slope during liquefaction. *Proceedings of the*

16th Symposium on Performance-based Seismic Design Method for Bridges of JSCE, Tokyo, Japan.

14) Nguyen Thanh Trung Osamu Kiyomiya (9/2013): Dynamic behavior of bridge foundation during liquefaction by shaking table test. *Proceedings of the 15th International summer Symposium of JSCE*, Chiba, Japan.

Chapter 6

Conclusions and Future Work

6.1 Summary

The behavior of SPSP foundation during liquefaction was investigated in this study by both the vibration test and numerical methods. The foundation models in the flat and slope ground of 15^{o} were simulated and verified by using both the total stress and effective stress analysis to display the effects of slope on the behavior of foundation. The research result would provide understanding of behavior of SPSP foundation in the revetment along river bank or coastal line where the liquefaction and liquefaction induced lateral ground movement occur. Moreover, it also produces necessary provisions for design work of SPSP foundation.

The research work is summarized in four main stages. Firstly, the damages of structure and previous researches about the behavior of foundation during liquefaction were reviewed to provide a background and basic foundations in setting up the vibration test and numerical models.

Secondly, 1G shaking table test was conducted to perform the dynamic responses of SPSP foundation during liquefaction by the flat and slope models. Especially, it also clarified the difference of their responses to present the significant effect of slope ground on the foundation.

Thirdly, the test models were simulated by the numerical method in the specification approach. The research result provided understandings about the applicability of specification to verify the seismic responses of SPSP foundation during liquefaction.

Finally, the dynamic behavior of two models were investigated by the effective stress analysis in both undrain and drain conditions. The difference of responses between two models and drainage conditions were also presented and compared with the vibration test to display the significant effect of slope ground and validity of numerical methods in this study.

6.2 Conclusions

There are some main findings as follows:

(6) The dynamic response of foundation and ground consists of pore water pressures, displacements, accelerations and strains increased were in accordance with the increase in the input acceleration in both the flat and slope models in the vibration test. The lateral movement on the foundation became large when liquefaction occurred, and residual displacement at the top of foundation was observed for both models. The residual displacement in the slope model was considerably larger than that in the flat model

(7) In the slope model, the foundation moved down the slope and inclined in the shaking table test and quickly generated the high acceleration in slope model, the immigration of pore water pressure became more complicated at the bottom of slope. The movement of the slope at the foundation that was inserted into non-liquefaction layer was smaller than that of the free field.

(8) The result of the TSA indicates that the dynamic response displacement of the TSA with a reduction of shear modulus agrees reasonably well with that of the experiment in the flat model. However, the TSA method cannot provide a reasonable response displacement for the slope model even for case reduced the shear modulus until 1/100 G_o. This is because the displacement of the ground was estimated to critical side when the sand was liquefied.

(9) The effective stress analysis partially performed the dynamic behavior of the flat and slope models with regard to the strain, pore water pressure, acceleration responses. It also displayed the difference of dynamic responses between two models. However, the calculated value of residual displacement, inclination of foundation, etc. was not in an agreement with the vibration test.

(10) Both multi-spring and cocktail-glass models were in the same trend with the vibration test is that: in the lower input ground motion from 50 to 100 Gal the difference of acceleration, displacement, inclination between two models was not much significant. However, in the higher input ground motions from 200 to 300 Gal the, soil was liquefied the displacement response of the pile cap and superstructure and inclination and strain of foundation in the slope model was almost larger than that in the flat

model then during liquefaction; whereas the acceleration in the slope model was smaller. Therefore, the lateral movement of liquefaction layer due to slope may partially affect to the foundation when liquefaction occurred.

(11) In lower input ground motion, the displacement of superstructure was out of phase with that of ground foundation in both models. However, in the case of higher input motion as the soil was liquefied the displacement of superstructure was in phase with that of foundation. Meanwhile, the acceleration of superstructure was almost out of phases with that of foundation in both models during shaking. This phenomenon would be investigated and explained in the Chapter 3.

(12) The bending and axial strains along the foundation axial were nearly uniform before the liquefaction of sand occurred. When liquefaction occurred, the strains in the non-liquefaction layer became larger instead of the strains in the liquefied layer. The reaction stress of the slope model was small in the liquefied layer. The reaction force at the front wall was small in the liquefied layer for the slope model. However, the reaction at the back wall was large to move the foundation to front direction. The foundation resisted the movement due to the non-liquefaction layer.

(13) The total stress analysis has the same trend with effective stress analysis is that : the horizontal reaction stress is smaller in the liquefaction layer when shear modulus of soil increases. It means that reaction stress in the liquefaction layer increases when the liquefaction occurs.

(14) The cocktail glass model that considers the dilative component of the sand and seepage of water can be used to estimate the dissipation of the pore water pressure and vertical displacement. However, the response displacement using the cocktail glass model is smaller than that using the multi-spring model. The cocktail model can explain the dissipation of the pore water pressure in the vibration test; however the calculation result had the vibration component and was not stable. Methods of determining the parameters in the ESA using both the multi-spring model and the cocktail glass model to coincide the test results should be examined in future studies.

(15) The second natural frequency of models is significantly affected by a reduction of soil shear modulus in the liquefaction verification. The difference of dynamic characteristic between the flat and slope models is also significant in the second frequency.

(16) Total stress analysis using the linear reduction of shear modulus produces a good agreement of horizontal acceleration with the experiment in the near field but in the far field there is not an agreement between them. The acceleration behavior of soil around the foundation in the slope model is really complex in the movement direction because of the soil movement in the slope ground.

6.3 Future work

Effective stress analysis under drainage condition will be considered in the next research. The 2-D model cannot consider the effect of soil movement at two sides of the foundation during liquefaction. The movement of liquefied soil may significantly affect to a seismic behavior of the foundation. Moreover, when the slope ground is unstable, the physical properties of the ground may be change during shaking and the behavior of the foundation will becomes complicated. Therefore, the mentioned problems should be considered detail in the next research.

The research shows that the effect of slope of 15^{o} on the dynamic response of SPSP in the revetment was significant and the liquefaction verification using reductions of shear modulus in JRA 2002 specification approach cannot provide the good displacement responses in the slope model. Therefore, it is necessary to give the further researches in determination of reduction of soil strength and/or in consideration of the effect of lateral ground movement to coincide the proposal conclusion of vibration test in this study.

The observation of acceleration time histories during shaking in the slope model expressed the larger acceleration value in the downslope direction. The study only explained the behavior phenomenon of the instability of slope ground generates the higher acceleration. The numerical methods cannot explain this phenomenon. Therefore, the further researches in both vibration test and theory numerical models need to be conducted to clarify.

早稲田大学　博士（工学）　学位申請　研究業績書

(List of research achievements for application of doctorate (Dr. of Engineering), Waseda University)

氏 名(Full Name) NGUYEN Thanh Trung　　印(seal or signature　　)

（As of May, 2014）

種 類 別 (By Type)	題名、　発表・発行掲載誌名、　発表・発行年月、　連名者（申請者含む） (theme, journal name, date & year of publication, name of authors inc. yourself)
Paper	
○1	Dynamic behavior of a steel pipe sheet pile foundation in a liquefied layer during an earthquake. *Journal* of *Structural Eng. & Earthquake Eng., JSCE*, 2014. *Nguyen Thanh TRUNG*. Osamu KIYOMIYA and Makoto YOSHIDA. (Accepted)
Others	
1)	Impact on the seismic performance of steel pipe sheet pile foundation by the joint mechanical properties. *Proceedings of the 36th of IABSE Symposium in Long Span Bridge and Roofs-Development, Design and Implementation,* Kolkata, India, Sept. 2013. Tongxiang AN. Osamu KIYOMIYA and *Nguyen Thanh TRUNG*.
○2)	Seismic performance of steel pipe sheet pile foundation on soft ground. *Proceedings of the 15th of World Conference in Earthquake Engineering,* Lisbon, Portugal, Sept. 2012. Tongxiang AN. Osamu KIYOMIYA and *Nguyen Thanh TRUNG*
3)	Dynamic behavior of bridge foundation during liquefaction by shaking table test. *Proceedings of the 15th International summer Symposium of JSCE*, Chiba, Japan, Sept. 2013. *Nguyen Thanh TRUNG* and Osamu KIYOMIYA.
○4)	Shaking table test on steel pipe sheet pile foundation in slope during liquefaction. *Proceedings of the 16th Symposium on Performance-based Seismic Design Method for Bridges of JSCE*, Tokyo, Japan, July 2013. *Nguyen Thanh TRUNG*. Osamu KIYOMIYA. Tongxiang AN and Makoto YOSHIDA.
○5)	Verification of influence on seismic performance of SPSP foundation under the 2011 pacific coast of Tohoku earthquake. *Proceedings of the 1th International Symposium on Earthquake engineering of JAEE*, Tokyo, Japan, Dec. 2012. *Nguyen Thanh TRUNG*. Osamu KIYOMIYA and Tongxiang AN.
6)	Dynamic response analysis of steel sheet pipe pile foundation conducted on three simple models. *Proceedings of the 14th International summer Symposium of JSCE*, Nagoya, Japan, CS4-0019, Sept. 2012. *Nguyen Thanh TRUN*G. Osamu KIYOMIYA and Tongxiang AN.
○7)	Comparison of three seismic analysis models of Steel sheet pile bridge foundation. *Proceedings of the 15th Symposium on Performance-based Seismic Design Method for Bridges of JSCE*, Tokyo, Japan, July 2012. *Nguyen Thanh TRUNG*. Osamu KIYOMIYA and Tongxiang AN.
8)	Response analysis of steel sheet pipe pile foundation by three simple types of models. *Proceedings of the 39th Annual Conference of JSCE*, Yokohama, Japan, Kanto Branch, March 2012. *Nguyen Thanh TRUNG*. Osamu KIYOMIYA and Tongxiang AN.